UNIVERSIDADE FEDERAL DO RIO GRANDE DO SUL
INSTITUTO DE QUÍMICA
PROGRAMA DE PÓS-GRADUAÇÃO EM QUÍMICA

TESE DE DOUTORADO

STRUCTURE-PROPERTY RELATIONSHIPS IN HIGH BARRIER MULTILAYER FILM/FOAM SYSTEMS

CLAUDIO ROBERTO LIMA DE SOUZA

Orientador: Prof. Drª. Raquel Santos Mauler

Orientador: Prof. Dr. Gary Wnek

Porto Alegre, Novembro/2020

UNIVERSIDADE FEDERAL DO RIO GRANDE DO SUL
INSTITUTO DE QUÍMICA
PROGRAMA DE PÓS-GRADUAÇÃO EM QUÍMICA

CLAUDIO ROBERTO LIMA DE SOUZA

STRUCTURE-PROPERTY RELATIONSHIPS IN HIGH BARRIER MULTILAYER FILM/FOAM SYSTEMS

Tese apresentada como requisito parcial para a
obtenção do grau de Doutor em Química

Prof. Drª. Raquel Santos Mauler
Orientador

Prof. Dr. Gary Wnek
Orientador

Porto Alegre, Novembro/2020

A presente tese foi realizada inteiramente pelo autor, exceto as colaborações as quais serão devidamente citadas nos agradecimentos, no período entre (abril/2016) e (novembro/2020), no Instituto de Química da Universidade Federal do Rio Grande do Sul sob Orientação do(a) Professor(a) Doutor(a) Raquel Santos Mauler e Orientação do(a) Professor(a) Doutor(a) Gary Wnek. A tese foi julgada adequada para a obtenção do título de Doutor em Química pela seguinte banca examinadora:

Comissão Examinadora:

Prof. Dr. Eric Baer	Prof. Dr. Andrew Olah
Prof. Dr. Xiong Yu	Prof. Dr. Cesar L. Petzhold
Prof. Drª. Raquel Santos Mauler	Prof. Dr. Gary Wnek
Claudio Roberto Lima de Souza	

Dedication

To my wife, Alana, and my daughter, Natália.

TABLE OF CONTENTS

LIST OF TABLS

Chapter 2

Chapter 3

Chapter 4

LIST OF FIGURES

Chapter 1

Chapter 2

Chapter 3

ACKNOWLEDGEMENTS

First, I would like to express my sincere gratitude to my advisors, Dr. Gary Wnek and Dr. Raquel Mauler, for their support and guidance throughout my graduate career.

Second, I would also like to acknowledge the opportunity to work in the science and technology Center for Layered Polymeric System (CLiPS) funded by National Science Foundation under supervision of Professor Eric Baer and Dr. Andrew Olah. CLiPS provided me with a professional and unique circumstance to collaborate with interdisciplinary colleagues. The weekly group meetings led by Professor Baer were extremely helpful through refining the logic of my research and training on the methodology of constructing the process-structure-properties of polymeric materials. It was an unforgettable experience and will be a great fortune to my further research.

Third, I thank the previous and current colleagues, Jingxing Feng, Ziyou Zhang, Mohammed Alanazi, Zhenpeng Li, Ci Zhang, Xinting Wang, Cong Zhang, Ruolin Sun, Susan Kozawa, Erik Price and Haofei Nian for contributing to my research projects, and for experiencing microlayer runs and group meetings together. I thank my Brazilian friends from Capes/CWRU program for supporting my research and for facilitating my campus life. The scholarship and financial support from Capes are gratefully acknowledged. I also want to thank to Dr. João Maia for the support during the Capes/CWRU program.

Finally, I sincerely thank my mother, parents-in-law, and especially my lovely wife and daughter for their great support, patience, and love during my Ph.D studies.

Structure-Property Relationships in High Barrier Multilayer Film/Foam Systems

Claudio Souza

ABSTRACT

Thermoplastic foams nowadays are widely used in a variety of applications, such as packaging, construction, and the automotive industry because of their wide range of properties such as lightweight, excellent strength/weight ratio, insulation properties, energy absorption performance, and material cost. However, there are still issues on the gas barrier and mechanical properties in use because of the cellular structure. This work targeted to unveil the processing-structure-property relationships of three film/foam multilayer polymeric systems with diverse transport properties.

The first part of the thesis (Chapter 2) focuses on the understanding of the effect of the number of layers and composition on mechanical properties and barrier properties of multilayer film/foam material with alternating ethylene-vinyl alcohol copolymer (EVOH) film layers and low-density polyethylene (LDPE) foam layers. Tensile properties of the film/foams at elevated temperatures were used to optimize thermoforming conditions. Uniaxial orientation was discovered as an efficient approach to evaluate the potential for thermoforming. Oxygen transmission showed a strong correlation with the thickness reduction which could be used as an indicator for barrier properties of the packaging materials. Film/foam materials with 32 layers demonstrated optimum performance with low oxygen transmission along with high drawing capability.

In the third chapter, the previous system (Chapter 2) was innovated with high-density polyethylene (HDPE) skin layer. High oxygen and water vapor barrier film/foam system had been developed using multilayer co-extrusion technology. The film/foams contained alternating low-density polyethylene (LDPE) foam layers and ethylene–vinyl alcohol (EVOH) copolymer film layers with HDPE skin layer. The lightweight film/foams showed oxygen and water vapor transmission rate are correlated with the EVOH film layer and HDPE skin layer composition. The layered film/foam was successfully thermoformed at 80 °C with low oxygen transmission along with high drawing capability.

The fourth chapter introduces a novel approach, to produce PLA/PLA multilayer film/foams structures having 16, 32, and 64 alternating layers. The lightweight multilayered PLA/PLA film/foam has a unique solid/porous alternating horizontal architecture, in which the film layers can effectively control the growth of the cells and suppress the premature rupture of cells during coextrusion process. Tensile properties at elevated temperatures of the PLA film were used to optimize thermoforming conditions. The effects of annealing temperature and time on the crystallinity and oxygen permeability of PLA/PLA multilayer film/foams were investigated. Oxygen transmission showed a strong correlation with the crystallinity of PLA/PLA multilayer film/foam. The material demonstrated high performance with low oxygen transmission which could be used as high barrier material.

Chapter 1

Introduction

1.1 Introduction to thermoplastic foams

Plastic foams are widely used for different applications because of their outstanding properties such as lightweight, mechanical, thermal, electrical, insulation, and acoustic properties. These outstanding properties lead cellular plastics to have a wide range of applications and end-use industries, namely, construction, medical, automotive, and packaging industries [1]. The global market size of polymer foam is estimated to reach 30 million metric tons by 2020 at an average compounded annual growth rate CAGR of 3.5% [2]. However, the major foamed products are less effective than desired in regards to water vapor and oxygen barrier properties.

1.2 Foam and Foam formation

Foam can be defined as spherical gaseous voids dispersed in a continuum denser phase, which usually shows a liquid or solid phase. Foam materials are made when there is an abruptly change in the surrounding conditions and free gas molecules in the material are converted into spherical bubbles. The gas phase keeps growing until it is balanced by adjacent cells and polymeric tension. The bubble expansion work, melt elasticity and latent heat are present in a nonisothermal system. This behavior is a form of the system dissipated the disturbances created in the environment. On the others words, this is a transition from a stable (homogeneous) state to a meta-stable or unstable (heterogeneous) state. This kind

of structure is widely found in nature like as wood, cork, tree trunk. Material with this kind of structure also can be made through of synthetic processes using polymers as a matrix [3].

Plastic foams or cellular plastics also referred to as expanded polymer consist of a minimum of two phases: a solid polymer matrix as a continuous phase and a gaseous phase as dispersed bubbles. Generally, such structure is produced by introducing a blowing agent in a polymer matrix, then foaming the gas, and subsequently cooling of the melt to retain the useful effects of the dynamically intensive foaming process and thereby deliver stable foamed products. Besides, different types of particles can be added into the polymer matrix as nucleating agents. When a material is foamed, voids are created and dispersed inside the matrix, however, the continuity of the matrix keep present, the basic property does not change, even with lower density. A composite with different range of properties can be created changing the quantity, distribution, and size of the cells. That is, the relationship between performance/weight can be significantly different from foam-free material [4].

Plastic foam may be flexible or rigid, depending of their glass-transition temperature, degree of crystallinity, chemical composition and degree of crosslinking of the materials. The structure may be present in the form of closed cell or open cell in different sizes and shapes, these properties greatly affect the foam performance. Thus, open cell foams are most suitable for filtration and acoustical insulation, while closed cell are best for thermal insulation. Plastics foams can be manufactured in a broad spectrum of densities, ranging from very low density about (1.6 Kg/m^3) to high density about (960 Kg/m^3) [3]. The mechanical properties of the foam are generally proportional to the foam density; the end applications determine which range of densities are required. In general, load bearing

requires high density and (or) fiber-reinforced foams, while thermal insulation requires low density. Foam system has several variables that can profound impact its properties and thereby applications. Those are, the amount of voids (blowing agent percentage) and its interconnection, their dispersion and distribution [3].

1.3 Foam Extrusion

Thermoplastic foams have been evolved since 1941 as an extension of the extrusion application. The extruder is a powerful tool to converter mechanical power and thermal energy into processing heat for polymer phase change and create sufficient positive pumping force for fast material transport. The extrusion process has been achieved the critical processing conditions for foaming and become widely adopted for foam processing since the 1970s. Develop of gas bubbles is a critical factor in foam extrusion seems that the process is favorable at higher temperature. However, the melt strength is a limiting parameter to maintain the bubbles. In foaming extrusion, coalescence and collapse of the bubble are not desirable, to avoid this phenomenon the parameters of the system need to be optimized. Other properties, such as foam density, cell size, cell size distribution, type of cells and cell geometry are important parameters to control the mechanical properties of a foam [5].

Figure 1.1 shows the relevant point in foam extrusion. Foaming process is a complex system because the viscoelastic properties of the polymers depends of the temperature, pressure and the amount of blowing agent used. Furthermore, dynamic foaming using extrusion makes the system even more complex. Thermoplastic foams processing remains a challenge in some fields and is a huge challenge for new foaming technologies. The key

point is to overcome these issues and understand some important properties of polymers, such as melting, flow, foaming and forming. Also, the relationship between properties and structure of the materials [5].

1.4 Bio-based Foam

The market of polymeric foams materials is growing rapidly because of their outstanding properties [2]. However, there are concerns about the possible environmental impact of these materials. Bio-based foams have been extensively studied as a potential substitute for conventional polymeric foams. Among these materials, polylactic acid (PLA) has received special attention because of its good mechanical properties, and low cost [6]. PLA based foam has two main drawbacks, its poor melt elasticity and slow crystallization kinetics, which produce poor cellular structures with cell coalescence, and large cells [5].

It is well known that melt elasticity is an important property during the foaming process. In the molten state elastic properties are enhanced by incorporation of long-chain branches and larger molecular weight distribution. For this reason, low-density polyethylene (LDPE) is widely used for foaming. Since Poly (lactic acid) (PLA) has shorter-chain branches with a narrow molecular weight distribution [5]. Different approaches have been explored to solve the lack of elasticity required for foaming, as reported in the Chapter 4. However, in all cases, the cellular morphologies after foaming was not strongly enhanced in relation to the neat material. Therefore, new technologies to improve PLA melt elasticity are highly desired.

1.5 Food Polymeric Packaging

Polymeric materials are widely used in food packaging because it is properties. The main function of package is to protect the food products, not only during the transportation, but extended shelf life as well as protection from the loss of nutrients, color, taste, aroma, functional properties, and preserve the general appearance [7].

A good food package material should create an acceptable barrier between external environment and the food, especially in terms of oxygen, water vapor and microorganisms. Atmospheric gases and water vapor if allowed to permeate in or out of the package can strongly affect the shelf life, the length of time that product may be stored without becoming unfit for use.

Finally, a food package should present clear information about the product and attract consumers to buy it.

Polymeric materials need to have some attributes to be suitable for packaging applications, such as low permeability to gases and mechanical properties to allow the packaged food to withstand the rigors of transportation, handling, storage and refrigeration. Other key market driver is a trend toward conversion to biodegradable, recyclable and sustainable polymeric food packaging to improve the environmental footprint of packaging [7].

Plastic foams are widely used for single use food packaging. However, the low oxygen barrier has made its use difficult in general food packaging. The industry used lamination to improve barrier properties on foams. This process had high material and equipment cost because it is necessary use a tie layer to improve adhesion between the foam and the barrier film. Moreover, for many applications is necessary a skin layer to protect the barrier film.

Such process had a complex structure comprising at least five layers, which largely limited the popularity of foam with barrier properties [1].

1.6 Barrier Property

The barrier property of a polymer refers to its ability to restrict the permeation of vapors, gases, and organic liquids through their boundaries. The transmission rate or permeability of gases and vapor through the material is dependent on two factors: The solubility and the rate of diffusion of the permeant through the barrier material. The solubility of the permeant in the polymer is related with the chemical relationship between the polymer and the permeant molecule. The diffusion rate is dependent upon the amorphous morphology of the polymer and the size of the permeant molecule [7].

When a polymeric material is exposed to a permeant molecule having different in partial pressure on its two sides, the permeant passes through by net effect from the high-pressure to the low-pressure side in three steps: Absorption into the polymer, diffusion through the polymer and desorption through the polymer and evaporation for the surface[7], [8].

Permeability is a material property defined as the product of permeance and thickness. Under steady-state conditions, the permeance is defined as "the ratio of the gas transmission rate (the quantity of permeant passes through a unit surface area of a barrier material in unit time under specified test conditions) to the difference in partial pressure of penetrant on both sides of the material. The permeation rate of a material can be calculated from Eq. 1. This equation is derived from Fick's first law of mass transfer. Permeation happens due to the movement of a species through the molecules of another material. This

process does not take into account transport of material through physical flaws, such as voids and cracks of the second material [7], [8].

$$\mathbf{P = D.S} \qquad \mathbf{(1)}$$

Where P (cm^3(STP)/cm.s.atm) is the permeability of the gas, D (cm^2/s) is the diffusion coefficient, and S (cm^3(STP)/cm^3.atm) is the solubility coefficient.

The amount of permeant molecules that penetrate into a polymeric material depends on the properties of the polymer, such as chemical structure, the degree of crystallinity, and in some cases the thermal and mechanical histories of the polymer and the properties of the penetrating molecules, the temperature, their interaction and cross-effects, and the permeant partial pressure inside and outside the package [8].

Many factors affect the permeation rate in a polymer. The temperature is one of them when the temperature increase the permeation rate raises nearly exponentially. At above the glass transition temperature, the segmental mobility of the polymer chains increases, thus creating larger "holes" for the passage of permeant molecules. The permeation rate follows the Arrhenius equation, albeit with some limitations [7].

Actually, conventional monolayer polymer films are not able to meet all the requirements of food packaging. Instead, multilayer films are usually designed to attend all the characteristics of food packaging, such as mechanical and barrier properties. There are several technologies able to produce multilayer films, the most common are thermal lamination, coating and coextrusion process. These techniques can design multilayer polymeric structure in order to achieve excellent barrier properties, mechanical and optical properties combining different polymers. However, developing high oxygen and water

vapor barrier materials, particularly in food packaging, without significant cost increase continues to be a challenge [7].

1.7 Thermoforming Process

Thermoforming is considered as one of the oldest methods to produce useful formed parts of plastic and compete well with parts manufactured by other processes [9]. Thermoforming is a low-pressure, low-temperature process. It normally requires relatively inexpensive mold materials which are usually fabricated in relatively short times. In thermoforming, plastic products are made by heating a plastic sheet to its rubbery or forming condition, it is then stretched over or into a cool rigid mold surface. The formed sheet is then cooled until it retains the shape of the mold, the sheet and the formed part are removed from the mold without subsequent change in shape. The excess plastic is trimmed form the part and recycled to produce additional sheet.

Thermoforming is a differential stretching process. The sheet is stretched in a non-uniform biaxial way to produce the formed part, the product wall thickness is non-uniform [9]. Improvements in terms of wall thickness uniformity can be achieved by pneumatic or mechanical stretching of the heated sheet before bringing it in contact with the mold surface. Local wall thickness variation is strongly related to the geometry of the part and processing parameters such as mold temperature variation, cycling of heaters, ambient air temperature, plug temperature variation, and sheet sag. These factors combine with polymer properties strongly influence final part dimensions [9].

The forming window is defined as the temperature-dependent stress-strain region where the polymer can be stretched into its desired shape. It is material property driven. The lowest forming temperature is then determined by examining the mold characteristics to determine the maximum extent of stretch required to form the part. As expected, the maximum amount of stretching increases with increasing temperature. When the stress-strain data for a given polymer are depicted in this fashion, the cross-hatched area below the horizontal line is called the thermoforming area or forming area diagram (Figure 1.2) [9].

Thermoforming is widely used to form multilayer packaging materials. As multilayer sheet is stretched, every ply is stretched to the same extent. When thermoforming multilayer sheet into barrier packaging, care must be taken to ensure that the barrier layer remains thick enough in the thinnest portion of the formed product to minimize gas diffusion.

1.8 Forced Assembly Multilayer Co-extrusion

In recent decades, forced assembly multilayer coextrusion technology has been evolving and attracting both academic and industrial interest for the production of advanced polymeric material systems with a wide range of applications. This novel process has been demonstrated that it is an effective technology to develop new high value-added polymeric systems by creating complex hierarchical structures which novel or enhanced properties due to synergistic effect of the multiple components. This sophisticated hierarchical structures is inspired from biological systems. The benefits of this technology include, versatility, flexibility, solvent-free process, precise control of the structural levels and continuous processing of the material [10]–[12].

Forced assembly multilayer coextrusion combines two or three distinct polymers into a layered morphology with controllable hierarchical structure. This technology is able to produce hierarchical architectures by manipulating the scale, interaction and organization of the layers. The number of layers of multilayer films ranges from 2 to 4096 layers and the layer thickness ranges from microns down to around 10 nm by manipulating the number of layers. Moreover, this controlled interface of the alternating layered structure provides an interesting platform for fundamental studies on polymeric materials, such as interface, adhesion and interdiffusion [10].

This technology enables the fabrication of the multilayer polymeric materials into distinct architectures including films, fibers, film/foams, and gradient structures[10]. Furthermore, benefiting from the controlled scale, interaction and architecture, forced multilayer coextrusion has developed polymeric materials with outstanding properties in mechanics, permeability, dielectrics, and optics over conventional polymer materials [13]–[16].

Forced assembly process produces multilayer film structures by alternating micro or nano-layers of two or three components through sequential layer multiplication or "multipliers". Initially, polymer melts forming an initial two or three layered structure in a convention feedblock flow through several multipliers undergoing layer multiplication. A melt pump is used to control the relative volume composition that is proportional to the ratio between the layer thickness of the polymers. In each multiplication element, the layered melt is cut vertically into two parts, where one part flows and spreads into a bottom channel and the other part flows and spreads into a top channel, to stack. Through this process of splitting, spreading and stacking, the layer number is doubled by each of the multiplication element, producing from tens to thousands of individual layers within a single film. The layer

number are controlled by the number of the multipliers that are used and calculated as 2^{n+1} for the A/B structure and 2^{n+1+1} for the A/B/A structure. By changing the number of multipliers in the system, multilayer films having tens to thousands of layers are produced as shown in Figure 1.3.

The forced multilayer coextrusion utilizes the viscoelastic behavior of polymer melts under a shear field to produce the layered structure. The layer integrity and uniformity are highly influenced by the polymer melt viscosities. Several studies have been reported that large viscosity differences can induce instabilities, such as the low viscosity layer encapsulates the high viscosity layer, layer instability and layer break-up [10], [17]. Consequently, polymer pairs are coextruded at a temperature at which the polymer components have similar viscosities in order to optimize the layered structure.

Finally, the multilayer film is collected from an exit die by using a temperature controlled take-off chill roll. The total thickness of the fabricated multilayer films can range from 2 mm to 10 μm with individual layer thickness from microns to ∼10 nm [10].

1.9 Multilayer Film/Foam Co-extrusion

A novel technique to produce multilayer film/foam structure was recently proposed and developed by Baer and coworkers [18]–[21]. The process to prepare film/foam using multilayer coextrusion is basically the same used to prepare multilayer films. However, one of the extruders contains the polymer and a foaming agent which decomposed at the exit die where the foam cell grew into microcells throughout the foam layer. Previous researches demonstrated that film/foam produced by this technology using the same

polymer for film and foam layer has good layer structure, closed cell and cell size less than 100 μm [18], [19]. They also showed that changing composition and materials several properties can be tunable, such as density, mechanical properties, and permeability. These desirable properties are related to the small closed cells in its alternating film and foam layered architecture.

Rahman et al. discovered that film/foam systems have better control of layers and cell migration when the film layer material has higher viscosity than the foam layer material. The coextrusion process can be stabilized and more uniform layered structure can be achieved using the viscosity contrast yielded [19].

This technology has been demonstrated to be an efficient way to produce cellular materials with precise control of the cell size based on the layer confinement.

1.10. References

[1] J. Feng, Z. Li, A. Olah, and E. Baer, “High oxygen barrier multilayer EVOH/LDPE film/foam,” J. Appl. Polym. Sci., vol. 135, no. 26, p. 46425, Jul. 2018, doi: 10.1002/app.46425.

[2] E. B. Obi, Polymeric foams structure-property-performance: a design guide. William Andrew, 2018.

[3] S. T. Lee, C. B. Park, and N. S. Ramesh, Polymeric foams: Mechanisms and materials. 2006.

[4] L. J. Gibson and M. F. Ashby, Cellular Solids. Cambridge University Press, 1997.

[5] S. T. Lee and C. B. Park, Foam Extrusion: Principles and Practice, Second Edi. CRC Press, 2014.

[6] L.-T. Lim, R. Auras, and M. Rubino, “Processing technologies for poly(lactic acid),” Prog. Polym. Sci., vol. 33, no. 8, pp. 820–852, Aug. 2008, doi: 10.1016/j.progpolymsci.2008.05.004.

[7] S. Ebnesajjad, Plastic Films in Food Packaging Materials, Technology, and Applications. Elsevier, 2013.

[8] S. E. M. Selke, Understanding Plastic Packaging Technology. New York: Hanser Publications, 1997.

[9] J. L. Throne, Understanding Thermoforming. München: Carl Hanser Verlag GmbH & Co. KG, 2008.

[10] Z. Li, A. Olah, and E. Baer, “Micro- and nano-layered processing of new polymeric systems,” Prog. Polym. Sci., vol. 102, p. 101210, Mar. 2020, doi: 10.1016/j.progpolymsci.2020.101210.

[11] E. Baer, A. Hiltner, and H. Keith, “Hierarchical structure in polymeric materials,” Science (80-.)., vol. 235, no. 4792, pp. 1015–1022, Feb. 1987, doi: 10.1126/science.3823866.

[12] E. Baer, A. Hiltner, and D. Jarus, “Relationship of hierarchical structure to mechanical properties,” Macromol. Symp., vol. 147, no. 1, pp. 37–61, Dec. 1999, doi: 10.1002/masy.19991470106.

[13] C.-Y. Lai, A. Hiltner, E. Baer, and L. T. J. Korley, “Deformation of Confined Poly(ethylene oxide) in Multilayer Films,” ACS Appl. Mater. Interfaces, vol. 4, no. 4, pp. 2218–2227, Apr. 2012, doi: 10.1021/am300240r.

[14] J. M. Carr, D. S. Langhe, M. T. Ponting, A. Hiltner, and E. Baer, “Confined crystallization in polymer nanolayered films: A review,” J. Mater. Res., vol. 27, no. 10, pp. 1326–1350, May 2012, doi: 10.1557/jmr.2012.17.

[15] S. Ji, K. Yin, M. Mackey, A. Brister, M. Ponting, and E. Baer, “Polymeric nanolayered gradient refractive index lenses: technology review and introduction of spherical gradient refractive index ball lenses,” Opt. Eng., vol. 52, no. 11, p. 112105, Jul. 2013, doi: 10.1117/1.OE.52.11.112105.

[16] M. Mackey et al., “Reduction of Dielectric Hysteresis in Multilayered Films via Nanoconfinement,” Macromolecules, vol. 45, no. 4, pp. 1954–1962, Feb. 2012, doi: 10.1021/ma202267r.

[17] J. Feng et al., “Breakup behavior of nanolayers in polymeric multilayer systems — Creation of nanosheets and nanodroplets,” Polymer (Guildf)., vol. 143, pp. 19–27, May 2018, doi: 10.1016/j.polymer.2018.03.049.

[18] A. P. Ranade, A. Hiltner, E. Baer, and D. G. Bland, “Structure-Property Relationships in Coextruded Foam/Film Microlayers,” J. Cell. Plast., vol. 40, no. 6, pp. 497–507, Nov. 2004, doi: 10.1177/0021955X04048425.

[19] M. A. Rahman, R. Andrade, J. Maia, and E. Baer, “Viscosity contrast effects on the structure – Property relationship of multilayer soft film/foams,” Polymer (Guildf)., vol. 69, pp. 110–122, Jul. 2015, doi: 10.1016/j.polymer.2015.05.051.

[20] M. A. Rahman, J. Wang, C. Zhang, A. Olah, and E. Baer, “Novel micro-/nano-porous cellular membranes by forced assembly co-extrusion technology,” Eur. Polym. J., vol. 83, pp. 99–113, Oct. 2016, doi: 10.1016/j.eurpolymj.2016.08.015.

[21] H. Wu, J. Zhang, C. Zhang, J. Feng, M. A. Rahman, and E. Baer, “Structure–Properties Relationship of a Novel Multilayer Film/Foam Material Produced through Co-extrusion and Orientation,” Ind. Eng. Chem. Res., vol. 55, no. 41, pp. 10947–10954, Oct. 2016, doi: 10.1021/acs.iecr.6b03418.

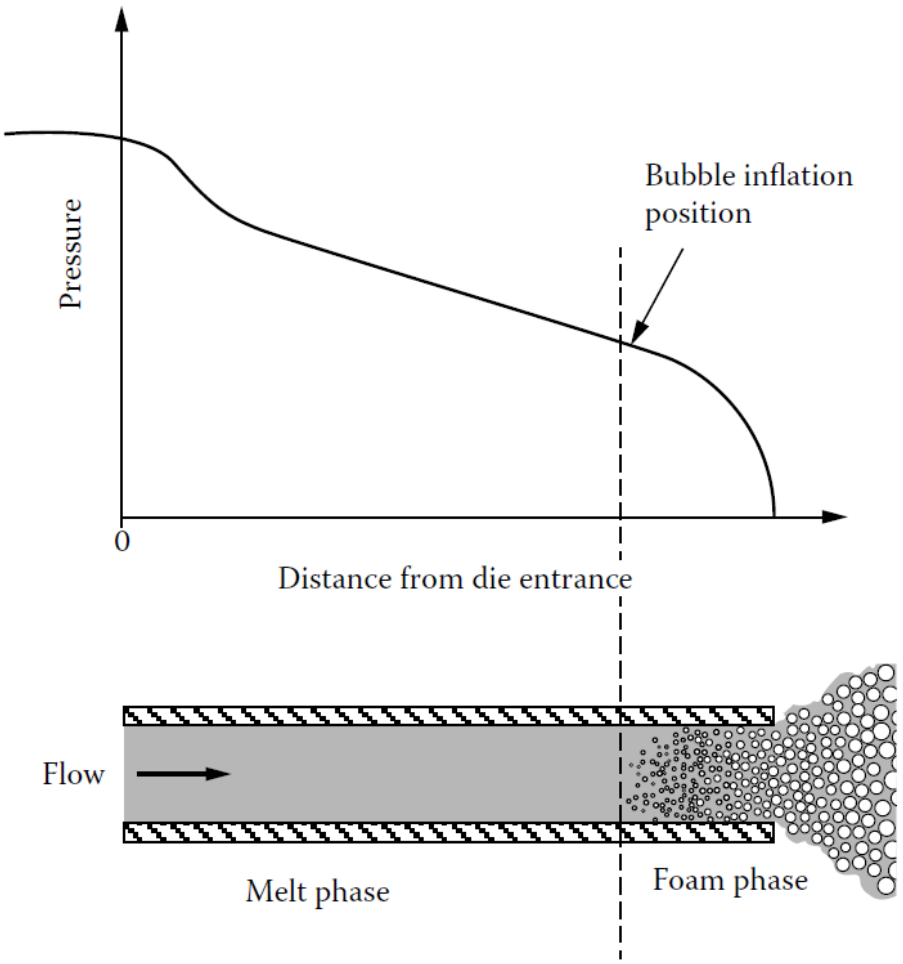

Figure 1.1 Axial pressure profile along a die of constant cross section: beyond entrance effects, a linear pressure drop is followed by a deviation from linearity as bubbles are nucleating [5].

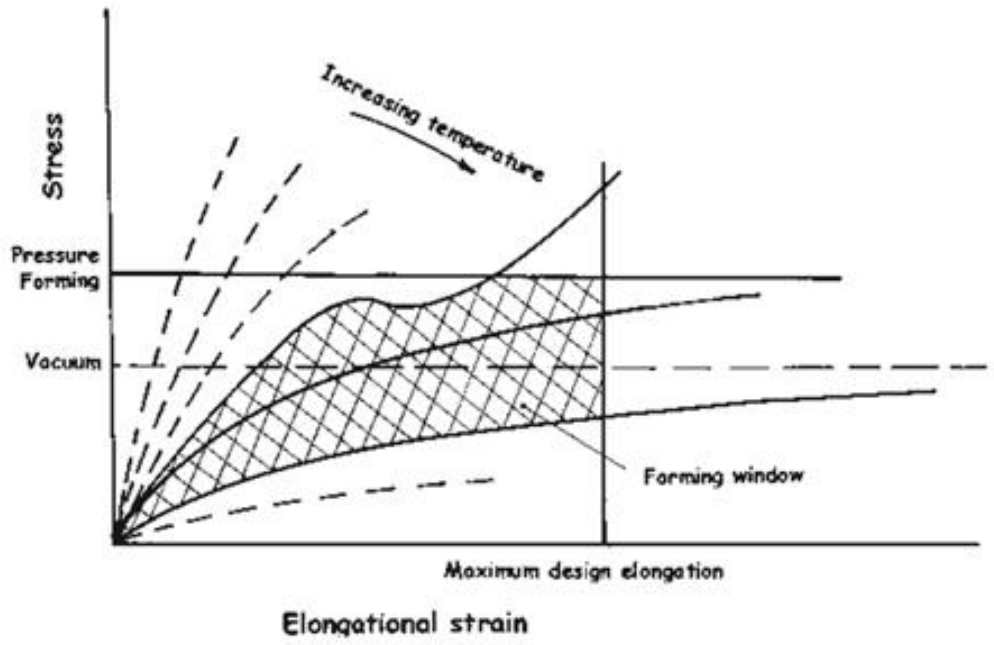

Figure 1.2 Temperature-dependent stress-strain curves with forming area [9].

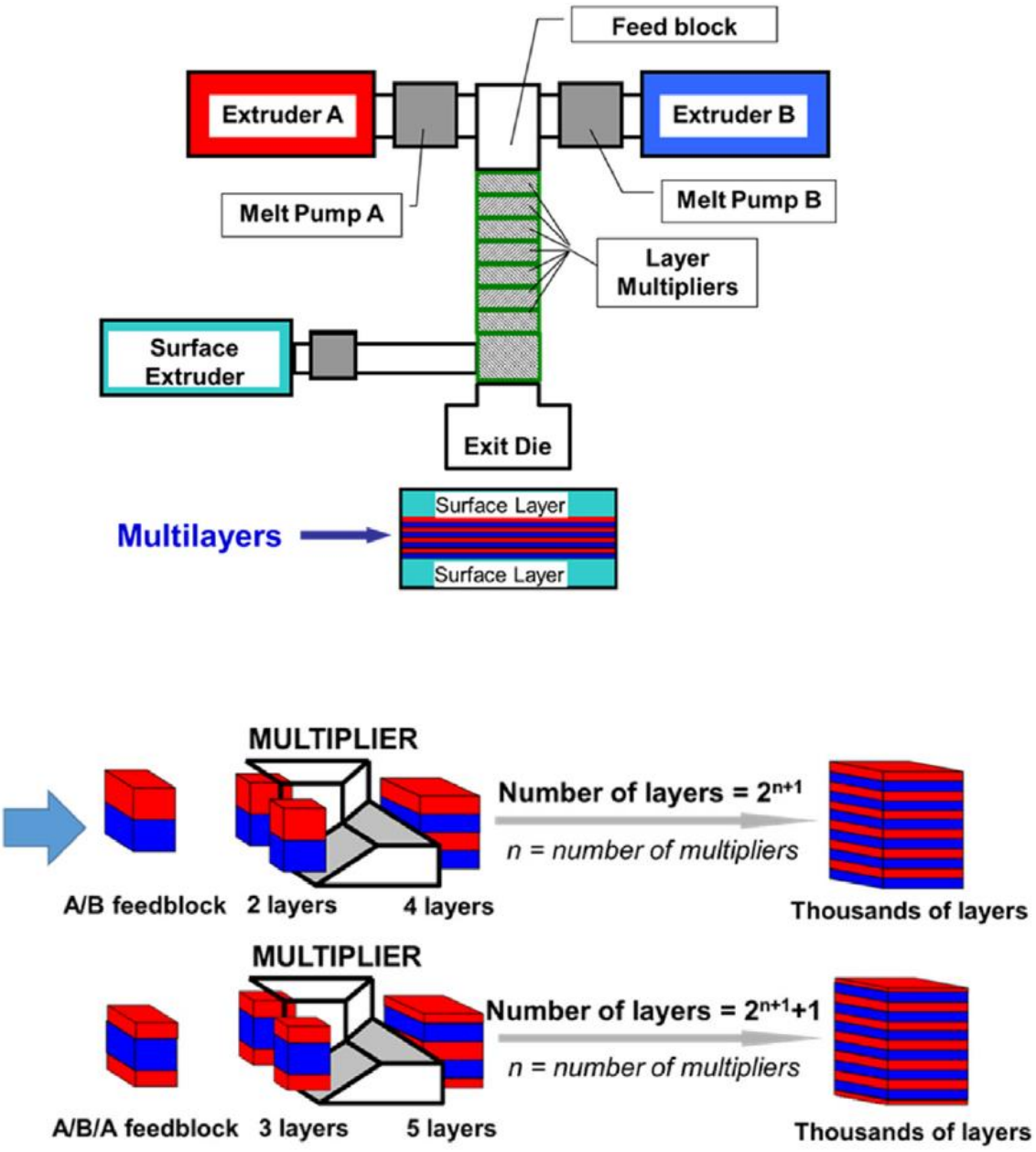

Figure 1.3 Schematic of two-component multilayer coextrusion process [10].

Chapter 2

Thermoformable High Oxygen Barrier Multilayer EVOH/LDPE Film/Foam

Abstract

The effect of the number of layers on oxygen transmission and thermoformability of novel multilayer film/foam materials was investigated. Ethylene-vinyl alcohol copolymer (EVOH) / low-density polyethylene (LDPE) multi-layered film/foam composites having 16, 32, and 64 alternating layers were developed using continuous multilayer co-extrusion process, and the morphology, density, oxygen transmission, and mechanical properties of the as-extruded film/foams were characterized. Tensile properties of the film/foams at elevated temperatures were used to optimize thermoforming conditions. Uniaxial orientation was discovered as an efficient approach to evaluate the potential for thermoforming. Oxygen transmission showed a strong correlation with the thickness reduction which could be used as an indicator for barrier properties of the packaging materials. Film/foam materials with 32 layers demonstrated optimum performance with low oxygen transmission along with high drawing capability.

2.1 Introduction

Plastic foam is widely used in several applications due to outstanding properties such as its low density, thermal and acoustic isolation, impact and shock absorption, and low production cost [1][2]. However, most common foamed products have high oxygen and water vapor transmission due to their porous structure. The current technology used to meet the demand for high barrier foams is based on lamination processes. In this approach one or more barrier layers are laminated with the foam layer. The lamination process is usually complex and expensive due to the use of bonding layers to ensure good adhesion between the materials and skin layer to protect the barrier film in post-processing steps such as thermoforming. Due to these challenges there are few commercial high barrier foams available in the market [1].

Thermoforming is widely used in industry to produce polymeric products with complex geometries [3][4]. Despite the great success in large-scale manufacturing of high barrier products, thermoforming of multilayered structures with foam layers has not been studied. Thermoforming imparts non-uniform deformation in the material which affects several properties such as mechanical strength, crystallinity of the constituent layers, thickness in corners, bottom and walls, and specifically gas transmission rates [5]–[7]. There is a concern, particularly in the food packaging industry, whether the final formed product will maintain the barrier properties after the thermoforming process [8].

Evaluation of barrier performance of thermoformed polymeric products is challenging. Standard test methods are available for measuring oxygen and water permeation rates through flat materials such as films and sheets. However, this measurement can be

complex for shaped products, due to package geometry and size. Moreover, the samples need to be very carefully prepared and sealed to avoid leakage problems during testing. There is a strong interest to estimate oxygen transmission rate (OTR) in the package based on the OTR and thickness of the unconverted film or sheet [8][9].

A novel technique to prepare co-extruded multilayer film/foam structures was recently proposed and developed by Baer and coworkers [1][2]. Multilayer polymer co-extrusion consists basically in a system of multiple single screw extruders with melt pumps, a co-extrusion feedblock, a sequence of layer multiplier elements, and an exit die. The flow rate of each component layer can be easily controlled by the melt pumps. In the feedblock, the melt streams are merged as parallel layers. In the multiplier sequence each element doubles the number of layers by first slicing vertically the layer, spreading them horizontally, and finally recombining. An assembly of n multiplier elements produces a film with $2^{(n+1)}$ layers. The thickness of the material can vary from 1 mm thick tape to as thin film as 25 μm with individual layer thickness down to less than 10 nm [10][11].

Multilayer polymer coextrusion is a scalable, cost-effective processing technique that can be used to combine polymers with widely dissimilar properties. These multilayered structures can exhibit a synergistic combination of properties that would be unavailable in a single material. Layered polymeric systems are important in achieving films that exhibit a desired mix of end-use characteristics. Mechanical, optical, gas barrier, electronic, and aesthetic properties can all be improved through multilayering. Multilayer coextrusion technology also provides a unique research tool for studying phenomena including layer interdiffusion, continued crystallization, and inter-layer adhesion due to their large interface to volume ratio [10], [12], [13].

This paper describes the development of multi-layered film/foam structures having 16, 32 and 64 alternating film and foam layers. High oxygen barrier composites were based on EVOH/LDPE film/foam. These materials exhibited adjustable properties, such as density, cell size, mechanical properties and oxygen transmission by changing the number of layers and overall composition. In addition, we evaluated the ability to predict the OTR of final thermoformed parts using uniaxial orientation. Thermoforming tests were performed at 80°C using two different molds. The foam composite showed good formability and the final OTR had a strong correlation with the final thickness.

2.2 Experimental

2.2.1 Materials

A two-component microlayer coextrusion setup was used to co-extrude film/foam layered structures. The foam layer material was a blend of LDPE 5004l and LDPE-grafted-maleic anhydrate (LDPE-g-MA) GR202 with melt flow indices of 4.2 and 8.0 g/10 min (190ºC/2.16 kg) supplied by the Dow Chemical Company. The blend composition was 80 wt % LDPE and 20 wt % LDPE-g-MA. This particular ratio was optimized in previous work [1]. The dry blend of LDPE and LDPE-g-MA was further blended with both a chemical blowing agent and a nucleating agent. The film layer was EVOH E171 copolymer supplied by Kuraray based with 44% ethylene content and a melt flow index of 1.7 g/10 min (190ºC/2.16 kg). Azodicarbonamide (Galata Chemicals) at 2 wt% was the chemical blowing agent for foaming the LDPE blend. The nucleating agent in the foam layer was 1 wt% Talc (Jetfine® 1H, IMERYS Talc).

2.2.2 Film/Foam Processing

One extruder contained the foam layer polymer (LDPE), chemical blowing agent (azodicarbonamide) and nucleating agent (talc) and the other extruder contained the film layer polymer (EVOH). After merging in the two-component feedblock, the foam and the film layers were processed into multilayers using the layer multipliers. Figure 2.1 illustrates the two-component coextrusion setup. The total pump rate in each extruder was adjusted to change the volumetric composition of film and foam layers for each sample.

Three-, four- and five-layer multiplication elements were used to produce 16, 32 and 64 layered film/foam structures. The temperature of the extrusion system and the layer multiplication elements were set at 195 °C. A 3 inch exit die at 170 °C was used after multiplication in order to control cell expansion. A 60 °C chill roll was used as a take-off. The thickness of the film/foam composites was maintained at 1.2 mm by adjusting the speed of the chill roll. The extruder screw speed and the melt pump rates were adjusted to control the composition of the film/foam composite. The temperature of the extrusion system was below the decomposition temperature of the chemical blowing agent so that the azodicarbonamide did not fully decompose to create large foam cells.

2.2.3 Scanning Electron Microscope Morphology

Scanning electron microscopy (SEM) (JEOL) was used to observe the film/foam layered structures in each sample. Film/foam samples were cut in the extrusion direction with sharp blades at room temperature. Then cross sections were sputter-coated with gold (10

nm). An emission voltage of 30 kV was used. The cell size and layer thickness of each film/foam sample were determined from SEM micrographs.

2.2.4 Density

The density of as-extruded film/foam specimens were measured using a density balance (Mettler Toledo, Columbus, OH). The liquid medium was ethanol to ensure wetting of the sample surface. Because the film/foams had a closed-cell structure, the mass/volume method for density determination was accurate. Each sample was tested at least 5 times, and the average value was taken.

2.2.5 Oxygen Transmission Rate

Oxygen transmission measurement was conducted with a MOCON-OX-TRAN 2/20 at 0% relative humidity, 1 atm and 23°C. The film/foam samples were cut into a circular shapes with a diameter of 3 cm and sandwiched between two aluminum foils providing a test area of 5 cm^2. The oxygen transmission through the aluminum foil was ignored since the aluminum is a very high oxygen barrier. The oxygen transmission of the samples were calculated using the flux and samples thickness.

The oxygen transmission measurement of the thermoformed samples were performed using a MOCON-OX-TRAN 2/20 at 0% relative humidity inside the package, 1 atm and 23°C using a package environmental chamber. The thermoformed parts were exposed to oxygen from the atmosphere. The results were converted in [$cm^3/(m^2.day)$]. All measurements were performed in triplicate and an average value was adopted.

2.2.6 Mechanical Properties

Tensile tests of as-extruded film/foam samples were conducted using a mechanical testing machine (Instron, Norwood, MA) at different temperatures. The film/foam samples were cut into rectangular microtensile bars having dimensions of 1.0 x 6.0 cm^2. The strain rate for the tensile study was 100%/min. The load–displacement data obtained from the testing equipment was converted into stress–strain curves. The Young's moduli of the specimens were calculated using the stress–strain ratio for 1% deformation. Each sample was tested at least 5 times, and the average value was taken.

2.2.7 Uniaxial Orientation

Uniaxial Orientation behavior of each film/foam multilayer system was investigated on microtensile bars (1.2 × 60 × 40) mm^3 at different temperatures. Tensile tests were performed in a mechanical testing machine (MTS Alliance RT/30) at a strain rate of 100%/min and the stress-strain curves were generated from the load-displacement curve obtained from the machine.

2.2.8 Mechanical Thermoforming

The as-extruded film/foam samples were cut into square specimens with a dimension of 60 mm by 60 mm square for thermoforming. Two different shapes for molding the film/foam samples were used to evaluate the thermoformability of the film/foam materials. The first consisted of a semi-spherical mold of two matched stainless steel parts with a diameter of 23 mm and a height of 13 mm. The second was an aluminum truncated cone mold shape, typical of the design in food packaging. This mold had a top

diameter of 30 mm, a base diameter of 25 mm, corners with radius of 2 mm, and a variable depth to 15 mm.

A film/foam specimen was loaded in the mold and was compressed at different temperatures. At room temperature, the pressure was maintained for 10s and afterwards the specimen was removed from the mold. When molded at higher temperatures the pressure was maintained for 5s. The composites were formed at a constant speed of 200 mm/min. To identify of the local strain across the film/foam sample during thermoforming, uniform grids were drawn on the sample to map the deformation. The change of distance between grid lines was used to determine local strain.

2.3 Results and discussion

Multilayer film/foam specimens having 16, 32, and 64 layers and several compositions were successfully produced by microlayer coextrusion process. Microcellular film/foam samples with good layer structure was achieved and investigated to determine the effect upon several properties, such as layer morphology, mechanical strength, oxygen transmission and thermoformability.

The morphologies of EVOH/LDPE film/foam with 16, 32 and 64 Layers at 50/50 compositions are shown in Figure 2.2. The materials show well defined layer structure and cell boundaries in all film/foam composites. By changing the composition and number of layers of LDPE foam and EVOH film, it is possible to achieve different foam and film layer thicknesses. An increase in the number of layers causes the foam layer and the film layer thickness to decrease as expected. The 16 layers system has the average film layer thickness about 70 μm which decreases to around 10 μm in the system with 64

layers. However, the structure remained continuous, which is essential for high barrier materials.

The film/foam samples with 16 and 32 layers show mostly single and bilayer cell structures with straight and parallel layer boundaries. The cells were confined to the foam layer without the cells causing any break-up of the film layers. However, the system with 64 layers was comprised of single layer cell and the cells were larger than the individual layer thickness, therefore deforming and squeezing the film layers. Although the film layer becomes more tortuous, film layer break-up was not observed. In addition, the confinement effect was very significant in this system as the foam had to develop and expand with less freedom. Figure 2.2 shows sharp interfaces and good layer structure without delamination in all three systems. This result was achieved because the materials were selected based on the principle of viscosity contrast and due to the use of LDPE-g-Ma in the foam layer. The latter works as a compatibilizer to improve the adhesion between the film and foam layer [1][14]. Furthermore, EVOH copolymer is partially compatible with LDPE, due to 44% polyethylene content. The strong adhesion between the film and foam layers are due to the reaction between the MA group from LDPE-g-MA with the hydroxyl groups in EVOH during the extrusion process. The samples were processed to have the same final thickness (1.2 mm) by controlling the speed of chill roller.

2.3.1 Properties EVOH/LDPE film/foam Composites

The characteristics of the as-extruded EVOH/LDPE multilayer film/foam materials are described in Table 2.1. As expected, the cell size and total density decreased with the increase of foam layer composition. As an example, the average cell size of the system with 16 layers decreased from 104 to 58 μm and the total density decreased from 0.67 to 0.50 g/cm^3 when the foam layer composition increased from 50% to 90%. It was observed that in this system the total density of the multilayer film/foam and cell size were highly variable with the composition of the system. In terms of the number of layers, by increasing the numbers of layers in the system with 10/90 EVOH/LDPE composition reduces cell size from 58 to 53 μm without adversely affecting the total density. The two factors found to mainly affect the total density and cell size were the film/foam composition and the number of layers. In the system with 16 layers the composition effect was more pronounced in terms of cell size. The measured cell size of multilayer film/foam composite (10/90 composition) approximately follows lognormal distribution, as shown in Figure 2.3.

The oxygen transmission rates of as-extruded multilayer film/foam samples are listed in Table 2.1. All samples show very good oxygen barrier properties. Film/foam samples with high concentration of EVOH show very low oxygen transmission. By decreasing the EVOH film layer content, the oxygen transmission increases due the reduction of EVOH film layer thickness. However, for all compositions and systems the OTR (oxygen transmission rate) values were below 1.0 cm^3/(m^2.day) which meet or exceed the requirements for the most oxygen barrier applications, such as food packaging. The EVOH grade used in this project had 44% ethylene content. The oxygen barrier

properties can be improved by using a EVOH grade having lower ethylene content. There are commercial grades of EVOH from 24 mol% to 48 mol% ethylene. The lower mol% ethylene content would provide higher gas barrier properties.

The 10/90 EVOH/LDPE multilayer film/foam was chosen for subsequent studies because it yielded properties closer to those of commercial products, such as film layer content, film thickness and oxygen transmission rate.

2.3.2 Mechanical Properties of EVOH/LDPE film/foam

Figure 2.4 shows the tensile properties of as-extruded film/foam EVOH/LDPE (10/90) with 16, 32 and 64 layers at room temperature and strain rate of 100%/min. The load-displacement data were obtained from the testing equipment and converted into stress-strain curves. The data reveal good mechanical properties and typical plasto-elastomeric behavior under tension for all systems. The highest maximum stresses, elongations at break, and Young's modulus for all three systems are shown in Figure 2.4. Initially samples show a reversible elastic deformation. At a certain amount of stress, deformation becomes irreversible, which is recognizable by a yield point in the true stress-strain curves. After the yield point, the samples exhibit a constant stress with the increase of strain. At low strain, all systems demonstrate a typical elastomeric behavior with the yield point around 7% strain.

The tensile test experiment indicate that the film/foam samples have a good layering and good adhesion without delamination at break or at maximum strain. Moreover, all samples have maximum strain larger than 100% indicating their potential for thermoforming.

Details of mechanical properties of EVOH/LDPE film/foams are presented in Table 2.2. It was observed that increasing the number of layers the maximum stress and the elongation at break increase. However, the Young's modulus remained almost constant. The Young's modulus was modeled using Equation (1). The volume ratio of EVOH and LDPE in the equation was selected by the melt pump rate during the multilayer coextrusion process. The void ratio was determined from the density of the foamed and unfoamed film/foam.

$$E_{Film/Foam} = (E_{EVOH} \times V_{EVOH}\% + E_{LDPE} \times V_{LDPE}\%) \times (1 - V_{Void}\%) \quad (1)$$

Where E_{EVOH} is the tensile modulus of the EVOH (1040MPa) and E_{LDPE} is the tensile modulus of the unfoamed LDPE (300MPa). The model assumes that the material had a good layer structure and follows the layer series model. In addition, this model ignores the voids in the material and assumes that the polymeric matrix contributed to Young`s modulus. The results obtained using the model were consistent with the experimental results, which validates the assumptions and confirms the good layer structure of the film/foam materials.

Several studies have been made to understand the mechanical behavior of polymers through tensile tests at different temperatures and strain rates, in order to derive information on optimum thermoforming conditions. The tensile test experiments at different temperatures were applied to the as-extruded film/foam samples to determine the limits of a thermoforming processing window. Figure 2.5 shows the stress–strain relationships at different temperatures for a 10/90 composition. The testing temperatures

ranged between 20°C and 100°C and the testing strain was 100%/min. Table 2.3 shows the details of mechanical properties of EVOH/LDPE film/foams composite at several temperatures. These results can be characterized by a yield stress followed by a yield plateau with strain hardening behavior. While the tensile moduli, determined from the secant modulus at 1% deformation, hardly vary with temperature, the tensile strengths and yield stresses tends to decrease and the elongations at break tend to increase with an increase in the temperature. However, at 100ºC, the behavior changes and the elongation at failure decreases. Moreover, the EVOH/LDPE multilayer film/foam samples show non-uniform deformation and rupture of the LDPE cells, hence, significant deterioration of the microstructure occurs at this temperature. The transition in mode of micro-deformation is around the melt temperature of LDPE (110 ºC), where the deformation is more severe and flow-like behavior arises.

It was observed that the mechanical properties of multilayer EVOH/LDPE film/foam samples were very dependent on temperature. A processing temperature around 80°C appears optimal as it offers a good compromise between large deformations and low stresses. This temperature was selected for uniaxial orientation and thermoforming studies.

2.3.3 Uniaxial Orientation

The uniaxial tensile performance of multilayer EVOH/LDPE film/foams was investigated. The uniaxial deformation process was used to understand the influence of temperature and strain on the final thickness and oxygen transmission rate of the oriented material. These are important parameters during typical post processing steps such as

thermoforming. Thermoforming is typically a biaxial deformation process; however when the material contacts the mold surface the deformation may be mainly uniaxial [15]. Bhattacharyya et al. showed that the deformation is basically uniaxial in the critical area where there is the maximum wall thickness reduction during the thermoforming process when using a semi-spherical and a truncated cone mold shape [16]. Due to the complexity of a biaxial deformation process involved in thermoforming, uniaxial deformation was first studied in this work.

Uniaxial deformation behavior of the as-extruded EVOH/LDPE multilayer film/foam was investigated on microtensile bars (1.2 x 60 x 40 mm^3). Tensile tests were performed with a strain rate of 100%/min at 80ºC. A grid pattern (0.5 x 0.5 cm) was drawn on each film/foam sheet to follow the deformation behavior during the orientation experiments.

Similar to the thermoforming procedure, specimens were heated prior to testing. Figure 2.6 shows the multilayer film/foam samples having 16 layers with 10/90 composition before and after uniaxial orientation to 100% strain. The composite shows different patterns of deformations at different zones after the uniaxially drawn. However, the material shows more homogeneous deformation in the center of the sample with a maximum local strain of 120%. The maximum local wall thickness reduction was around 40%. We selected this center zone with the maximum deformation for the following thickness and OTR measurements.

The oxygen transmission rates as a function of the deformation after uniaxial orientation at 80°C of EVOH/LDPE (10/90) multilayer film/foam samples are shown in Figure 2.7 and Table 2.4. The system with 64 layers showed the lowest oxygen barrier properties after the uniaxial orientation. At a relatively early stage of deformation, around 30%, the

oxygen transmission of the material increase strongly. This behavior can be explained by the layer thickness reduction of the material. During the uniaxial deformation process the continuous EVOH layer thickness decreases resulting in an increase of oxygen transmission of the film layer. At this point, the film/foam material does not provide an oxygen barrier as effectively as the as-extruded material.

The system with 16 layers had the thicker film layer, and therefore the sample can maintain the barrier properties during the deformation process. However, due to the mechanical properties of the film/foam with 16 layers the samples break around 120% of strain.

The EVOH/LDPE film/foam with 32 layers had the best combination in terms of both mechanical and barrier properties. Due to the mechanical properties of this system, it is possible to draw the sample to more than 240% strain without break or to lose the oxygen barrier properties. Moreover, the film/foam sample at 240% strain maintained the oxygen transmission rate below 2 $cm^3/(m^2.day)$, a value required for shelf-stable food in packaging applications [8]. In addition, this result suggested that the material can be subjected to more deep draw forming without losing the barrier properties.

Based upon the OTR results after uniaxial orientation, the thermoforming work continued only with the film/foam composites with 16 and 32 layers.

2.3.4 Thermoforming

Thermoforming is a processing that clearly affects the transmission of the materials, due to both increased area and thinning of the material. The thickness distribution of a

thermoformed product is dependent on a variety of processing parameters, such as sheet temperature, mold temperature, heating time, thermoforming pressure and plug speed [7]. Film/foam samples with 16 and 32 layers were thermoformed with a semi-spherical mold at 80 °C. Figure 2.8 shows the shape and dimensions of the mold used and the appearance of samples after the thermoforming process. The thermoformed film/foam parts were cross sectioned for final thickness measurements using a micrometer. The wall thickness reduction of thermoformed material in the bottom, the walls, and the corners was evaluated by choosing strategic locations (Figure 2.9).

The distribution of the material thickness in the thermoformed sheets was identified, showing the locations that were most affected by the thermoforming process. It is clear that in the corners the impact upon material thinning was more pronounced. It can be seen that wall thickness reduction at the edges was approximately 40% after the thermoforming process. The oxygen transmission rate of the formed part was 0.9 and 1.1 $cm^3/(m^2.day)$ for the system with 16 layers and 32 layers respectively. These results are in agreement with the uniaxial orientation tests where the samples stretched to around 100% strain had this range of wall thickness reduction and oxygen transmission.

Figure 2.10 shows the design and dimensions of the second mold used for thermoforming studies and the appearance of sample after the thermoforming process. This is a truncated cone mold, designed to produce formed parts with a variable depth by controlling the final position of the mold plug. Moreover, the mold used allows a final draw ratio in the thermoformed film/foam sample that may be considered as deep draw [8].

The film/foam samples with 16 and 32 layers were thermoformed at 80 °C. The percentage thickness of each material as a consequence of the thermoforming process

was determined. Figure 2.11 shows the results for the system with 16 and 32 layers, respectively. The system with 16 layers was able to be formed until 75% of the draw depth using the truncated cone mold, after which sample started to break. However, the film/foam maintained the barrier properties at this level of deformation. The final thickness reduction at 75% of draw depth was around 40% at the critical point and the oxygen transmission was 1.4 $cm^3/(m^2.day)$.

The film/foam with 32 layers exhibits the best mechanical properties was able to be completely formed using the deep draw mold. The reduction of thickness in the material after the thermoforming process were strongly dependent on the design of the mold and the draw depth. The profile of the thin sheet materials clearly show that the edges are more thinned than the walls and the bottom. No difference in wall thickness distribution was observed after thermoforming. The non-uniform wall thickness distribution is caused by differential stretching during the thermoforming process. The final thickness reduction at the critical point at 75% of draw depth was around 40% and the oxygen transmission was 1.6 $cm^3/(m^2.day)$. However, at 100% of draw the final thickness was around 40% of the original thickness and the oxygen transmission increase to 38 $cm^3/(m^2.day)$. This behavior is in accordance with the uniaxial orientation test because this level of thickness reduction is associated with a uniaxial deformation more than 250%. However, some improvements in wall thickness uniformity can be achieved by using optimized processing parameters and/or using a pre-stretching process.

2.4 Conclusions

Microcellular film/foam structures having 16, 32, and 64 alternating EVOH film layers and LDPE foam layers can be successfully produced by microlayer coextrusion process. The as-extruded film/foams showed good layer structure with clear layer boundaries and continuous film layers. The cell size can be reduced considerably by increasing the numbers of layers without affecting the density significantly. The materials demonstrated high oxygen barrier properties and good mechanical properties. Moreover, the oxygen transmission and mechanical properties could be adjusted by varying the number of layers and composition of the film/foam. The structure-property relationships of EVOH/LDPE film/foam are significant for the development of film/foam materials with extraordinary barrier properties that can be produced at large scale. The mechanical properties of EVOH/LDPE are attractive since these can be achieved with more than 100% of elongation at break, which allows an evaluation of thermoforming performance. These film/foam materials demonstrate a level of oxygen barrier properties which can meet stringent food packaging requirements.

Due to the simplicity of this technique, uniaxial orientation was used as a preliminary tool to study the EVOH/LDPE film/foam deformation behavior and the effect of the strain on the final thickness and oxygen transmission of the material. Samples were subjected to uniaxial tensile deformation at different final strains at 80°C. The tests showed that the film/foam had a uniform deformation in the center of the sample. This region was characterized in term of deformation ratio, thickness, and oxygen transmission rate.

Finally, the EVOH/LDPE film/foams were successfully thermoformed using two different mold shapes. Optimum forming capacity was achieved at 80°C. Wall thickness distribution obtained in the thermoformed parts was significantly affected by the design of the mold and the drawing depths. The OTR of the thermoformed parts increased with the drawing depth. The EVOH/LDPE film/foam composites with 32 layers showed the best combination between mechanical and barrier properties. Therefore, it is recognized that there is a close relationship between the results from uniaxial orientation tests and actual thermoforming tests. The final thickness and OTR results from uniaxial deformation could be used as a rough approximation to predict the formability and final OTR of thermoformed parts.

2.5. References

[1] J. Feng, Z. Li, A. Olah, and E. Baer, “High oxygen barrier multilayer EVOH/LDPE film/foam,” J. Appl. Polym. Sci., vol. 135, no. 26, p. 46425, Jul. 2018, doi: 10.1002/app.46425.

[2] M. A. Rahman and E. Baer, “Layer Integrity in Polyethylene Based Multilayer Film/Foams and their Properties,” in SPE ANTEC: Orlando, FL., 2015.

[3] E. Giménez, J. M. Lagarón, L. Cabedo, R. Gavara, and J. J. Saura, “Study of the thermoformability of ethylene-vinyl alcohol copolymer based barrier blends of interest in food packaging applications,” J. Appl. Polym. Sci., vol. 91, no. 6, pp. 3851–3855, Mar. 2004, doi: 10.1002/app.13584.

[4] J. L. Throne, Understanding Thermoforming. München: Carl Hanser Verlag GmbH & Co. KG, 2008.

[5] N. Rosenzweig, M. Narkis, and Z. Tadmor, “Wall thickness distribution in thermoforming,” Polym. Eng. Sci., vol. 19, no. 13, pp. 946–951, Oct. 1979, doi: 10.1002/pen.760191311.

[6] L. S. Kochar and J. L. Throne, “Thermoforming Multilayer Sheet; I: General Criteria,” J. Plast. Film Sheeting, vol. 5, no. 3, pp. 186–208, Jul. 1989, doi: 10.1177/875608798900500308.

[7] F. M. Duarte and J. A. Covas, “Multilayer plug concept to enhance thickness distribution control of deep thermoformed parts,” Plast. Rubber Compos., vol. 37, no. 7, pp. 293–300, Sep. 2008, doi: 10.1179/174328908X314316.

[8] M. Buntinx et al., “Evaluation of the Thickness and Oxygen Transmission Rate before and after Thermoforming Mono- and Multi-layer Sheets into Trays with Variable Depth,” Polymers (Basel)., vol. 6, no. 12, pp. 3019–3043, Dec. 2014, doi: 10.3390/polym6123019.

[9] M. K. Pettersen, A. Nilsson, A. Espedal, and A. Kohler, “Prediction of oxygen transmission rate for thermoformed trays,” Packag. Technol. Sci., vol. 17, no. 6, pp. 321–332, Nov. 2004, doi: 10.1002/pts.669.

[10] T. Schuman, S. Nazarenko, E. . Stepanov, S. . Magonov, A. Hiltner, and E. Baer, “Solid state structure and melting behavior of interdiffused polyethylenes in microlayers,” Polymer (Guildf)., vol. 40, no. 26, pp. 7373–7385, Dec. 1999, doi: 10.1016/S0032-3861(99)00013-0.

[11] D. Jarus, A. Hiltner, and E. Baer, “Barrier properties of polypropylene/polyamide blends produced by microlayer coextrusion,” Polymer (Guildf)., vol. 43, no. 8, pp.

2401–2408, Apr. 2002, doi: 10.1016/S0032-3861(01)00790-X.

[12] E. Baer and A. Moet, High performance polymers- Structure, properties, composites, fibers(Book). Munich/New York: Hanser Publishers/Oxford University Press, 1991.

[13] J. Feng et al., “Breakup behavior of nanolayers in polymeric multilayer systems — Creation of nanosheets and nanodroplets,” Polymer (Guildf)., vol. 143, pp. 19–27, May 2018, doi: 10.1016/j.polymer.2018.03.049.

[14] M. A. Rahman, R. Andrade, J. Maia, and E. Baer, “Viscosity contrast effects on the structure – Property relationship of multilayer soft film/foams,” Polymer (Guildf)., vol. 69, pp. 110–122, Jul. 2015, doi: 10.1016/j.polymer.2015.05.051.

[15] E. Giménez, J. M. Lagarón, M. L. Maspoch, L. Cabedo, and J. J. Saura, “Uniaxial tensile behavior and thermoforming characteristics of high barrier EVOH-based blends of interest in food packaging,” Polym. Eng. Sci., vol. 44, no. 3, pp. 598–608, Mar. 2004, doi: 10.1002/pen.20054.

[16] D. Bhattacharyya, M. Bowis, and K. Jayaraman, “Thermoforming woodfibre–polypropylene composite sheets,” Compos. Sci. Technol., vol. 63, no. 3–4, pp. 353–365, Feb. 2003, doi: 10.1016/S0266-3538(02)00214-2.

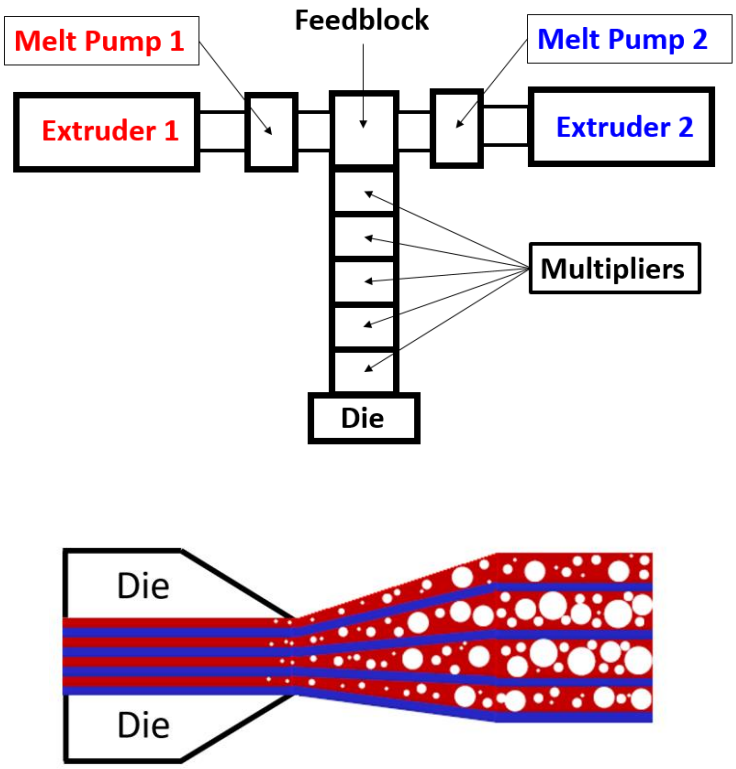

Figure 2.1 Schematic of multilayer film/foam coextrusion process.

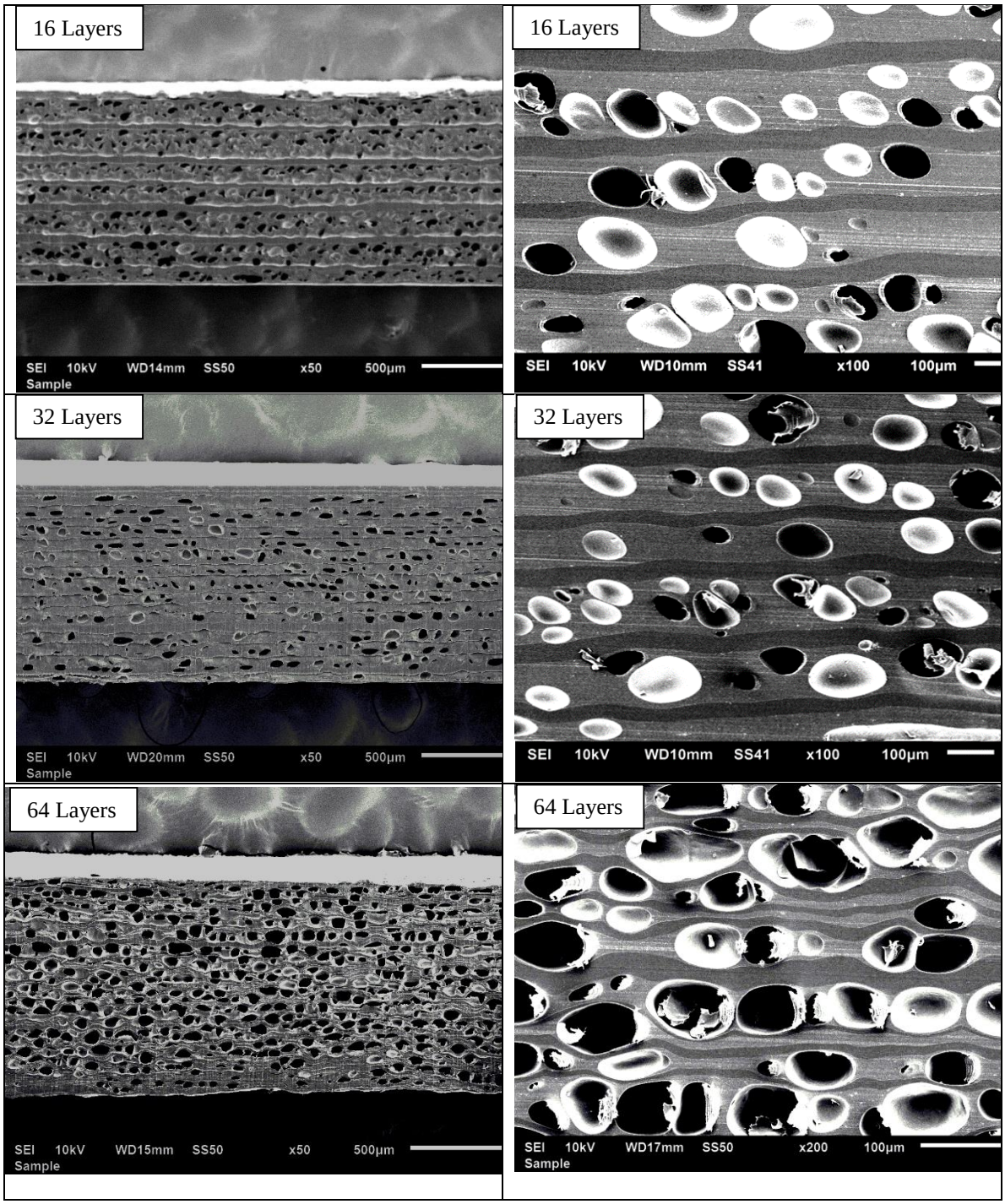

Figure 2.2 EVOH/LDPE film/foam (50/50) morphology extrusion-direction as-extruded with 16 Layers, 32 Layers and 64 Layers.

Table 2.1 Characteristics of EVOH/LDPE Multilayer Film/Foam.

	Film/Foam Composition in Volume	**Number of Layers**	**Total Thickness (mm)**	**Density (g/cm^3)**	**Average Cell Size (μm)**	**OTR ($cm^3/(m^2.day)$)**
1	50/50	16	1.2 ± 0.1	0.67 ± 0.07	104 ± 35	0.10 ± 0.01
2	30/70	16	1.2 ± 0.1	0.65 ± 0.06	84 ± 25	0.16 ± 0.02
3	20/80	16	1.2 ± 0.1	0.57 ± 0.05	62 ± 19	0.27 ± 0.03
4	10/90	16	1.2 ± 0.1	0.50 ± 0.05	58 ± 21	0.57 ± 0.06
5	10/90	32	1.2 ± 0.2	0.52 ± 0.05	56 ± 22	0.60 ± 0.06
6	10/90	64	1.2 ± 0.1	0.54 ± 0.05	53 ± 13	0.93 ± 0.09

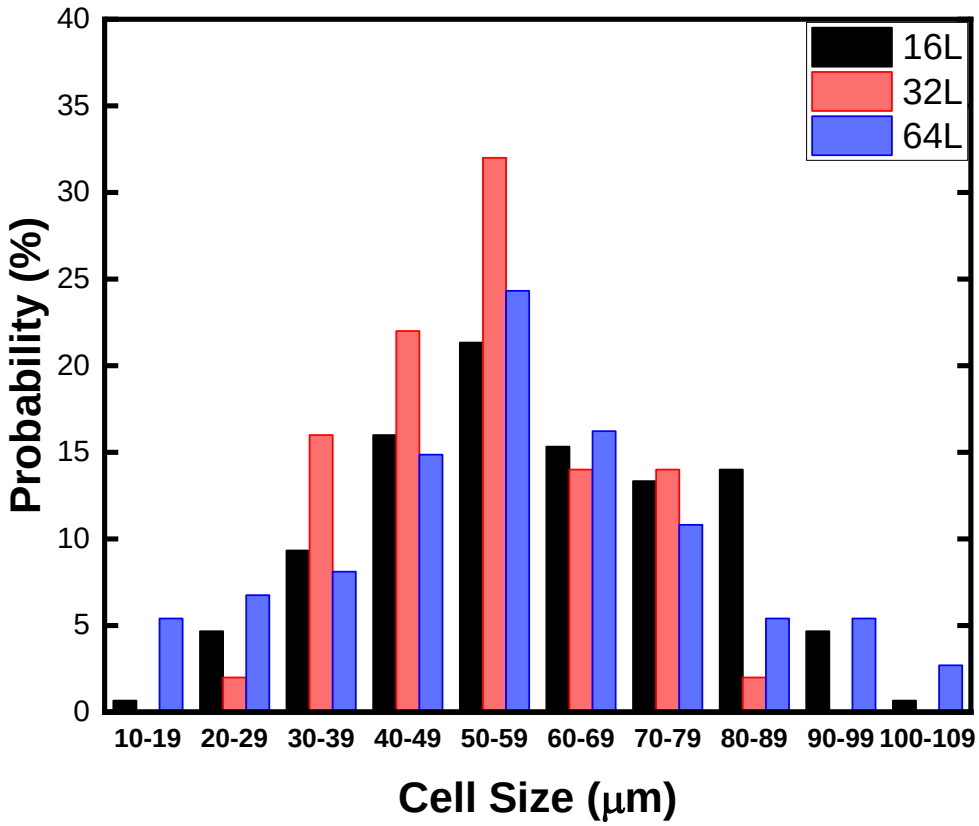

Figure 2.3 Measured Cell Size distribution and its probability distribution fit of as-extruded EVOH/LDPE multilayer film/foam (10/90 composition) with 16, 32 and 64 layers.

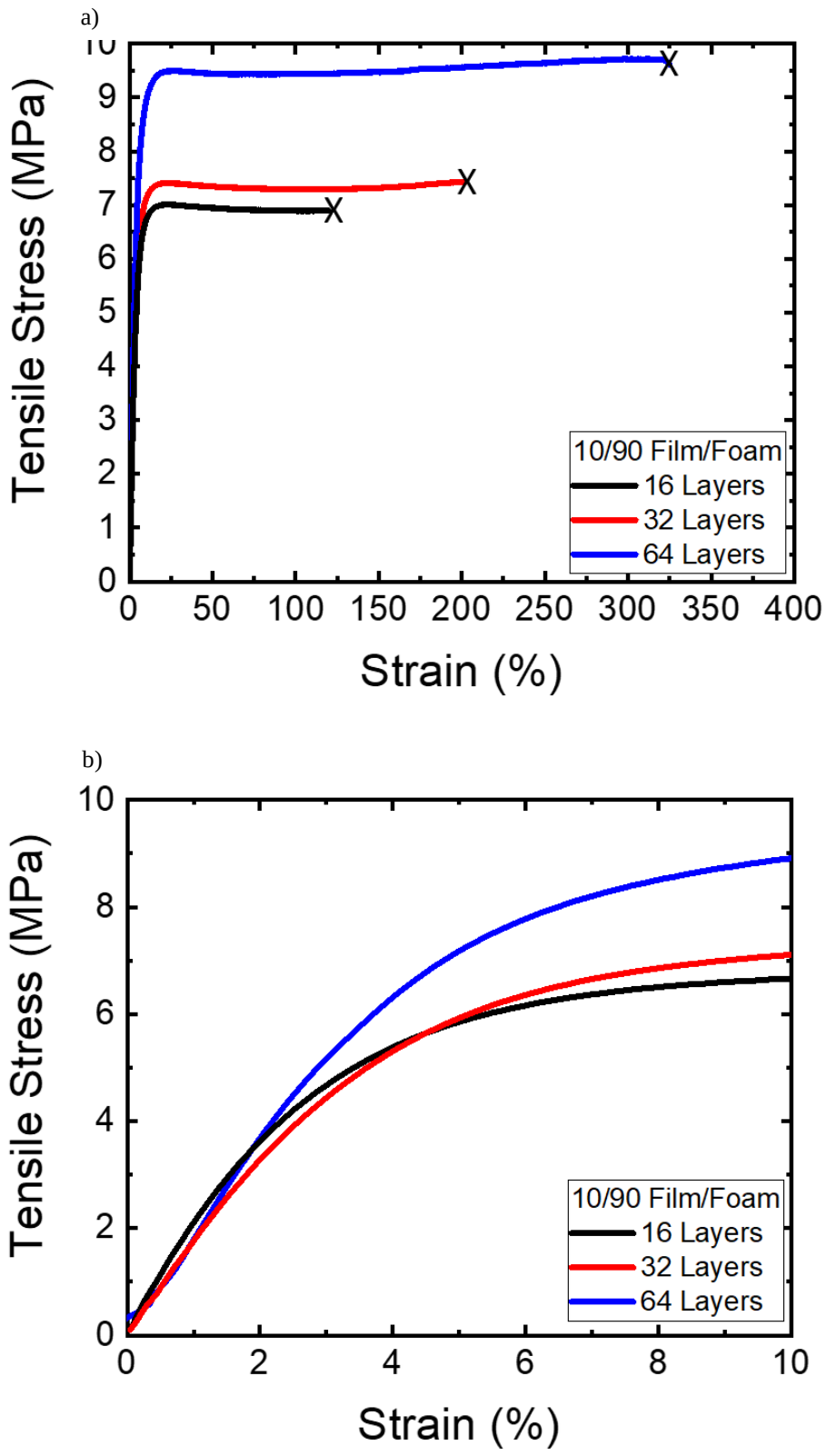

Figure 2.4 (a) Mechanical properties of as-extruded EVOH/LDPE multilayer film/foam at room temperature; (b) Mechanical properties of film/foam at low strain.

Table 2.2 Mechanical properties of as-extruded EVOH/LDPE multilayer film/foam at room temperature.

EVOH/LDPE Film/Foam	Tensile Strength (MPa)	Elongation to Break (%)	Measured Young`s Modulus (MPa)	Calculated Volume Fraction of Void (%)	Calculated Young`s Modulus (MPa)
16 Layers	6.9 ± 0.2	122 ± 15	180 ± 32		
32 Layers	7.3 ± 0.3	202 ± 60	181 ± 9	0.45	206
64 Layers	9.0 ± 0.3	325 ± 19	179 ± 34		

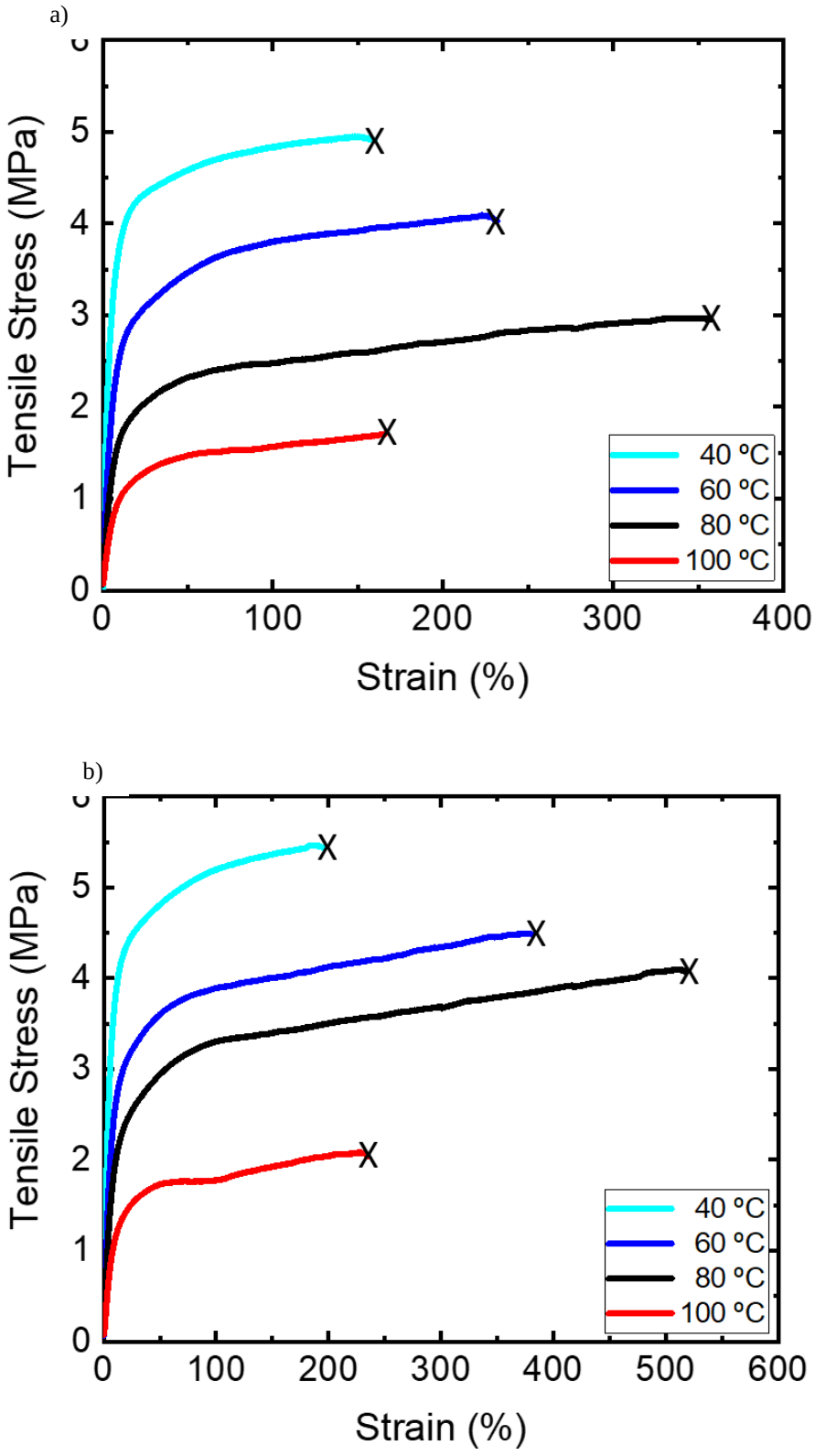

Figure 2.5 (a) Mechanical properties of as-extruded EVOH/LDPE multilayer film/foam (10/90 composition) at different temperature. a) 16 Layer system and b) 32 Layer system.

Table 2.3 Mechanical properties of as-extruded EVOH/LDPE multilayer film/foam (10/90 composition) at different temperature.

EVOH/LDPE Film/Foam	Temperature (°C)	Tensile Strength (MPa)	Elongation to Break (%)	Measured Young`s Modulus (MPa)
16 Layers	40	5.2 ± 0.1	161 ± 25	110 ± 1
16 Layers	60	4.1 ± 0.1	235 ± 52	47 ± 2
16 Layers	80	2.9 ± 0.2	352 ± 77	26 ± 1
16 Layers	100	1.6 ± 0.1	172 ± 34	16 ± 1
32 Layers	40	5.5 ± 0.5	192 ± 34	98 ± 3
32 Layers	60	4.4 ± 0.5	375 ± 70	51 ± 2
32 Layers	80	4.1 ± 0.4	502 ± 108	28 ± 2
32 Layers	100	2.1 ± 0.2	235 ± 64	16 ± 1

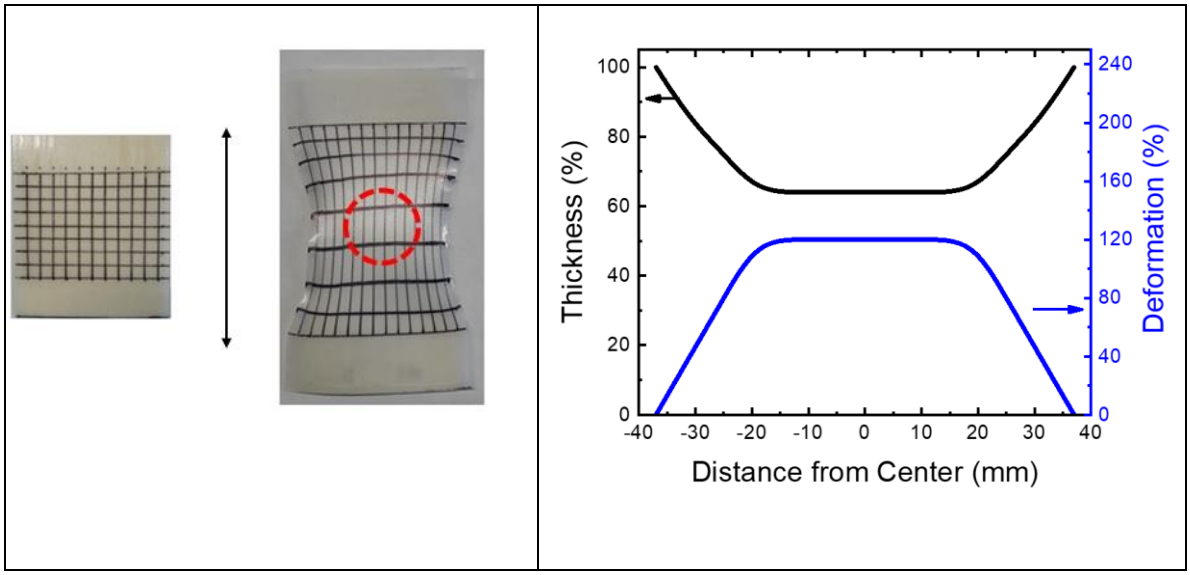

Figure 2.6 Film thickness reduction as a function of deformation after uniaxial orientation at 80°C of a 16 layer 505/50, EVOH/LDPE multilayer film/foam composite.

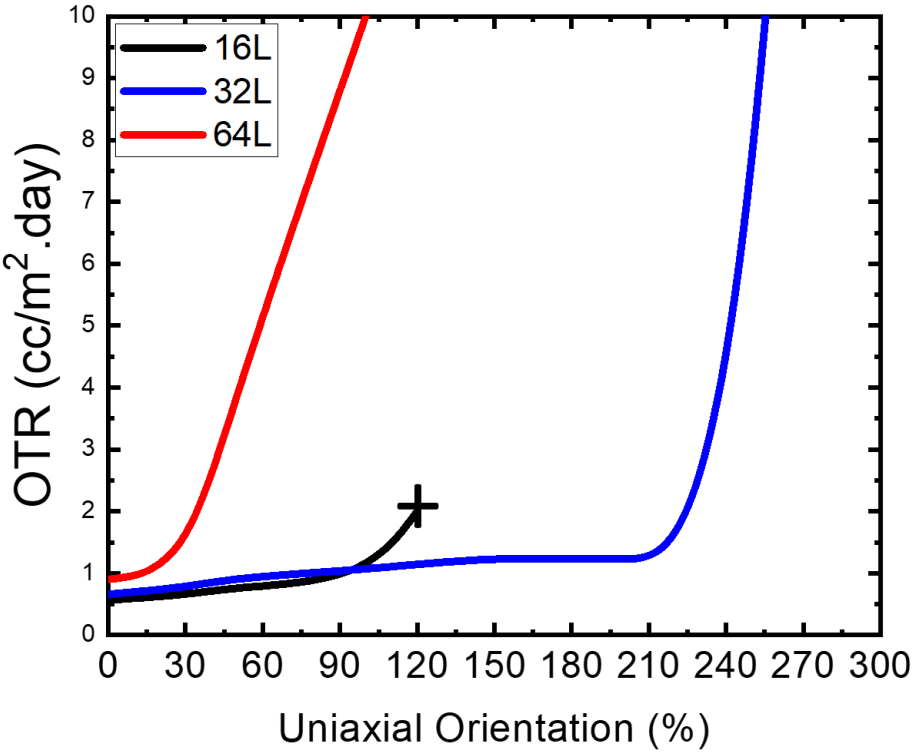

Figure 2.7 Oxygen Transmission Rate of EVOH/LDPE (10/90) multilayer film/foam at 80°C after uniaxial orientation with varied strain.

Table 2.4 Oxygen Transmission Rate **(**$cm^3/(m^2.day)$**)** of EVOH/LDPE multilayer film/foam composite (10/90 composition) as a function of deformation after uniaxial orientation at 80 °C.

EVOH/LDPE Film/Foam	**Deformation 50%**	**Deformation 100%**	**Deformation 150%**	**Deformation 200%**
16 Layers	0.78 ± 0.06	0.9 ± 0.05	-	-
32 Layers	0.93 ± 0.08	1.1 ± 0.09	**1.3 ± 0.1**	**1.6 ± 0.2**
64 Layers	4.1 ± 0.5	10.2 ± 0.2	23.1 ± 2.2	34.7 ± 2.8

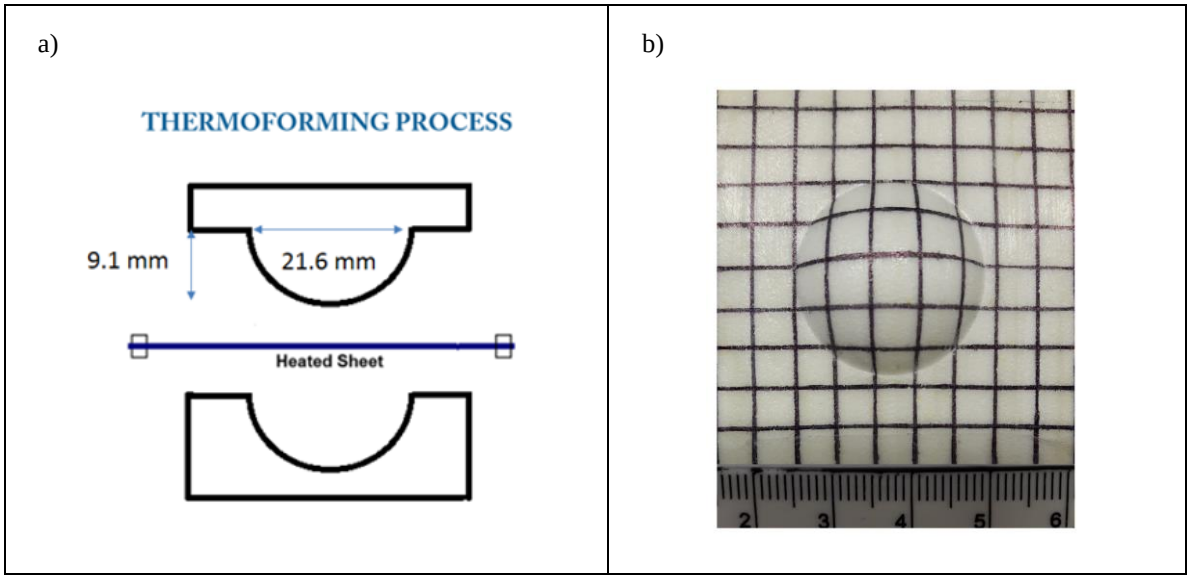

Figure 2.8 (a) Semi-spherical mold dimensions. (b) Mechanically thermoformed film/foam with composition of 10/90 in volume.

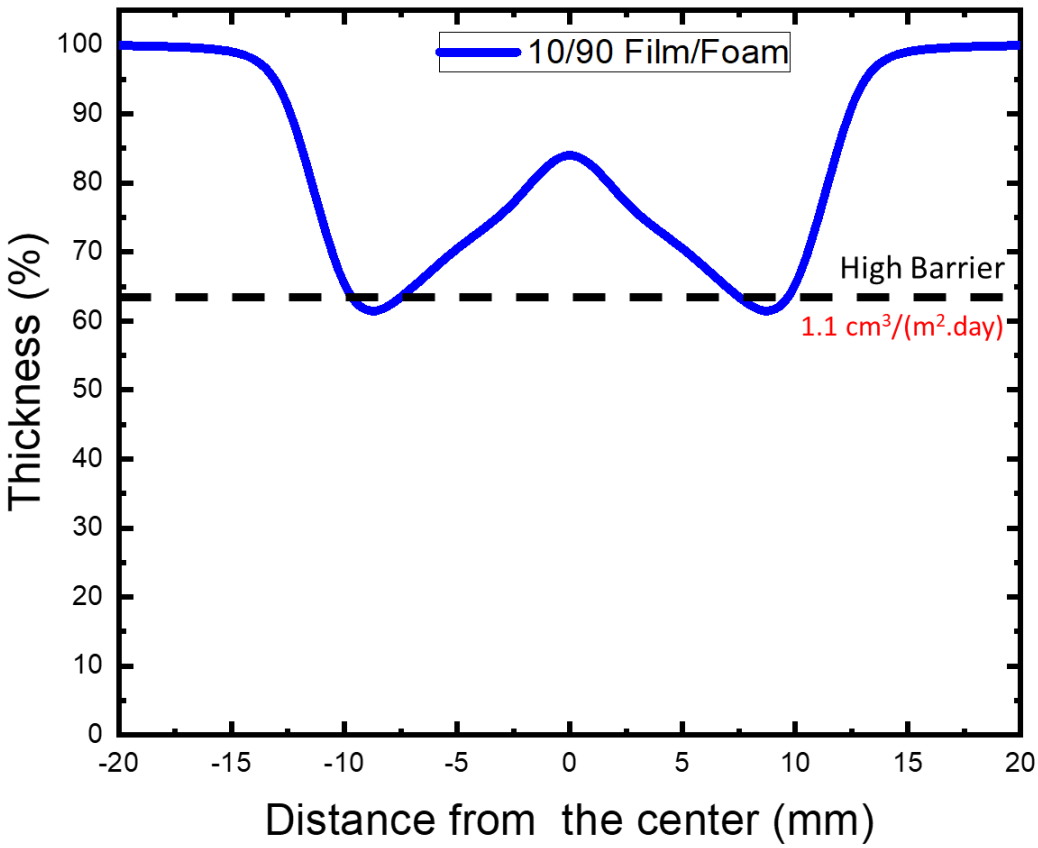

Figure 2.9 Wall thickness distribution (%) along a cross-section of thermoformed film/foam with composition of 10/90 in volume.

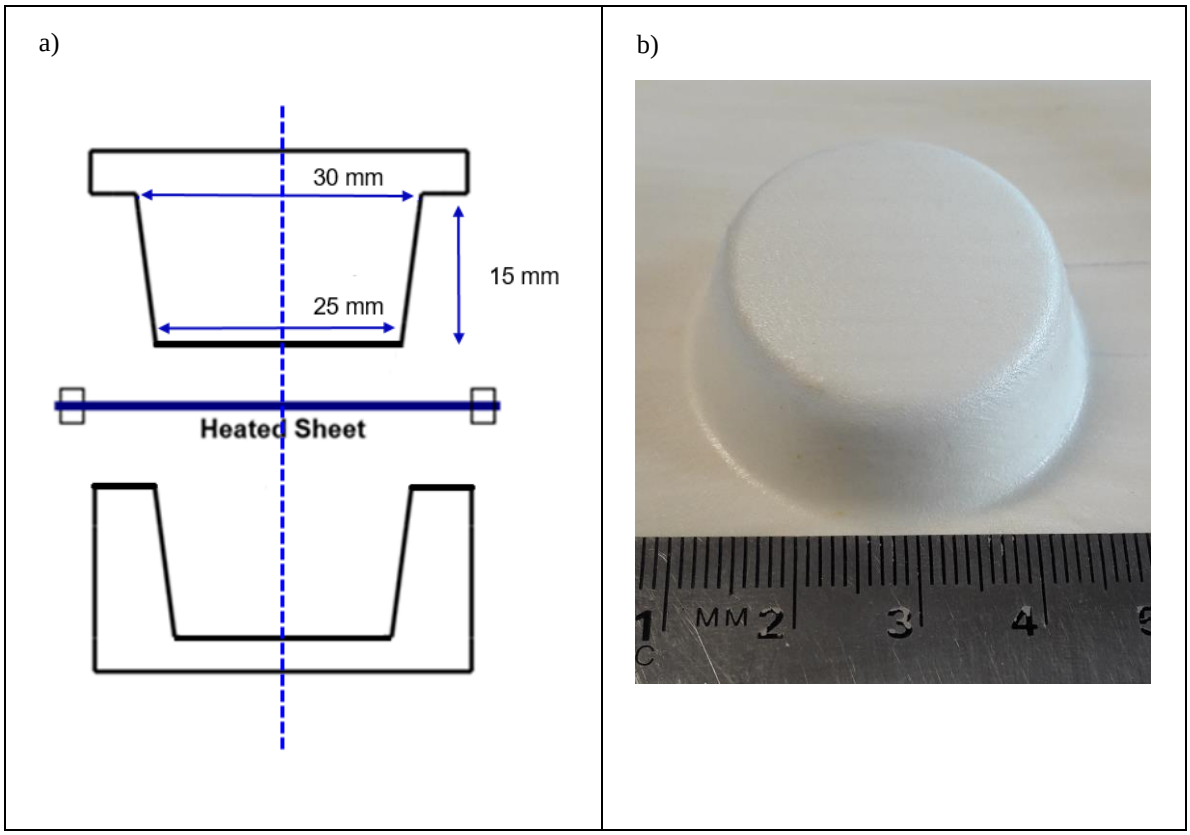

Figure 2.10 (a) Truncated cone mold dimensions. (b) Mechanically thermoformed film/foam with composition of 10/90 in volume.

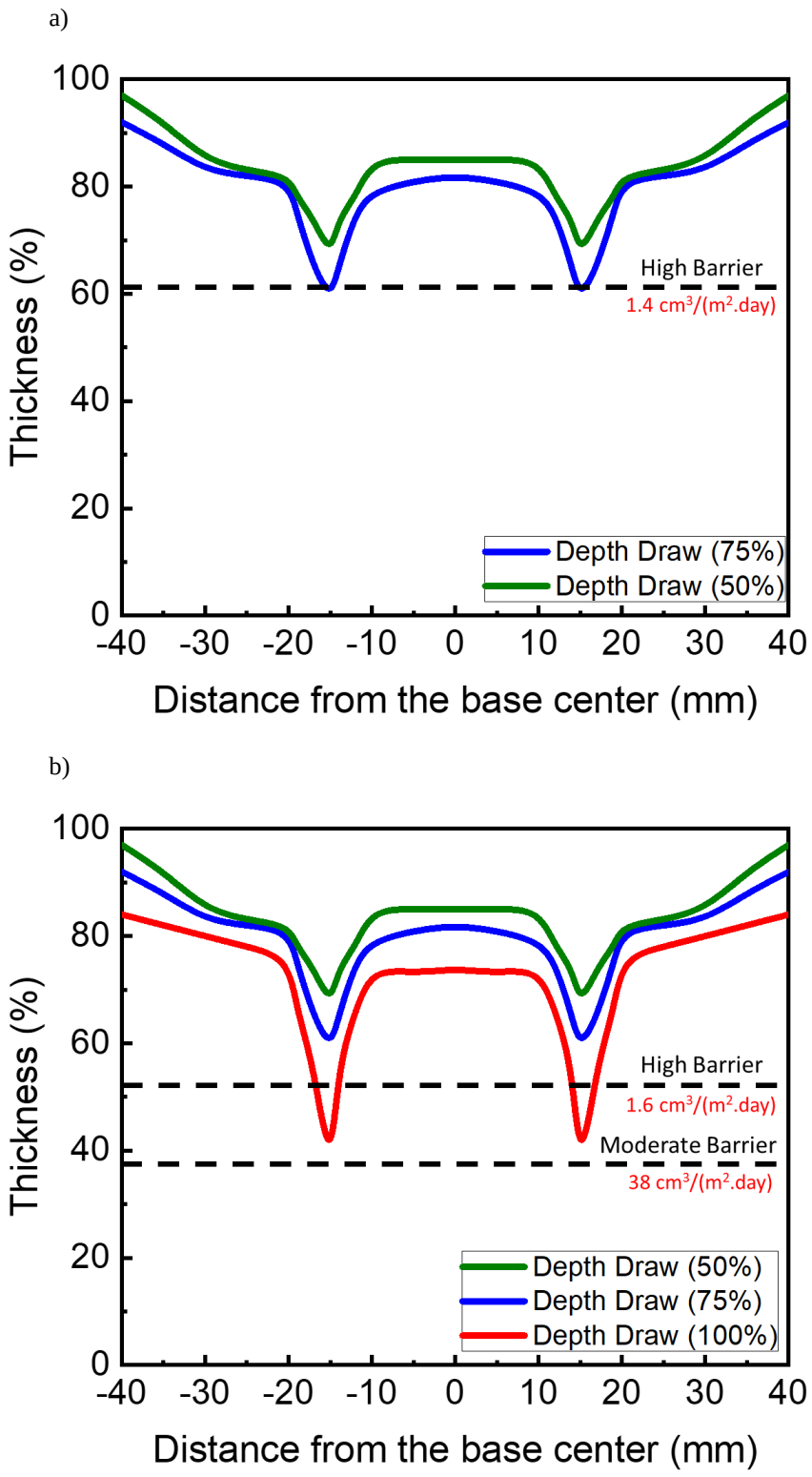

Figure 2.11 Wall thickness distribution (%) along a cross-section of thermoformed film/foam with composition of 10/90 in volume. a) 16 Layer system and b) 32 Layer system.

Chapter 3

High Barrier Multilayer (EVOH/LDPE)/HDPE Film/Foam

Abstract

High oxygen and water vapor barrier film/foam system had been developed using multilayer co-extrusion technology. The film/foams contained alternating low-density polyethylene (LDPE) foam layers and ethylene–vinyl alcohol (EVOH) copolymer film layers with HDPE skin layer. The morphology, density, oxygen, and water vapor transmission, and mechanical properties of the as-extruded film/foams were characterized. The lightweight film/foams showed oxygen and water vapor transmission rate are correlated with the EVOH film layer and HDPE skin layer composition. The layered film/foam was successfully thermoformed at 80 °C with low oxygen transmission along with high drawing capability.

3.1 Introduction

Food packaging can have a significant impact on food shelf life, taste, quality, and marketability. It is believed that using high quality packaging that prevents oxygen transmission and moisture between products and their environment can be a major factor to preserve the quality of the food from its manufacture to consumer use. Gain or loss of water and oxygen is a major cause of food deterioration [1], [2]. Oxygen water vapor transmission rate requirements vary depending on the nature of foods that need to be protected. Several parameters need to be considered during the package design process such as humidity and temperature associated with its end-use. Based on these requirements the material and thickness are chosen [1], [3]. It is a challenge to develop plastic material with oxygen and water vapor barrier properties. In general, commodity plastics often have poor oxygen barrier properties and good water vapor barrier. On the other hand, materials with high oxygen barrier properties, such as PA6, EVOH, PVA have poor water vapor barrier. In practice, coating and lamination with metals are two approaches to improve barrier properties of plastics. However, these packaging systems are expensive and hard to recycle[1], [4], [5].

The demand for materials to be used for food packaging is ever on the increase. Polymers, and based on polymers materials, have captured a large portion of the packaging market. The main advantage is their processability, light weight, mechanical and thermal properties, transparency, and low cost. However, the oxygen and water vapor barrier properties are not always satisfactory [6]. Different approaches have been developed to improve packaging in order to decrease the permeability of gases and vapors. These include, among others: layering of polymers by coextrusion process,

lamination or coating with different barrier materials, as well as orientation, blending with solids and metallization [6].

Forced assembly multilayer coextrusion is extremely flexible and cost-efficient technology to develop new high value-add polymeric materials by manipulating their hierarchical structural design. This technique allows the combination of several polymers with different viscosities and processing temperatures into a multilayer structure alternating micro or nano-layers of two or three components through a sequential layer multiplication process. The layer number depends on the number of the multipliers that are used and can be produced a single film with tens to thousands of layers [7], [8].

This study is aimed to develop a novel film/foam structure based on two polyolefins (LDPE and HDPE) and EVOH. This system was attractive due to its good mechanical properties, high gas barrier properties, and low moisture absorbance. The low density polyethylene (LDPE) provides excellent processability and foamability due to their high levels of long-chain branching and desirable rheological properties. On the other hand, high density polyethylene (HDPE) and EVOH provides the balance of oxygen and water vapor permeability [9]. This novel multilayer film/foam system had great potential to be used in high barrier packaging applications.

3.2 Experimental

3.2.1 Material

A three-component microlayer coextrusion setup was used to produce the multilayer film/foam structure with a skin layer. The foam layer material was a blend of LDPE 5004l and LDPE-grafted-maleic anhydrate (LDPE-g-MA) GR202 supplied by the Dow Chemical Company. The blend composition was 80 wt % LDPE and 20 wt % LDPE-g-MA. This particular ratio was optimized in previous work [10], [11]. The dry blend of LDPE and LDPE-g-MA was further blended with both a chemical blowing agent and a nucleating agent. The film layer was EVOH E171 copolymer supplied by Kuraray based on 44% ethylene content. Azodicarbonamide (Galata Chemicals) at 2 wt% was the chemical blowing agent for foaming the LDPE blend. The nucleating agent in the foam layer was 1 wt% Talc (Jetfine® 1H, IMERYS Talc). The skin layer was High density polyethylene (HDPE DMDA 8007) supplied by Dow Chemical Company. The characteristics of the materials used were shown in Table 3.1.

3.2.2 Film/Foam Processing

One extruder contained the foam layer polymer (LDPE), chemical blowing agent (azodicarbonamide), and nucleating agent (talc) and the other extruder contained the film layer polymer (EVOH). After merging in the two-component feedblock, the foam and the film layers were processed into multilayers using the layer multipliers. A three-component coextrusion setup can introduce a third polymer component (HDPE Skin Layer) to the above two-component film/foam multilayer structure forming an $S/(A/B)_n/S$ structure. Figure 3.1 illustrates the three-component coextrusion setup. The

total pump rate in each extruder was adjusted to change the volumetric composition of film, foam, and skin layers for each sample. Four-layer multiplication elements were used to produce 32 layered (EVOH/LDPE) film/foam structures with HDPE skin layer. The temperature of the extrusion system and the layer multiplication elements were set at 195 °C. A 3 inch exit die at 170 °C was used after multiplication in order to control cell expansion. A 60 °C chill roll was used as a take-off. The thickness of the film/foam composites was maintained at 1.1 mm by adjusting the speed of the chill roll. The extruder screw speed and the melt pump rates were adjusted to control the composition of the film/foam with a skin layer composite. The temperature of the extrusion system was below the decomposition temperature of the chemical blowing agent so that the azodicarbonamide did not fully decompose to create large foam cells.

3.2.3 Scanning Electron Microscope Morphology

The cross-sectional morphology of the as-extruded film/foams was imaged by a scanning electron microscopy (SEM) (JEOL). Film/foam samples were cut in the extrusion direction with sharp blades at room temperature. Then cross section samples were sputter-coated with gold (10 nm) before the SEM analysis. An emission voltage of 30 kV was used. The cell size and layer thickness of each film/foam sample were determined from SEM micrographs.

3.2.4 Density

The density of as-extruded film/foam specimens were measured using a density balance (Mettler Toledo, Columbus, OH). The liquid medium was ethanol to ensure wetting of

the sample surface. Because the film/foams had a closed-cell structure, the mass/volume method for density determination was accurate. Each sample was tested at least 5 times, and the average value was taken

3.2.5 Mechanical Properties

Mechanical properties of as-extruded film/foam samples were evaluated in uniaxial tension on an Instron 5565 universal tester at different temperatures. The strain rate for the deformation study was 100%/minute. The film/foam samples were cut into rectangular microtensile bars having dimensions of 1.0 x 6.0 cm^2. The load–displacement data obtained from the testing equipment was converted into stress–strain curves and Young's modulus (E), yield strength (σ) (maximum stress) and strain at break (ε) values were determined from these curves. The Young's moduli of the specimens were calculated according to the slope of the initially linear part of the stress-strain curve. Each sample was tested at least 5 times, and the average value was taken. The model the Young's moduli was applied using the follow equation (1):

$$E_{Film/Foam} = (E_{EVOH} \times V_{EVOH}\% + E_{LDPE} \times V_{LDPE}\% + E_{HDPE} \times V_{HDPE}\%) \times (1 - V_{Void}\%) \quad (1)$$

The volume ratio of EVOH, LDPE and HDPE in the equation was determined by the pump rate during the multilayer coextrusion process. The void volume was calculated from the density.

3.2.6 Oxygen Transmission Rate

The oxygen flux at 0% relative humidity, 1 atm, and 23 ºC was measured with a MOCON OX-TRAN 2/20 which uses the continuous-flow cell method approved by ASTM (Designation: D3985-81). The film/foam samples were cut into a circular shapes with a diameter of 3 cm and sandwiched between two aluminum foils providing a test area of 5 cm^2. The oxygen transmission through the aluminum foil was ignored since the aluminum is a very high oxygen barrier. The oxygen transmission of the samples were calculated using the flux and samples thickness.

The oxygen transmission measurement of the thermoformed samples were performed using a MOCON-OX-TRAN 2/20 at 0% relative humidity inside the package, 1 atm and 23°C using a package environmental chamber. The thermoformed parts were exposed to oxygen from the atmosphere. The results were converted in [$cm^3/(m^2.day)$]. All measurements were performed in duplicate and an average value was adopted.

3.2.7 Water Vapor Transmission Rate

The water vapor transmission rate (WVTR) was measured using the wet cup method approved by ASTM (Designation: E96/E96M-10. According to this method, an acetal homemade dish filled with distilled water is covered by the tested material and placed in a chamber under controllable conditions of humidity and temperature. During the experimental procedure, the weight change of the complete test set up is measured. Water vapor transmission rate (WVTR) is defined as the steady water vapor flow in unit of time through unit of area, under specific conditions of humidity and temperature. The tested

area was A = 20.27 cm^2. The slope of the water loss as a function of time normalized to the testing area A was taken as the WVTR with units of $g.m^{-2}.day^{-1}$.

$$WVTR = \text{Mass } H_2O \text{ lost / time x area}$$

3.2.8 Mechanical Thermoforming

The as-extruded film/foam samples were cut into square specimens with a dimension of 60 mm by 60 mm square for thermoforming. The thermoformability of the film/foam material was evaluated using an aluminum truncated cone mold shape, typical of the design in food packaging. This mold had a top diameter of 30 mm, a base diameter of 25 mm, corners with radius of 2 mm, and a variable depth to 15 mm. A film/foam specimen was loaded in the mold and was compressed at 80 °C. The pressure was maintained for 5s and afterward, the specimen was removed from the mold. The composites were formed at a constant speed of 200 mm/min. The details for the film/foam thermoforming process were discussed in previous publications [11]. To identify the local strain across the film/foam sample during thermoforming, uniform grids were drawn on the sample to map the deformation. The change of the distance between grid lines was used to determine the local strain.

3.3. Results and Discussion

3.3.1 Morphology and Properties of As-extruded EVOH/LDPE Film/Foam with HDPE skin layer

In order to understand the effect of the HDPE skin layer on the morphology of the extruded film/foams, the cellular structure of as-extruded film/foam with different compositions of HDPE skin layer was analyzed. Figure 3.2 shows the cross-sectional morphologies of as-extruded EVOH/LDPE film/foam with 32 layers having a composition of 10% EVOH and 90% LDPE with HDPE skin layer with three different compositions (10%, 20%, and 30% (v/v)). Based on the images can be observed that the film/foams have a good layered structure and well defined cell boundaries with a clear skin layer in all film/foam systems. By changing the HDPE skin film layer composition, it is possible to achieve different film skin thickness. The film/foam systems show an average EVOH film thickness around 10 μm for all skin layer compositions and the EVOH film layer structure remained continuous. This means that the oxygen barrier properties of the material are preserved, which is essential for high barrier materials.

The (EVOH/LDPE)/HDPE film/foam systems show mostly single and bilayer ellipsoidal bubble cell structures with straight and parallel layer boundaries. This indicates that the film layer can suppress cell growth due to the higher melt strength and produce appropriate layer confinement of the cells. This means that the cells were confined to the foam layer without the cells causing any break-up of the film layers. This result is in accord with previous works where the film/foam materials were selected based on the principle of viscosity contrast [12]. In addition, Figure 3.2 shows sharp interfaces and good layer structure without delamination in all three systems. This result was achieved

due to use of LDPE-g-MA as a compatibilizer in the foam layer improving the adhesion between the EVOH film layer and LDPE foam layer. Moreover, the strong adhesion between the film layer and the foam layer is due to the reaction between the MA group from LDPE-g-MA with the hydroxyl groups in EVOH [10].

Figure 3.2 shows that changing the HDPE skin layer composition does not impact the bubble growth and shape of the cells during the foaming process. All systems can suppress cell growth and create a layered film/foam structure. To further highlight the effect of the HDPE skin layer on the cell structure and compare the cellular structure more quantitatively, the average cell diameter and the cell and cell size distribution were determined by image analysis of the SEM images in Figure 3 using ImageJ® software. The characteristics of the as-extruded (EVOH/LDPE)/HDPE multilayer film/foam materials are described in Table 3.2.

The average cell size of the system was 89 ±30, 75 ±18, and 89 ±27 for the system with 10%, 20%, and 30% HDPE skin layer composition respectively. The total density was 0.50 ±0.3, 0.53 ± 0.2, and 0.54 ±0.1 when the skin layer composition increased from 10% to 30%. This indicates that the average cell size of multilayer film/foam was not affected by changing the HDPE skin layer composition. However, as expected, the total density was affected by changing the HDPE skin layer composition. The measured cell size of multilayer film/foam composite with HDPE skin layer (all three composition) approximately follows lognormal distribution, as shown in Figure 3.3.

The DSC profiles in Figure 3.4 shows the melting behaviors of the as-extruded (EVOH/LDPE)/HDPE multilayer film/foam. The melting temperature of EVOH, LDPE, and HDPE were 160, 111, and 131°C which were constant among all tested systems.

3.3.2 Mechanical Properties of (EVOH/LDPE)/HDPE film/foam

Figure 3.5 demonstrates the mechanical properties of the as-extruded (EVOH/LDPE)/HDPE film/foam in tension at room temperature and strain rate of 100%/min. All three systems suggested ductile behavior in tension. The abrupt yield took place at about 7% strain followed by necking and elongation of the neck. The data indicate that (EVOH/LDPE)/HDPE film/foam shows good mechanical properties with good layering and adhesion without delamination. Moreover, the material shows high maximum elongation indicating high potential for thermoforming. Table 3.3 summarizes the maximum stresses, elongations at break, and Young's modulus for all three film/foam system and film/foam control.

It was observed that increasing the HDPE skin layer composition the maximum stress and the Young's modulus increase. As expected, the composite with HDPE skin layer of 30% composition had the highest Young's modulus and the composite with HDPE skin layer of 10% was the lowest among all the three compositions. In addition, the engineering stress reached maximum at the yield point. The film/foam with higher HDPE composition showed the maximum stress and the composite with lower HDPE content showed the maximum elongation to break suggesting that increasing amount of the HDPE harden the material.

The Young's modulus was modeled using Equation (1). The volume ratio of EVOH, LDPE, and HDPE in the equation was selected by the melt pump rate during the multilayer coextrusion process. The void ratio was determined from the density of the

foamed and unfoamed film/foam. The model ignores the voids in the material and assumes that the polymeric matrix contributed Young's modulus. Moreover, this model assumes that the composite follows the layer series model and had a good layer structure. The results obtained based on the model were consistent with the experimental results, which validates the assumptions and confirms the good layer structure of the multilayer (EVOH/LDPE)/HDPE film/foam material.

3.3.3 Oxygen and Water Vapor Transmission Rate

Oxygen and water vapor transmission rate measurements on the as-extruded multilayer (EVOH/LDPE)/HDPE film/foam were performed to study the barrier properties of the material. According to material properties listed in Table 3.1, EVOH has excellent oxygen barrier properties but poor water vapor barrier properties, on the other hand, HDPE has good water vapor barrier properties with poor oxygen properties. Consequently, the oxygen and water vapor permeability of the multilayer (EVOH/LDPE)/HDPE film/foam were highly dependent on the EVOH/HDPE ratio.

The results indicate that the film/foam composite exhibited very low oxygen permeability for all three systems. This high oxygen barrier suggested that the EVOH film layer were continuous without break up. The oxygen transmission rates of as-extruded multilayer (EVOH/LDPE)/HDPE film/foam are shown in Table 3.2.

Figure 3.6 shows the water vapor transmission of all three (EVOH/LDPE)/HDPE film/foam systems and film/foam control (without HDPE skin layer). As expected, the film/foam with HDPE skin layer had superior water vapor barrier property. The water vapor permeability increase with a decrease of the HDPE skin layer content.

The oxygen permeability and water vapor permeability of all three film/foam systems and film/foam control were measured at room temperature.

3.3.4 Thermoforming

The formability of the multilayer (EVOH/LDPE) film/foam with HDPE skin layer of 20% composition was studied. In this study was used a truncated cone mold, designed to produce formed parts with a variable depth by controlling the final position of the mold plug. Figure 3.7 shows the shape and dimensions of the mold and the appearance of the sample after the thermoforming process. Based on the DSC results, the temperature of forming was fixed on 80 °C.

A grid strain analysis was used to assess the formability of parts and track the local strain in strategic positions of thermoformed film/foam samples. The strain analysis was conducted using square grids, printed on the sheets before the thermoforming process and the thickness of the sample.

Figure 3.8 shows the thickness distributions of the material and the locations that were most affected by the thermoforming process. It is clear that in the corners the impact upon material thinning was more pronounced than the walls and the bottom. It can be seen that maximum thickness reduction was approximately 50 % on the edge of the mold after the thermoforming process. Moreover, the mold used allows a final draw ratio in the thermoformed film/foam sample that may be considered as deep draw [13]. The non-uniform wall thickness distribution is caused by differential stretching during the thermoforming process.

It was not observed delamination between the HDPE skin layer and the EVOH/LDPE film/foam during the mechanical and thermoforming tests. The system was set up for the larger HDPE skin layer (downside) to be in contact with the mold.

During the thermoforming process, the material is heated and subsequently deformed through the application of mechanical stretching and/or pressure. This process clearly affects material properties such as gas permeability, due to both increased area and thinning of the material. The strain distribution of a thermoformed product is dependent on a variety of processing parameters, such as sheet temperature, mold temperature, heating time, thermoforming pressure, and plug speed[14].

The multilayer EVOH/LDPE film/foam with 32 layers and with HDPE skin layer exhibits good mechanical properties and was able to be completely formed using the deep draw mold. No difference in appearance of samples was observed after thermoforming. The oxygen transmission rate of the thermoformed part was 1.9 $cm^3/(m^2.day)$ at 75% of draw depth and 41 $cm^3/(m^2.day)$ at 100% of draw depth.

3.4. Conclusions

In this study, multilayer EVOH/LDPE film/foam with HDPE skin layer had been successfully extruded and characterized in terms of morphology, mechanical properties, and gas permeabilities. The film/foams systems were prepared by multilayer coextrusion process using three extruders and four layer multiplication elements. The foam layer extruder was responsible for extruding a dry blend of LDPE, LDPE-g-MA, and foaming agents and the film layer extruder was responsible for extruding EVOH film. After the multiplication elements, a third extruder added the HDPE skin layer in the system.

The foam layers were contained closed cell structures with cell size less than 100 μm and the EVOH film layers were continuous and had lithe variation of local thickness. The lightweight material shows good mechanical properties without delamination between the foam layers, film layers, and skin layer. The film/foam had excellent oxygen and water vapor barrier properties and could easily be thermoformed at low temperature. After the thermoforming process, the final formed product maintains good oxygen barrier properties.

The (EVOH/LDPE)/HDPE multilayer film/foam introduced in this article show interesting properties with excellent potential material for high barrier packaging applications.

3.5. References

[1] J. Wang, D. J. Gardner, N. M. Stark, D. W. Bousfield, M. Tajvidi, and Z. Cai, "Moisture and Oxygen Barrier Properties of Cellulose Nanomaterial-Based Films," ACS Sustain. Chem. Eng., vol. 6, no. 1, pp. 49–70, Jan. 2018, doi: 10.1021/acssuschemeng.7b03523.

[2] F. Tihminlioglu, İ. D. Atik, and B. Özen, "Water vapor and oxygen-barrier performance of corn–zein coated polypropylene films," J. Food Eng., vol. 96, no. 3, pp. 342–347, Feb. 2010, doi: 10.1016/j.jfoodeng.2009.08.018.

[3] B. A. Blakistone, Ed., Principles and Applications of Modified Atmosphere Packaging of Foods. Boston, MA: Springer US, 1998.

[4] J. Lange and Y. Wyser, "Recent innovations in barrier technologies for plastic packaging?a review," Packag. Technol. Sci., vol. 16, no. 4, pp. 149–158, Jul. 2003, doi: 10.1002/pts.621.

[5] F. Carosio et al., "Efficient Gas and Water Vapor Barrier Properties of Thin Poly(lactic acid) Packaging Films: Functionalization with Moisture Resistant Nafion and Clay Multilayers," Chem. Mater., vol. 26, no. 19, pp. 5459–5466, Oct. 2014, doi: 10.1021/cm501359e.

[6] M. R. Kamal, I. A. Jinnah, and L. A. Utracki, "Permeability of oxygen and water vapor through polyethylene/polyamide films," Polym. Eng. Sci., vol. 24, no. 17, pp. 1337–1347, Dec. 1984, doi: 10.1002/pen.760241711.

[7] Z. Li, A. Olah, and E. Baer, "Micro- and nano-layered processing of new polymeric systems," Prog. Polym. Sci., vol. 102, p. 101210, Mar. 2020, doi: 10.1016/j.progpolymsci.2020.101210.

[8] N. Alipour et al., "Structure and properties of polyethylene-based and EVOH-based multilayered films with layer thicknesses of 150nm and greater," Eur. Polym. J., vol. 64, pp. 36–51, Mar. 2015, doi: 10.1016/j.eurpolymj.2014.12.011.

[9] Daniel Klempner, Handbook of Polymeric Foams and Foam Technology, 2nd Editio. Hanser Publications, 2004.

[10] J. Feng, Z. Li, A. Olah, and E. Baer, "High oxygen barrier multilayer EVOH/LDPE film/foam," J. Appl. Polym. Sci., vol. 135, no. 26, p. 46425, Jul. 2018, doi: 10.1002/app.46425.

[11] C. Souza, J. Feng, A. Olah, G. Wnek, and E. Baer, "Thermoformable high oxygen barrier multilayer EVOH/LDPE film/foam," J. Appl. Polym. Sci., vol. 137, no. 30, p. 48903, Aug. 2020, doi: 10.1002/app.48903.

[12] M. A. Rahman, R. Andrade, J. Maia, and E. Baer, “Viscosity contrast effects on the structure – Property relationship of multilayer soft film/foams,” Polymer (Guildf)., vol. 69, pp. 110–122, Jul. 2015, doi: 10.1016/j.polymer.2015.05.051.

[13] M. Buntinx et al., “Evaluation of the Thickness and Oxygen Transmission Rate before and after Thermoforming Mono- and Multi-layer Sheets into Trays with Variable Depth,” Polymers (Basel)., vol. 6, no. 12, pp. 3019–3043, Dec. 2014, doi: 10.3390/polym6123019.

[14] F. M. Duarte and J. A. Covas, “Multilayer plug concept to enhance thickness distribution control of deep thermoformed parts,” Plast. Rubber Compos., vol. 37, no. 7, pp. 293–300, Sep. 2008, doi: 10.1179/174328908X314316.

[15] J. R. W. Jr., Multilayer Flexible Packaging, First Edit. Elsevier, 2010.

Table 3.1 Characteristics of Materials Used to Produce (EVOH/LDPE)/HDPE Multilayer Film/Foams.

Polymer	Trade name	Density (g/cm^3)	Tm (°C)	Melt Flow Index[a]	Oxygen Permeability Coefficient[b]	Water Vapor Transmission Rate[c]
EVOH	E171	1.14	159	1.7	0.02	2.0 – 4.5
LDPE	5004I	0.92	110	4.2	420	1.0 – 1.2
LDPE-g-MA	GR202	0.93	110	8.0	N.A	N.A
HDPE	DMDA 8007	0.96	133	8.3	150	0.4 – 0.8

a) (190 °C and 2.16 Kg) (g/10min).
b) (cc*mil/100in^2 *day*atm) [15].
c) (g*mil/100 in^2*day) [15].

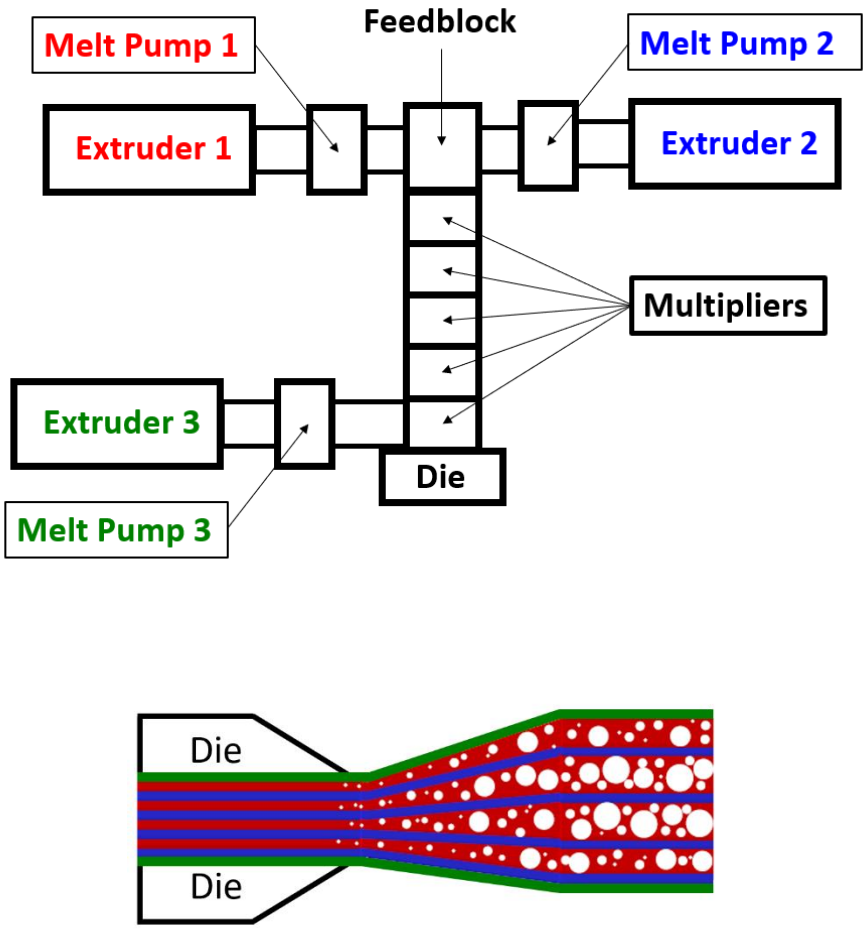

Figure 3.1 Schematic of multilayer film/foam coextrusion process.

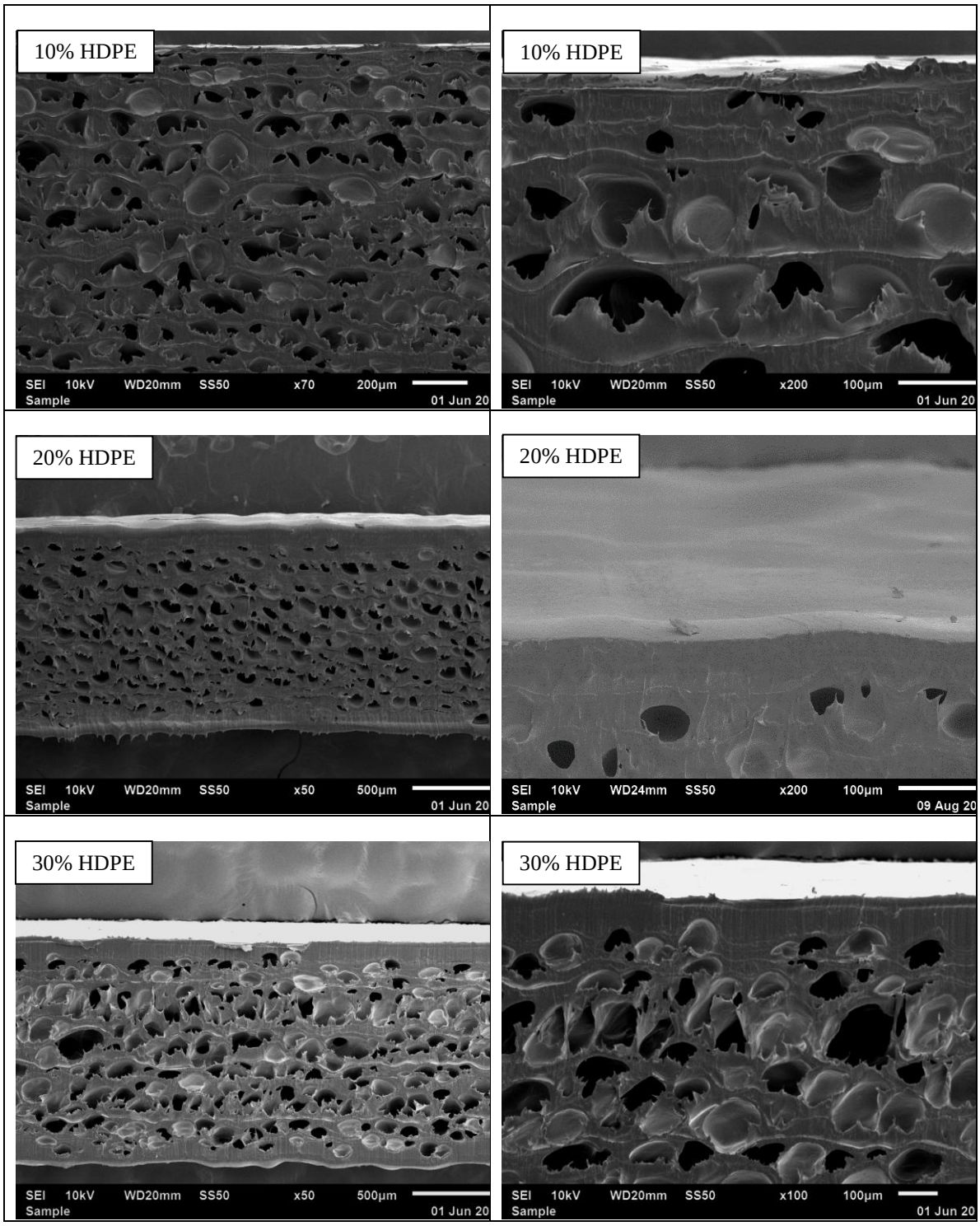

Figure 3.2 (EVOH/LDPE)/HDPE film/foam morphology extrusion-direction as-extruded with HDPE skin layer composition of 10%, 20% and 30% v/v.

Table 3.2 Characteristics of as-extruded (EVOH/LDPE)/HDPE Multilayer Film/Foam.

	EVOH/LDPE Film/Foam (10/90) Composition in Volume (%)	**HDPE Skin Layer Composition in Volume (%)**	**Total Thickness (mm)**	**Density (g/cm^3)**	**Average Cell Size (μm)**	**OTR[a] ($cm^3/(m^2.day)$)**
1	100	0	1.2 ± 0.1	0.52 ± 0.2	51 ± 15	0.60 ± 0.06
2	90	10	1.1 ± 0.1	0.50 ± 0.3	89 ± 30	0.72 ± 0.07
3	80	20	1.2 ± 0.1	0.53 ± 0.2	75 ± 18	0.84 ± 0.06
4	70	30	1.2 ± 0.1	0.54 ± 0.1	89 ± 27	0.86 ± 0.06

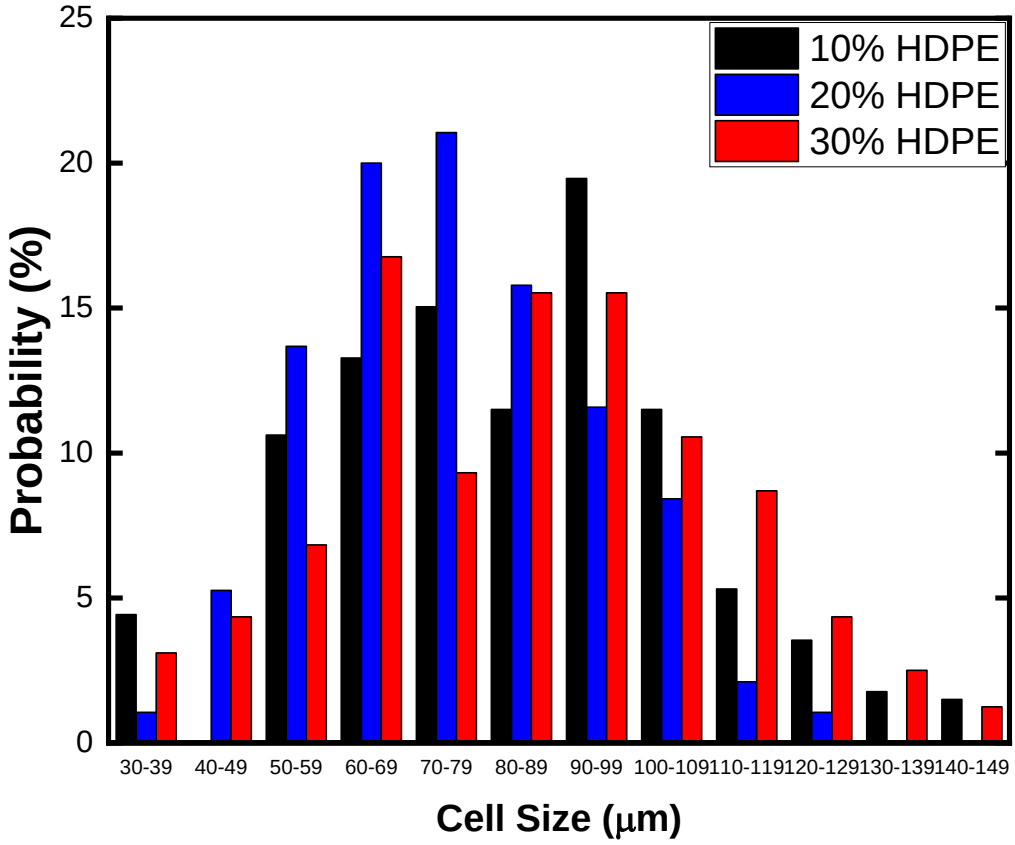

Figure 3.3 Measured Cell Size distribution and its probability distribution fit of as-extruded EVOH/LDPE multilayer film/foam (10/90 composition) with HDPE skin layer of 10%, 20% and 30% v/v composition.

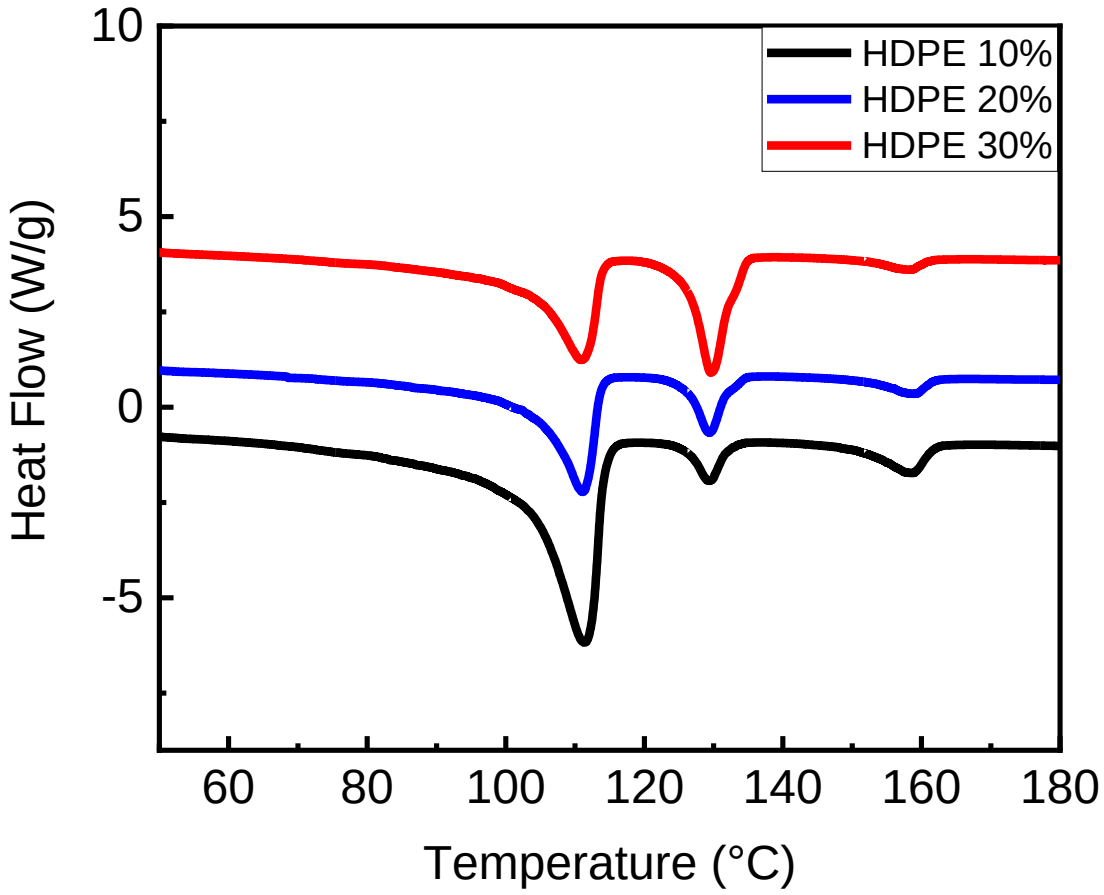

Figure 3.4. DSC heating thermograms of as-extruded EVOH/LDPE multilayer film/foam (10/90 composition) with HDPE skin layer of 10%, 20% and 30% v/v composition.

a)

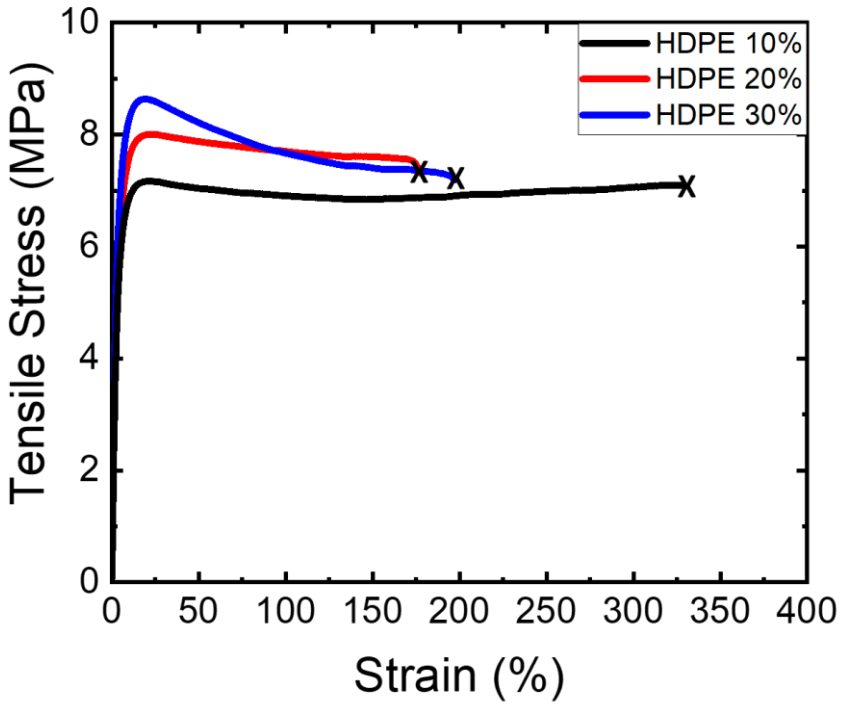

b)

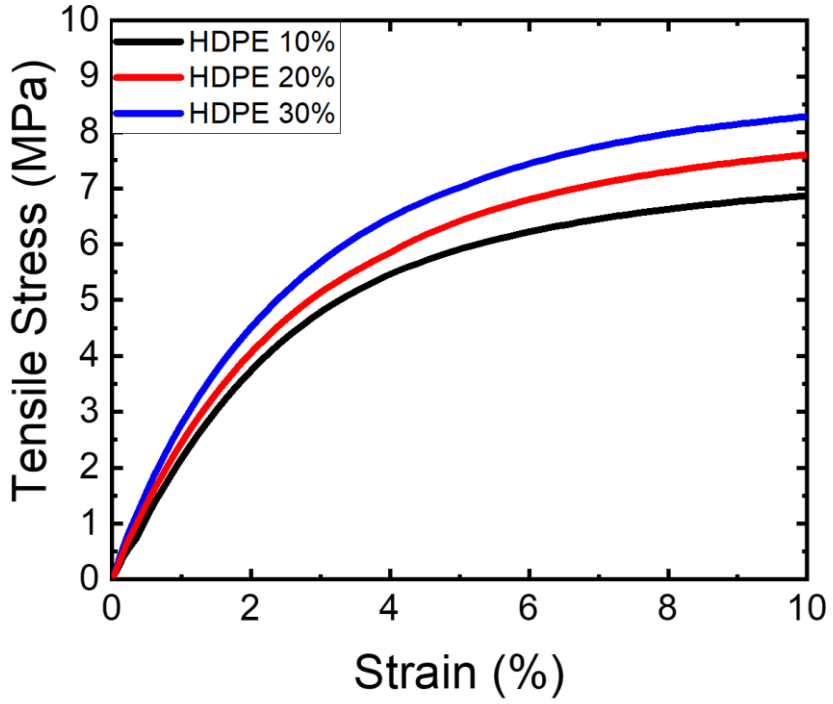

Figure 3.5 (a) Mechanical properties of as-extruded EVOH/LDPE multilayer film/foam (10/90 composition) with HDPE skin layer of 10%, 20% and 30% v/v composition at room temperature; (b) Mechanical properties of film/foam at low strain.

Table 3.3 Mechanical properties of as-extruded (EVOH/LDPE)/HDPE multilayer film/foam at room temperature.

HDPE Skin Layer Composition in Volume (%)	Tensile Strength (MPa)	Elongation to Break (%)	Measured Young`s Modulus (MPa)	Calculated Young`s Modulus (MPa)
10	7.0 ± 0.5	330 ± 25	218 ± 12	233
20	8.0 ± 0.6	180 ± 21	260 ± 14	290
30	8.7 ± 0.5	200 ± 23	306 ± 19	356

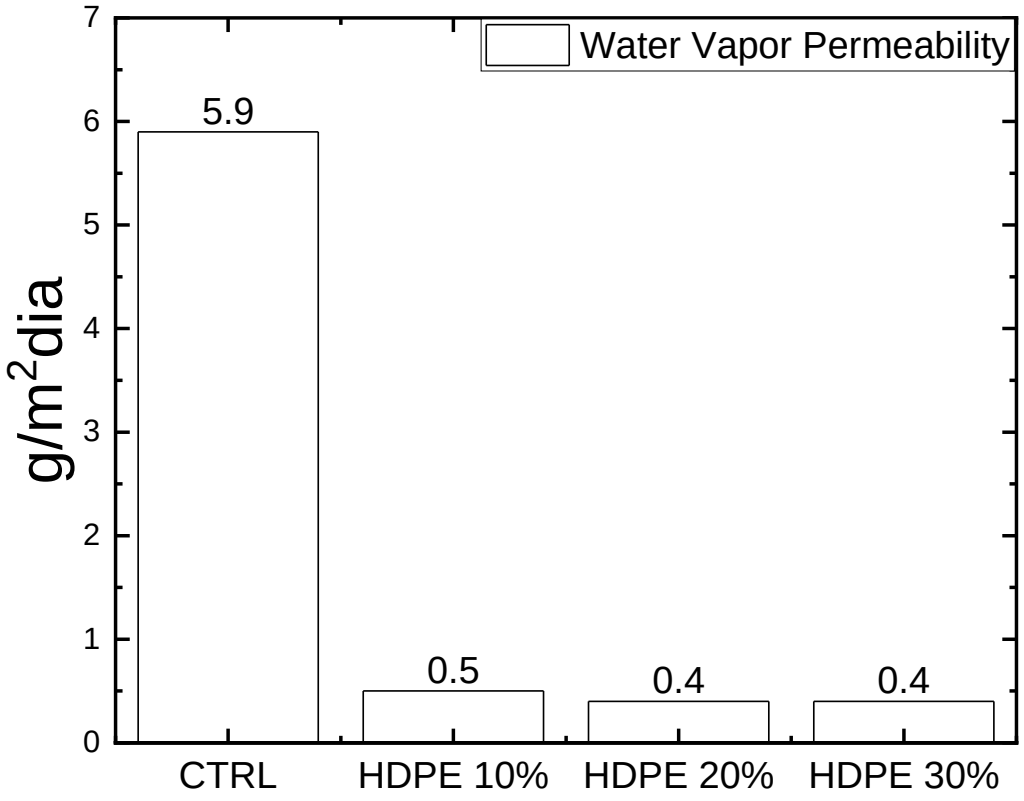

Figure 3.6 Water Vapor Transmission Rate of EVOH/LDPE multilayer film/foam (10/90 composition) with HDPE skin layer of 10%, 20% and 30% v/v composition.

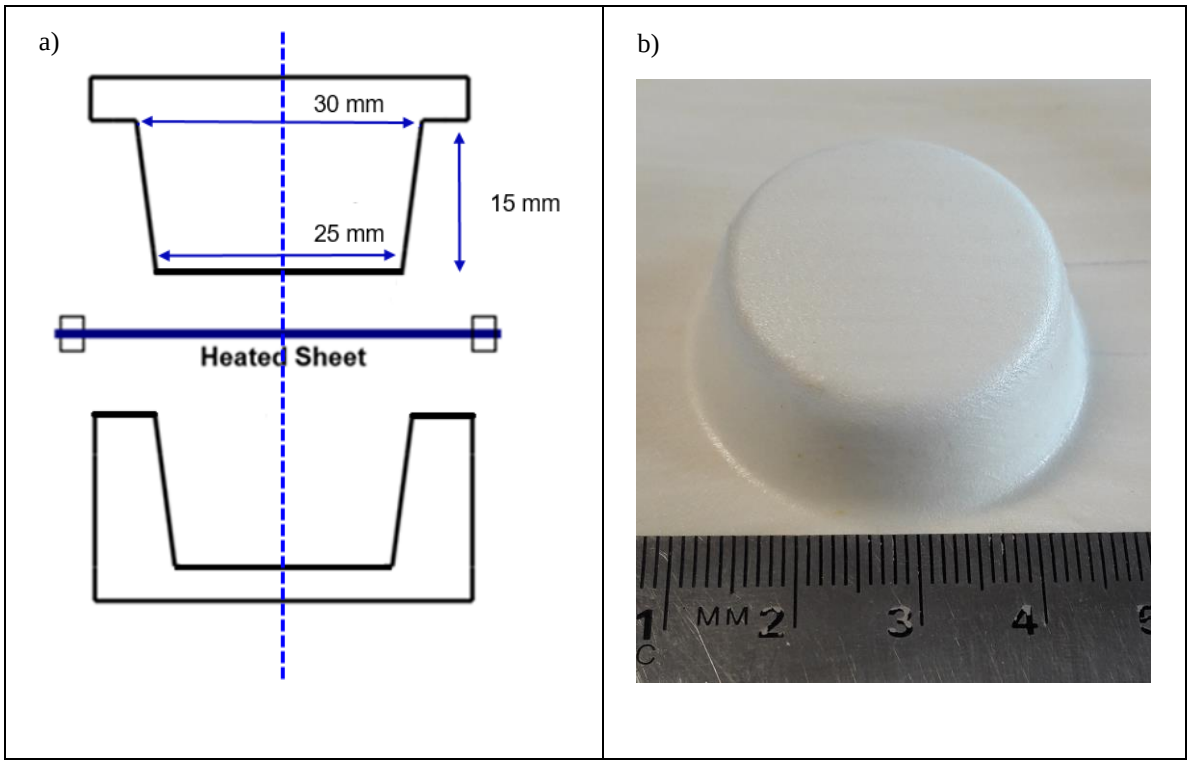

Figure 3.7 (a) Truncated cone mold dimensions. (b) Mechanically thermoformed EVOH/LDPE multilayer film/foam (10/90 composition) with HDPE skin layer of 20% v/v composition.

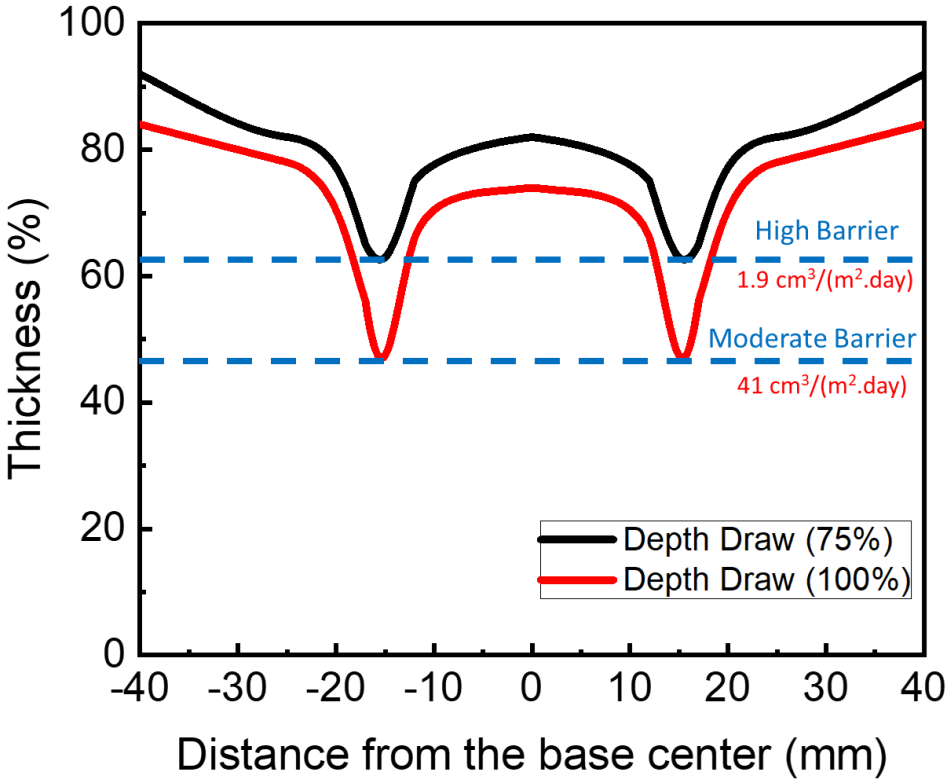

Figure 3.8 Wall thickness distribution (%) along a cross-section of thermoformed EVOH/LDPE multilayer film/foam (10/90 composition) with HDPE skin layer of 20% v/v composition.

Chapter 4

A Novel PLA High Oxygen Barrier Multilayer Film/Foam

Abstract

Production of biopolymer for packaging applications is still a burgeoning demand with the rising environmental concern about pollution due to non-degradable plastic waste materials. This paper introduces a novel approach, yet a continuous production method, to produce PLA multilayer film/foams structures having 16, 32, and 64 alternating layers were developed by multilayer coextrusion technique, and the morphology, density, mechanical properties and oxygen transmission of the as-extruded film/foams were characterized. The lightweight multilayered PLA film/foam has a unique solid/porous alternating horizontal architecture, in which the film layers can effectively control the growth of the cells and suppress the premature rupture of cells during coextrusion process. Tensile properties at elevated temperatures of the PLA film/foam were used to optimize thermoforming conditions. The effects of annealing temperature and time on the crystallinity and Oxygen permeability of PLA multilayer film/foams were investigated. Oxygen transmission showed a strong correlation with the crystallinity of PLA multilayer film/foam. The material demonstrated high performance with low oxygen transmission which could be used as high barrier material.

4.1. Introduction

Thermoplastics polymers are widely used in packaging and other consumer products due to outstanding properties such as low density, low process temperature, good printability, heat sealable, formability and barrier properties [1], [2]. While some plastics are being recycled and reused, petroleum-based polymers are not easily recyclable and are difficult to degrade completely in nature, creating environmental problems [3]. A great deal of effort is being made to overcome these issues [4]. Since PLA is derived from sustainable sources, compostable and low toxicity material, it has been viewed as a promising material for food contact and related packaging applications [5].

Poly (lactic acid) or polylactide (PLA) is a bio-based thermoplastic produced using renewable resources as cornstarch and sugarcane by either a chemical method or a biological process [1], [4], [6]. PLA is an enantiomeric polyester including L- and D-isomers. The degree of crystallinity is adjusted by the ratios between the isomers. Highly crystalline materials are achieved when the D content is below (2%) whereas fully amorphous materials can be obtained with high D content above (20%) [5]–[7]. PLA has been extensively studied as a potential substitute for petroleum-based polymers in several applications, such as biomedical materials and packaging, due to its mechanical properties, processability, material and processing costs [3], [4]. Despite these attractive properties, this environmentally-friendly biopolymer has some drawbacks that need to be addressed, as low impact resistance, poor heat stability and barrier properties [8], [9]. These factors may have limited its applicability in some areas, especially in applications where high oxygen and water barrier is important [10]. For instance, in food packaging where high barrier protection is important, replacement of PET by PLA may not be

feasible, since the barrier properties of PLA are not in par with PET [1], [5], [10]. Efforts are continuously made to produce new materials to overcome these issues included new polymerization routes to produce high molecular weight PLA, blending, addition of fillers, foaming, annealing and orientation [6], [8], [11]–[17].

Foaming technology is a well know process to enhance impact resistance and ductility of polymer matrix and widely used in industry to produce polymeric products with outstanding properties and low production cost [14]. There are several processing technologies that enable the production of PLA foams. PLA microcellular foam has several advantages over their unfoamed counterpart, such as low density, superior impact strength, improved toughness and higher heat and acoustic insulation properties [1], [3], [4]. Due to their large surface area and biocompatibility, PLA foams have a niche in medial implant applications and tissue engineering [18]–[20]. PLA foams have been considered as an interesting alternative for substitution of most current foamed petroleum-based products, such as polystyrene (PS) foam products as packaging, food trays and plastic utensils [11], [12]. However, the current technology used to develop PLA foam has some challenges to produce low-density foams with high surface to volume ratio and uniform cell structure in large scale. These are mainly due to PLA's low melt strength, low melt elasticity and slow crystallization kinetics that leads to cell coalescence and cell rupture during cell growth [4], [12]. Due to these challenges, there are few commercial PLA foams in the market.

Forced assembly multilayer coextrusion technology was demonstrated to be a reliable technique for producing multilayer film/foam structures in a continuous process. This technology is a scalable, solvent-free, cost-effective processing technique that can be

used to combine the physical and mechanical behaviors of both solid and foamed polymers. These coextruded polymeric systems can exhibit a synergistic combination of properties that would be unavailable in a conventional polymeric composite and have showed highly tunable properties, such as mechanical, optical, electrical and gas barrier by scaling and layer-layer interaction [2], [21], [22]. In the past two decades multilayer coextrusion process has evolved from two-component system with uniform layers and one-dimensional structure to more complex architectures including layered films, fibrous membranes, gradient structures and cellular film/foams. Such improvements are important in achieving materials that exhibit a broader property spectrum for various applications, including optical films, dielectric films, shape memory films, gas barrier films and packaging film/foams [21].

Forced assembly multilayer co-extrusion technology consists basically in a system of multiple single screw extruders with melt pumps, a co-extrusion feedblock, a sequence of layer multiplier elements, and an exit die. In the feedblock, the melt streams are merged as parallel layers. In the multiplier sequence each element doubles the number of layers by first slicing vertically the layer, spreading them horizontally, and finally recombining. The flow rate of each component layer can be easily controlled by the melt pumps. The layer number depends on the number of the multipliers that are used. An assembly of n multiplier elements produces a film with $2^{(n+1)}$ layers. This technology can produce structures from tens to thousands of individual layers within a single film. The thickness of the material can vary from 1 mm thick tape to as thin film as 25 μm with individual layer thickness down to less than 10 nm [21], [23].

In the present work, taking advantage of the unique solid/porous alternating architecture of the multilayer film/foam material. We developed an innovative approach to produce a PLA based foaming material having 16, 32 and 64 alternating film and foam layers through multilayer processing. The cellular morphology, mechanical properties, oxygen and water permeability, and thermoformability of the novel PLA cellular material have been discussed in detail.

4.2. Experimental

4.2.1 Materials

A two-component microlayer coextrusion setup was used to co-extrude film/foam layered structures. PLA (2003D, supplied by Nature Works) was used for the production of PLA multilayer film/foam. The physical and thermal properties of neat PLA are showed in Table 4.1.

The dry PLA used in the foam extruder was blended with both a chemical blowing agent and a nucleating agent. Azodicarbonamide (AZ-130 Galata Chemicals) at 1.5 wt% was used as the chemical blowing agent (CBA) for foaming PLA. The nucleating agent in the foam layer was 1 wt% Talc (Jetfine® 1H, IMERYS Talc).

4.2.2 Film/Foam Processing

One extruder contained the foam layer polymer (PLA), chemical blowing agent (azodicarbonamide) and nucleating agent (talc) and the other extruder contained the film layer polymer (PLA). After merging in the two-component feedblock, the foam and the film layers were processed into multilayers using the layer multipliers. Figure 4.1

illustrates the two-component coextrusion setup. The total pump rate in each extruder was adjusted to change the volumetric composition of film and foam layers for each sample.

Three-, four- and five-layer multiplication elements were used to produce 16, 32 and 64 layered film/foam structures. The temperature of the extrusion system and the layer multiplication elements were set at 195 °C. A 3 inch exit die at 180 °C was used after multiplication in order to control cell expansion. A 50 °C chill roll was used as a take-off. The thickness of the film/foam composites was maintained at 1.1 mm by adjusting the speed of the chill roll. The extruder screw speed and the melt pump rates were adjusted to control the composition of the film/foam composite. The temperature of the extrusion system was below the decomposition temperature of the chemical blowing agent so that the azodicarbonamide did not fully decompose to create large foam cells.

4.2.3 Scanning Electron Microscope Morphology

Scanning electron microscopy (SEM) (JEOL) was used to observe the film/foam layered structures in each sample. Film/foam samples were cut in the extrusion direction with sharp blades at room temperature. Then cross sections were sputter-coated with gold (10 nm). An emission voltage of 30 kV was used. The cell size and layer thickness of each film/foam sample were determined from SEM micrographs.

4.2.4 Density

The density of as-extruded film/foam specimens were measured using a density balance (Mettler Toledo, Columbus, OH). The liquid medium was ethanol to ensure wetting of

the sample surface. Because the film/foams had a closed-cell structure, the mass/volume method for density determination was accurate. Each sample was tested at least 5 times, and the average value was taken.

4.2.5 Oxygen Transmission Rate

Oxygen transmission measurement was conducted with a MOCON-OX-TRAN 2/20 at 0% relative humidity, 1 atm and 23°C. The film/foam samples were cut into a circular shapes with a diameter of 3 cm and sandwiched between two aluminum foils providing a test area of 5 cm^2. The oxygen transmission through the aluminum foil was ignored since the aluminum is a very high oxygen barrier. The oxygen transmission of the samples were calculated using the flux and samples thickness.

The oxygen transmission measurement of the thermoformed samples were performed using a MOCON-OX-TRAN 2/20 at 0% relative humidity inside the package, 1 atm and 23°C using a package environmental chamber. The thermoformed parts were exposed to oxygen from the atmosphere. The results were converted in [$cm^3/(m^2.day)$]. All measurements were performed in triplicate and an average value was adopted.

4.2.6 Mechanical Properties

Tensile tests of as-extruded film/foam samples were conducted using a mechanical testing machine (Instron, Norwood, MA) at different temperatures. The film/foam samples were cut into rectangular microtensile bars having dimensions of 1.0 x 6.0 cm^2. The strain rate for the tensile study was 100%/min. The load–displacement data obtained from the testing equipment was converted into stress–strain curves and Young's modulus

(E), yield strength (σ) (maximum stress) and strain at break (ε) values were determined from these curves. The Young's moduli of the specimens were calculated according to the slope of the initially linear part of the stress-strain curve. Each sample was tested at least 5 times, and the average value was taken.

4.2.7 Differential Scanning Calorimetry

Heating thermograms of PLA film/foam samples were determined by using a differential scanning calorimeter (DSC, TA Q2000 TA Instruments Inc., New Castle, DE) in nitrogen atmosphere at a constant heating rate of 10 °C/min in the temperature range 40 to 240 °C. The melting points was determined from the peak value of endothermic peak. The percent crystallinity of each as-extruded and annealed sample was determined by using the heat of fusion ΔHm and heat of crystallization ΔHc from DSC analysis. The following equation was used to calculate the degree of crystallinity within the samples:

$$\text{Crystallinity (\%)} = \frac{\Delta Hm - \Delta Hc}{93.1} \text{ x } 100 \qquad (1)$$

where the constant 93.1 J/g is the ΔHm for 100% crystalline PLLA or PDLA homopolymers [1].

4.2.8 Thermal treatment

Thermal treatment (annealing) was carried out in an oven. The PLA film/foam as-extruded samples were annealed at 80, 100 and 120 ºC, for varying lengths of time. These were used to compare crystallinity and oxygen permeability with samples without thermal treatment.

4.2.9 Mechanical Thermoforming

The as-extruded film/foam samples were cut into square specimens with a dimension of 60 mm by 60 mm square for thermoforming. The thermoformability of the film/foam material were evaluated using an aluminum truncated cone mold shape, typical of the design in food packaging. This mold had a top diameter of 30 mm, a base diameter of 25 mm, corners with radius of 2 mm, and a variable depth to 15 mm. A film/foam specimen was loaded in the mold and was compressed at different temperatures. At room temperature, the pressure was maintained for 10s and afterwards the specimen was removed from the mold. When molded at higher temperatures the pressure was maintained for 5s. The composites were formed at a constant speed of 200 mm/min. To identify of the local strain across the film/foam sample during thermoforming, uniform grids were drawn on the sample to map the deformation. The change of distance between grid lines was used to determine local strain.

4.3 Results and discussion

PLA/PLA multilayer film/foam specimens having 16, 32, and 64 layers and several compositions were successfully produced by microlayer coextrusion process. The foam process can be divided into three stages, as shown schematically in Figure 4.1: nucleation, bubble growth and stabilization stages. As the chemical blowing agent decomposes in the foam extruder, the gas is released. In the exit die the material experiences a pressure drop and the dissolved gas starts to nucleate in the form of bubbles. As more gas diffuses into the cell, the bubbles keep growing until the sheet cools down and the cell growth is stabilized and the multilayer PLA/PLA film/foam with enclosed cells is obtained.

The foam stability during this process is seen to be dependent of the exit die temperature, bubble growth stress, which is dependent of the blowing agent concentration, and the melt strength of the film layer [4], [14]. Moreover, an optimum concentration of the blowing agent and the optimum film layer composition ensure that there is maximum foaming without break-up. Microcellular material samples with good multilayer film/foam structure was achieved and investigated to determine the effect upon several properties, such as layer morphology, mechanical strength, oxygen transmission, and thermoformability.

Figure 4.2 shows the morphologies of PLA/PLA film/foam with 16, 32 and 64 Layers at 50/50 compositions. Layered morphology with cell boundaries is evident in the system with 16 and 32 layers. However, layered system is less evident when layer number exceeded 32 or the foam content was more than 50 %. Baer et al. reported similar observation based on the principle of viscosity contrast, working with a PE/PE multilayer

film/foam system [24]. The film/foam samples with 16 show mostly single and bilayer cell structures with straight and parallel layer boundaries. The cells were confined to the foam layer by film layer that enhanced the cell nucleation and suppressed the cell coalescence and thus contributed to single cell array in foam layers. However, in the system with 64 layers is less clear to identify the film layer, due to the decrease of film layer thickness and the system approach to a pure foam material. It can be imagined that when the thin layers are formed, the gas molecules close to the skin tends to migrate to the surface to, in turn, escape from the surface, which evidently reduces the efficiency of the foaming process as illustrated in Figure 4.2. Many attempts have been made in order to produce PLA foam with high surface to volume ratio and good cell structure, which is, cell integrity and cell size [13], [25], [26]. However, these studies have found that is complex to produce PLA foam with good cell structure and high surface to volume ratio. During PLA foam process of thin sheet, the low melt strength of PLA leads to cell coalescence and cell rupture during cell growth, which is, more gas tends to diffuse to the surface, and then vaporize from the surface [13]. Such gas loss during foam expansion evidently results in low foaming efficiency. Figure 4.2 shows that forced assembly multilayer coextrusion technology can be an effective way to overcome the weak viscoelastic properties of PLA and improve its foaming behaviors. Moreover, this technique can produce PLA microcellular structure with low density, high surface to volume ratio and good cell structure.

4.3.1 Properties Multilayer PLA/PLA Film/Foam

The characteristics of the as-extruded PLA/PLA multilayer film/foam materials are described in Table 4.2. As expected, it is possible to develop PLA/PLA film/foams with different properties, such as morphology, density, cell size and cell distribution by changing the composition and number of layers of the systems. As pointed out in the previous publications [22], [24], [27], the cell size and total density decreased with the increase of foam layer composition. As an example, the average cell size of the system with 16 layers decreased from 71 to 55 μm and the total density decreased from 0.89 to 0.74 g/cm^3 when the foam layer composition increased from 50% to 90%. As expected, the bulk apparent density of each film/foam system decreased as the foam content increases.

The density is governed by the total amount of gas released and dissolved in the system. It was observed that in this system total density of the PLA/PLA multilayer film/foam were highly variable with the composition of the system. In terms of the number of layers, by increasing the numbers of layers in the film/foam system, the cell size and total density did not change significantly. However, the 64 layers system with 90% foam composition shows a reduction on total density (0.65 g/cm^3) and a considerably increase in cell size (136 μm). This can be explained because in this system the film layer thickness is so thin that this system shows properties very similar to those of foam control material.

The two factors found to mainly affect the total density and cell size were the film/foam composition and the number of layers. In the system with 64 layers the composition effect was more pronounced in terms of cell size and total density. All system with 50%

foam composition has the average cell size around 70 μm which increase to about 136 μm in the system with 64 layers with 90% foam composition. The measured cell size of PLA/PLA multilayer film/foam (50/50 composition) approximately follows lognormal distribution, as shown in Figure 4.3.

The oxygen transmission rates (OTR) of as-extruded PLA/PLA multilayer film/foam samples are listed in Table 4.2. All samples show moderate oxygen barrier properties with OTR values below 40 $cm^3/(m^2.day)$ which meet or exceed the requirements for several applications, such as some kind of food packaging. However, the material is not suitable for high oxygen barrier applications where the requirements in terms of OTR is below 2 $cm^3/(m^2.day)$ [28].

Figure 4.4 shows the melting behavior of as-extruded film control and the PLA/PLA multilayer film/foam obtained from first DSC heating thermograms. The glass transition, cold crystallization and melt point of the samples are clearly seen in the curves. The melting points of PLA were 149 °C which were constant in both samples. The exothermic transition around 125 °C is due to the cold crystallization of PLA. The crystallinities of PLA film control and PLA multilayer film/foam can be determined based on the area under the melting peaks (ΔH_m) and cold crystallization (ΔH_C) following equation (1). The crystallinity of PLA film control and PLA/PLA multilayer film/foam as-extruded were less than 2% for all system and composition. This result was expected due to the semicrystalline PLA become quite amorphous after fast quenching from the melt phase during the extrusion process. The samples were processed to have the same final thickness (1.1 mm) by controlling the speed of chill roller.

4.3.2 Mechanical Properties of PLA multilayer film/foam

Figure 4.5 shows the tensile properties of as-extruded PLA/PLA multilayer film/foam at different compositions with 16, 32 and 64 layers at room temperature and strain rate of 100%/min. The load-displacement data were obtained from the testing equipment and converted into stress-strain curves. The data reveal good mechanical properties and typical plasto-elastomeric behavior under tension for all systems. The highest maximum stresses, elongations at break, and Young's modulus for all three systems are shown in Figure 4.5 and Table 4.3. Initially PLA/PLA multilayer film/foams samples show a reversible elastic deformation. At a certain amount of stress, deformation becomes irreversible, which is recognizable by a gradual yielding leading to a linear plastic deformation. After the yield point, the samples exhibit a constant stress with the increase of strain. At low strain, all systems demonstrate a typical elastomeric behavior with the yield point around 6% strain. Moreover, all samples have maximum strain larger than 15% indicating their potential for several applications.

PLA film control showed ductile behavior in tensile tests exhibiting a yield point, necking and strain softening after this point and a plateau before fracture.

Details of mechanical properties of PLA/PLA multilayer film/foams are presented in Table 4.3. It was observed that alternating the number of layers the maximum stress, elongation at break and Young's modulus were similar for all system with the same composition. However, as expected, by changing the composition between PLA foam and film is possible to achieve different results in terms of maximum stress and Young's modulus.

The Young's modulus was modeled using Equation (2)[2]. The void ratio was determined from the density of the foamed and unfoamed film/foam.

$$\boldsymbol{E_{Film/Foam} = (E_{PLA})\, X\, (1 - V_{Void}\%)} \quad (2)$$

Where E_{PLA} is the tensile modulus of the PLA (1082MPa). This model ignores the voids in the material and assumes that the polymeric matrix contributed to Young`s modulus. The results obtained using the model were consistent with the experimental results, which validates the assumption and confirm the good layer structure of the PLA/PLA film/foam materials.

Several studies have been made to understand the mechanical behavior of polymers through tensile tests at different temperatures and strain rates, in order to derive information on optimum thermoforming conditions. The tensile test experiments at different temperatures were applied to the as-extruded PLA film control samples to determine the limits of a thermoforming processing window. Figure 6 and 7 show the stress–strain relationships at different temperatures. The testing temperatures ranged between 60°C and 100°C and the testing strain was 100%/min. Table 4.4 shows the details of mechanical properties of PLA film control at several temperatures. These results can be characterized by a yield stress followed by a yield plateau with strain hardening behavior. The mechanical properties of PLA film control are dramatically affected by temperature. While the tensile moduli, determined from the secant modulus at 2% deformation, and the tensile strengths tend to decrease with an increase in the temperature the elongations at break tend to increase. However, at 100ºC, the behavior

changes and the elongation at failure decreases. Moreover, the PLA film samples show non-uniform deformation and significant deterioration of the microstructure occurs at this temperature. The transition in mode of micro-deformation is around the glass transition temperature of PLA (64 ºC), where the deformation is more severe and flow-like behavior arises.

It was observed that the mechanical properties of PLA film samples were very dependent on temperature. A processing temperature around 80°C appears optimal as it offers a good compromise between large deformations and low stresses. This temperature was selected for thermoforming studies.

4.3.3 Thermal treatment

Thermal treatment (annealing) of polymer is a well-known strategy to modify the microstructural features of polymer chains and buck properties, such as increasing stiffness and strength and improving barrier properties [6], [15], [16]. Moreover, the physical, mechanical and barrier properties of PLA are dependent on the solid-state morphology and its crystallinity, it can be anticipated that annealing treatment can be a useful strategy to improve the crystallinity of the PLA multilayered film/foam material with positive impact on the barrier properties.

Figure 4.8 shows the DSC thermograms from the first heating curve of annealing PLA/PLA multilayer film/foam 50/50 composition specimens with 32 layers at different annealing temperatures for 60 minutes. As noticed in Fig. 4.8 and Table 4.5, the crystallinity of PLA film/foam was enhanced during the annealing process. It can be seen that after annealing the exothermic transition around 120 °C, which is the cold

crystallization of PLA, was significantly affected by annealing process. The temperature and the peak area of cold crystallization decrease significantly after annealing at 80 °C. No cold crystallization endotherms were observed for the PLA multilayer film/foam after annealing at 100 and 120 °C. Figure 4.8 shows the evolution of crystallinity as a function on annealing temperature. The results show an increase on crystallinity by increasing temperature and the maximum crystallinity was around 34% at 120°C. After the annealing process at 100 °C was observed the presence of two melting peaks in the DSC thermogram. The same result was reported by Yasuniwa et al., they reported that the double-melting peak behavior was explained based on melt-recrystallization model, which is explained by the transition of small and imperfect crystals to more stable crystals form by melting and recrystallization. Moreover, different morphologies were formed at different temperatures [29]. As expected, maximum crystallization for PLA/PLA multilayer film/foam was achieved at 120 °C. Based on these results, that was the temperature choose for the kinetics studies.

Figure 4.9 shows the results obtained from DSC scans from the first heating curve of PLA/PLA multilayer film/foam 50/50 composition material with 32 layers heat treated for different length of time at annealing temperature of 120 °C. Based on the results from the Table 4.6, as we have expected, both time and temperature affect the process and longer annealing times and high temperature enhance PLA crystallization. It can be noticed that the melting peak for PLA is evident in each thermogram and the area under the melting peak changes with the annealing time, indicating the variation of the crystallinity of the samples. Table 4.6 shows that crystallinity changes from around 2% to a maximum of around 35% for the samples annealed more than 30 minutes. However,

there is a sharp increase from 2% to 30% when the sample was annealed for 15 minutes, indicating that the crystallinity of PLA multilayer film/foam was enhanced significantly at low annealing times. Such increase in crystallinity will reduce oxygen permeability on annealed PLA film/foam samples, which are discussed later. The crystallites produced during the annealing process also reduce the aging effect since they can act as physical crosslinks to stabilize the amorphous phase [1].

4.3.4 Oxygen Transmission Rate

PLA can in general be classified as a medium oxygen barrier polymer, its oxygen permeability is higher than for higher barrier materials, such as PVOH and EVOH, but below than PS, PE and PP. The annealing process of PLA result in better oxygen barrier properties. However, the values of oxygen permeability of PLA are still inferior to PET when both polymers have the same level of crystallinity [10]. Figure 4.10 shows the correlation of Annealing time to oxygen transmission rate of PLA multilayer film/foam, as anticipated, the enhance of crystallization of the material has a positive effect on the barrier properties.

As noticed in Fig. 4.10 and Table 4.7, the oxygen transmission rate decreases with increased crystallinity, interestingly, the oxygen transmission rate of the PLA film/foam structure is much lower than that of the PLA film control annealed at the same conditions, this behavior can be explained by the increased tortuosity of the path of oxygen molecules imposed by the crystals and the bubbles in the PLA multilayer film/foam.

In general, the gas transportation mechanism in a semicrystalline polymer is based on terms of a two phase model, which is an impermeable crystalline phase dispersed in a permeable amorphous matrix [10]. Based on this simple model, the decrease of permeability is mostly explained by the decrease the amount of amorphous material through which the gas molecules can permeate and the increase of the tortuosity of the transport path due to the impermeable crystallites.

4.3.5 Thermoforming

PLA multilayer 50/50 film/foam samples with 32 layers were thermoformed with a truncated cone mold at 80 °C. Figure 4.11 shows the design and dimensions of the mold used for thermoforming studies and the appearance of sample after the thermoforming process. This is a truncated cone mold, designed to produce formed parts with a variable depth by controlling the final position of the mold plug. A strain analysis in the thermoformed film/foam parts were conducted using a drawing grid to track the local strain in the bottom, the walls, and the corners during the thermoforming process (Figure 4.12).

The distribution of the material strain in the thermoformed sheets was identified, showing the locations that were most affected by the thermoforming process. It is clear that in the corners the impact upon material thinning was more pronounced. It can be seen that maximum deformation was approximately 65% on the edge of the mold after the thermoforming process. Moreover, the mold used allows a final draw ratio in the thermoformed film/foam sample that may be considered as deep draw [28].

Thermoforming is a processing that clearly affects the transmission of the materials, due to both increased area and thinning of the material. The strain distribution of a thermoformed product is dependent on a variety of processing parameters, such as sheet temperature, mold temperature, heating time, thermoforming pressure and plug speed [30].

The oxygen transmission rate of the PLA multilayer film/foam thermoformed part with subsequent annealing process for 30 minutes at 120 °C was 10 $cm^3/(m^2.day)$. The PLA film/foam with 32 layers exhibits good mechanical properties and was able to be completely formed using the deep draw mold. The strain profile of the thin sheet materials clearly show that the edges are more affected than the walls and the bottom. No difference in appearance of samples was observed after thermoforming. The non-uniform wall thickness distribution is caused by differential stretching during the thermoforming process.

The PLA multilayer film/foam introduced in this article show interesting properties with an excellent potential as a packaging material. The lightweight PLA material could easily be thermoformed at low temperature and after a short thermal treatment the final formed product shows good oxygen barrier properties.

4.4. Conclusions

PLA multilayer film/foam structures having 16, 32, and 64 alternating PLA film layers and PLA foam layers were successfully produced by microlayer coextrusion process. The as-extruded film/foams showed good layer structure with a uniform cell morphology. The cell size and the density can be adjusted by varying the number of layers and composition of the film/foam. The materials demonstrated good mechanical properties and low oxygen transmission. The structure-property relationships of PLA multilayer film/foam are significant for the development of film/foam materials with good barrier properties that can be produced at large scale.

The mechanical properties of PLA film at different temperatures was evaluated to determine the limits of a thermoforming processing window. The mechanical properties of PLA were very temperature dependent and processing temperature of 80 °C was selected as it offers a good compromise between large deformations and low stresses.

The effect of annealing time and temperature on the crystallinity and oxygen permeability of PLA/PLA multilayer film/foam parts was studied. The degree of crystallinity depended upon time and temperature and was measured using DSC. Annealing above Tg significantly enhanced the overall crystallinity, resulting in high improvements in terms of oxygen barrier properties of the material. The PLA multilayer film/foam showed extraordinary oxygen barrier after annealing process, which can meet high barrier oxygen requirements. Finally, the PLA multilayer film/foams were successfully thermoformed using a truncated cone mold. Optimum forming capacity was achieved at 80°C.

4.5. References

[1] L.-T. Lim, R. Auras, and M. Rubino, “Processing technologies for poly(lactic acid),” Prog. Polym. Sci., vol. 33, no. 8, pp. 820–852, Aug. 2008, doi: 10.1016/j.progpolymsci.2008.05.004.

[2] J. Feng, Z. Li, A. Olah, and E. Baer, “High oxygen barrier multilayer EVOH/LDPE film/foam,” J. Appl. Polym. Sci., vol. 135, no. 26, p. 46425, Jul. 2018, doi: 10.1002/app.46425.

[3] B. Jeon, H. K. Kim, S. W. Cha, S. J. Lee, M.-S. Han, and K. S. Lee, “Microcellular foam processing of biodegradable polymers — review,” Int. J. Precis. Eng. Manuf., vol. 14, no. 4, pp. 679–690, Apr. 2013, doi: 10.1007/s12541-013-0092-0.

[4] M. Nofar and C. B. Park, “Poly (lactic acid) foaming,” Prog. Polym. Sci., vol. 39, no. 10, pp. 1721–1741, Oct. 2014, doi: 10.1016/j.progpolymsci.2014.04.001.

[5] M. Murariu and P. Dubois, “PLA composites: From production to properties,” Adv. Drug Deliv. Rev., vol. 107, pp. 17–46, Dec. 2016, doi: 10.1016/j.addr.2016.04.003.

[6] Y. Srithep, P. Nealey, and L.-S. Turng, “Effects of annealing time and temperature on the crystallinity and heat resistance behavior of injection-molded poly(lactic acid),” Polym. Eng. Sci., vol. 53, no. 3, pp. 580–588, Mar. 2013, doi: 10.1002/pen.23304.

[7] B. Gupta, N. Revagade, and J. Hilborn, “Poly(lactic acid) fiber: An overview,” Prog. Polym. Sci., vol. 32, no. 4, pp. 455–482, Apr. 2007, doi: 10.1016/j.progpolymsci.2007.01.005.

[8] M. Siccardi, X. X. Garcia-Fonte, A. Simon, V. Pettarin, M. J. Abad, and C. Bernal, “Effect of the Processing-Induced Morphology on the Mechanical Properties of Biodegradable Extruded Films Based on Poly(lactic acid) (PLA) Blends,” J. Polym. Environ., vol. 27, no. 11, pp. 2325–2333, Nov. 2019, doi: 10.1007/s10924-019-01512-0.

[9] S. Saeidlou, M. A. Huneault, H. Li, and C. B. Park, “Poly(lactic acid) crystallization,” Prog. Polym. Sci., vol. 37, no. 12, pp. 1657–1677, Dec. 2012, doi: 10.1016/j.progpolymsci.2012.07.005.

[10] M. Drieskens, R. Peeters, J. Mullens, D. Franco, P. J. Lemstra, and D. G. Hristova-Bogaerds, “Structure versus properties relationship of poly(lactic acid). I. Effect of crystallinity on barrier properties,” J. Polym. Sci. Part B Polym. Phys., vol. 47, no. 22, pp. 2247–2258, Nov. 2009, doi: 10.1002/polb.21822.

[11] S. Pilla, S. G. Kim, G. K. Auer, S. Gong, and C. B. Park, “Microcellular extrusion-

foaming of polylactide with chain-extender," Polym. Eng. Sci., vol. 49, no. 8, pp. 1653–1660, Aug. 2009, doi: 10.1002/pen.21385.

[12] T. Standau, C. Zhao, S. Murillo Castellón, C. Bonten, and V. Altstädt, "Chemical Modification and Foam Processing of Polylactide (PLA)," Polymers (Basel)., vol. 11, no. 2, p. 306, Feb. 2019, doi: 10.3390/polym11020306.

[13] S. T. Lee, L. Kareko, and J. Jun, "Study of Thermoplastic PLA Foam Extrusion," J. Cell. Plast., vol. 44, no. 4, pp. 293–305, Jul. 2008, doi: 10.1177/0021955X08088859.

[14] L. M. Matuana, O. Faruk, and C. A. Diaz, "Cell morphology of extrusion foamed poly(lactic acid) using endothermic chemical foaming agent," Bioresour. Technol., vol. 100, no. 23, pp. 5947–5954, Dec. 2009, doi: 10.1016/j.biortech.2009.06.063.

[15] L. Yu, H. Liu, F. Xie, L. Chen, and X. Li, "Effect of annealing and orientation on microstructures and mechanical properties of polylactic acid," Polym. Eng. Sci., vol. 48, no. 4, pp. 634–641, Apr. 2008, doi: 10.1002/pen.20970.

[16] T. Takayama, M. Todo, and H. Tsuji, "Effect of annealing on the mechanical properties of PLA/PCL and PLA/PCL/LTI polymer blends," J. Mech. Behav. Biomed. Mater., vol. 4, no. 3, pp. 255–260, Apr. 2011, doi: 10.1016/j.jmbbm.2010.10.003.

[17] H. Li and M. A. Huneault, "Crystallization of PLA/Thermoplastic Starch Blends," Int. Polym. Process., vol. 23, no. 5, pp. 412–418, Nov. 2008, doi: 10.3139/217.2185.

[18] L. MATHIEU, T. MUELLER, P. BOURBAN, D. PIOLETTI, R. MULLER, and J. MANSON, "Architecture and properties of anisotropic polymer composite scaffolds for bone tissue engineering," Biomaterials, vol. 27, no. 6, pp. 905–916, Feb. 2006, doi: 10.1016/j.biomaterials.2005.07.015.

[19] V. Maquet et al., "Peripheral nerve regeneration using bioresorbable macroporous polylactide scaffolds," J. Biomed. Mater. Res., vol. 52, no. 4, pp. 639–651, Dec. 2000, doi: 10.1002/1097-4636(20001215)52:4<639::AID-JBM8>3.0.CO;2-G.

[20] W. Busby, N. R. Cameron, and C. A. Jahoda, "Tissue engineering matrixes by emulsion templating," Polym. Int., vol. 51, no. 10, pp. 871–881, Oct. 2002, doi: 10.1002/pi.934.

[21] Z. Li, A. Olah, and E. Baer, "Micro- and nano-layered processing of new polymeric systems," Prog. Polym. Sci., p. 101210, Jan. 2020, doi: 10.1016/j.progpolymsci.2020.101210.

[22] C. Souza, J. Feng, A. Olah, G. Wnek, and E. Baer, "Thermoformable high oxygen

barrier multilayer EVOH/LDPE film/foam," J. Appl. Polym. Sci., vol. 137, no. 30, p. 48903, Aug. 2020, doi: 10.1002/app.48903.

[23] D. Jarus, A. Hiltner, and E. Baer, "Barrier properties of polypropylene/polyamide blends produced by microlayer coextrusion," Polymer (Guildf)., vol. 43, no. 8, pp. 2401–2408, Apr. 2002, doi: 10.1016/S0032-3861(01)00790-X.

[24] M. A. Rahman, R. Andrade, J. Maia, and E. Baer, "Viscosity contrast effects on the structure – Property relationship of multilayer soft film/foams," Polymer (Guildf)., vol. 69, pp. 110–122, Jul. 2015, doi: 10.1016/j.polymer.2015.05.051.

[25] S.-T. Lee and N. S. Ramesh, "Gas loss during foam sheet formation," Adv. Polym. Technol., vol. 15, no. 4, pp. 297–305, 1996, doi: 10.1002/adv.1996.060150403.

[26] S.-T. Lee and N. S. Ramesh, Polymeric Foams Mechanisms and Materials. CRC Press, 2004.

[27] A. P. Ranade, A. Hiltner, E. Baer, and D. G. Bland, "Structure-Property Relationships in Coextruded Foam/Film Microlayers," J. Cell. Plast., vol. 40, no. 6, pp. 497–507, Nov. 2004, doi: 10.1177/0021955X04048425.

[28] M. Buntinx et al., "Evaluation of the Thickness and Oxygen Transmission Rate before and after Thermoforming Mono- and Multi-layer Sheets into Trays with Variable Depth," Polymers (Basel)., vol. 6, no. 12, pp. 3019–3043, Dec. 2014, doi: 10.3390/polym6123019.

[29] M. Yasuniwa, S. Tsubakihara, Y. Sugimoto, and C. Nakafuku, "Thermal analysis of the double-melting behavior of poly(L-lactic acid)," J. Polym. Sci. Part B Polym. Phys., vol. 42, no. 1, pp. 25–32, Jan. 2004, doi: 10.1002/polb.10674.

[30] F. M. Duarte and J. A. Covas, "Multilayer plug concept to enhance thickness distribution control of deep thermoformed parts," Plast. Rubber Compos., vol. 37, no. 7, pp. 293–300, Sep. 2008, doi: 10.1179/174328908X314316.

Table 4.1 Characteristics of Materials Used to Produce PLA/PLA Multilayer Film/Foams.

Polymer	Density (g/cm^3)	Tm (°C)	MFI[a] (g/10min)	Glass Transition Temperature (°C)
PLA	1.24	210	6	55-60

Tm = Melt point. MFI = Melt flow index; [a]At 210 °C and 2.16 Kg.

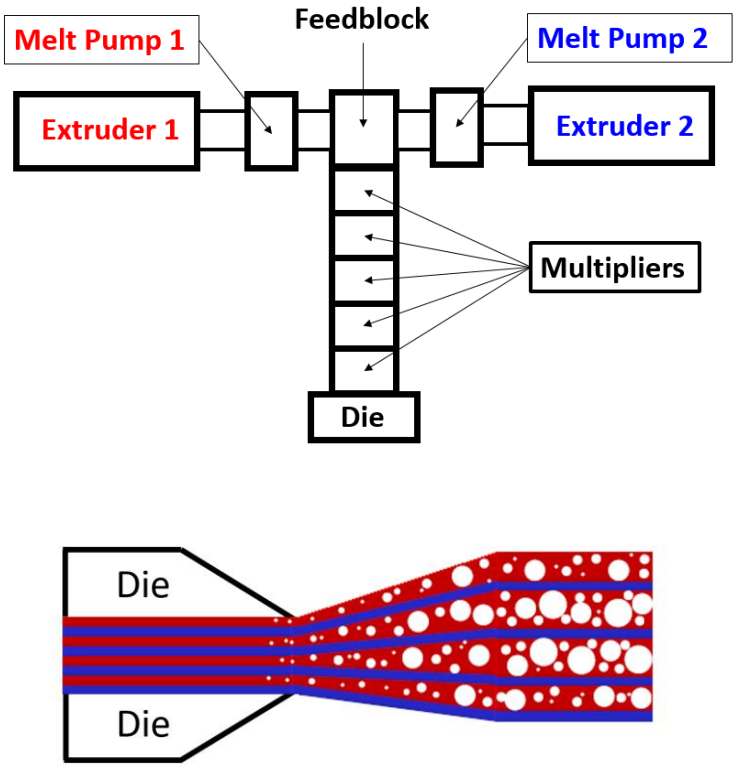

Figure 4.1 Schematic of multilayer film/foam coextrusion process.

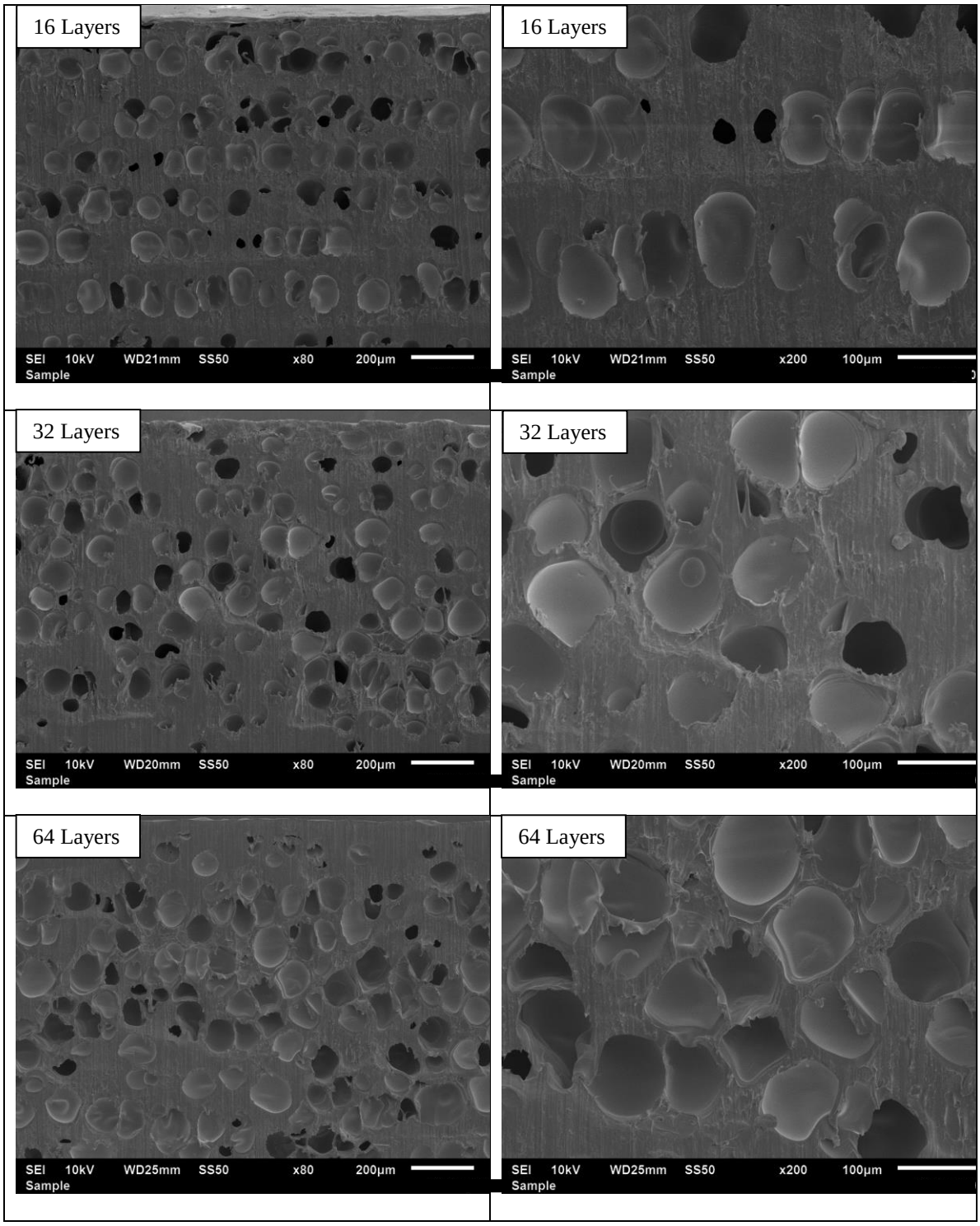

Figure 4.2 PLA/PLA film/foam (50/50) morphology extrusion-direction as-extruded with 16 Layers, 32 Layers and 64 Layers.

Table 4.2 Characteristics of as-extruded PLA/PLA Multilayer Film/Foam.

	Film/Foam Composition in Volume	**Number of Layers**	**Total Thickness (mm)**	**Density (g/cm^3)**	**Average Cell Size (μm)**	**OTR ($cm^3/(m^2.day)$)**
1	CTRL	1	0.49 ± 0.2	1.24 ± 0.01	124 ± 46	79.2 ± 0.9
2	50/50	16	1.1 ± 0.1	0.89 ± 0.03	71 ± 23	31.9 ± 0.7
3	30/70	16	1.1 ± 0.1	0.77 ± 0.03	57 ± 19	32.7 ± 0.5
4	10/90	16	1.1 ± 0.1	0.74 ± 0.02	55 ± 17	34.5 ± 0.9
5	50/50	32	1.1 ± 0.1	0.93 ± 0.01	70 ± 17	30.7 ± 0.3
6	30/70	32	1.1 ± 0.2	0.77 ± 0.03	60 ± 15	31.3 ± 0.6
7	10/90	32	1.1 ± 0.1	0.74 ± 0.02	80 ± 30	34.2 ± 0.9
8	50/50	64	1.1 ± 0.1	0.80 ± 0.01	77 ± 24	34.7 ± 0.4
9	30/70	64	1.1 ± 0.1	0.77 ± 0.07	73 ± 23	36.8 ± 0.5
10	10/90	64	1.1 ± 0.1	0.65 ± 0.05	136 ± 48	38.7 ± 0.7

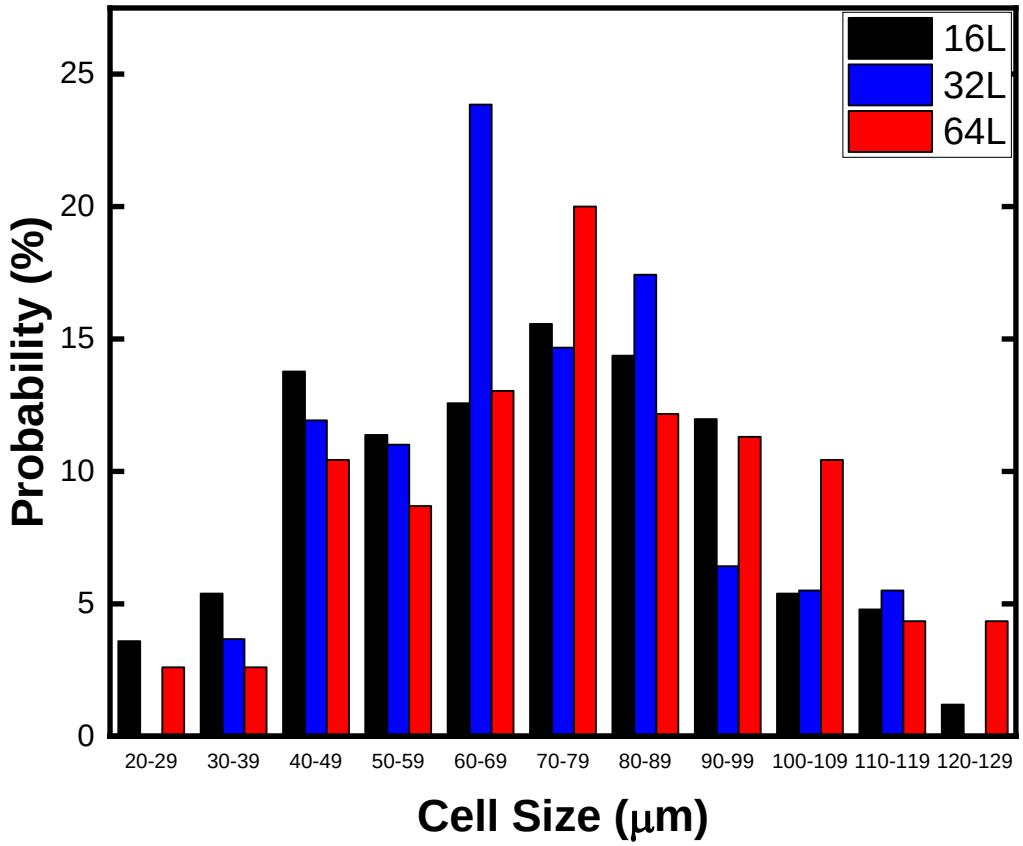

Figure 4.3 Measured Cell Size distribution and its probability distribution fit of as-extruded PLA/PLA multilayer film/foam (50/50 composition) with 16, 32 and 64 layers.

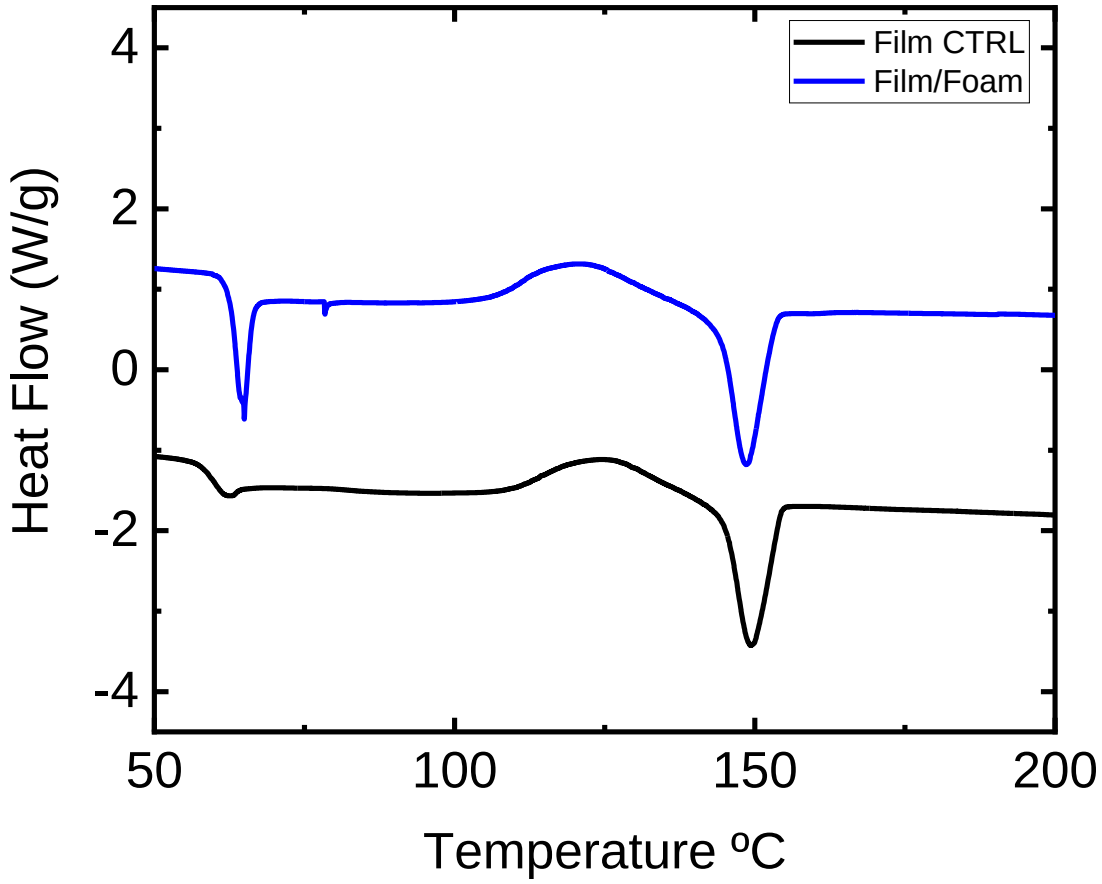

Figure 4.4 DSC heating thermograms of PLA control film and PLA/PLA film/foam material. The heating rate was 10°C/min.

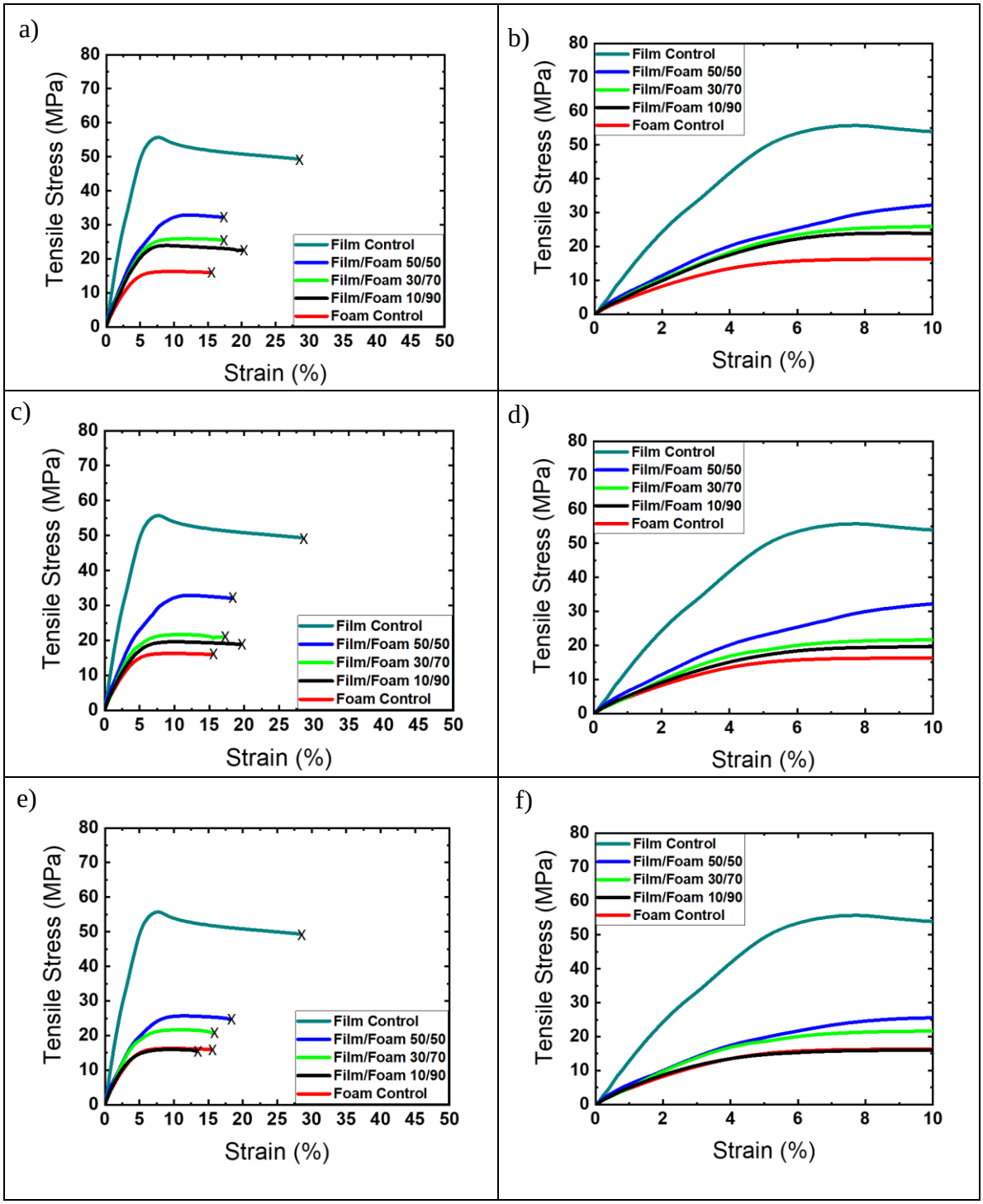

Figure 4.5 Mechanical properties of as-extruded multilayer PLA film/foam at room temperature; a) 16 Layers, c) 32 Layers and e) 64 Layers. Mechanical properties of film/foam at low strain; b) 16 Layers, d) 32 Layers and f) 64 Layers.

Table 4.3 Mechanical properties of as-extruded multilayer PLA film/foam at room temperature.

Number of Layers	Film/Foam Composition (%)	Tensile Strength (MPa)	Elongation to Break (%)	Measured Young`s Modulus (MPa)	Calculated Volume Fraction of Void (%)	Calculated Young`s Modulus (MPa)
1	100/0	55.4 ± 2.6	28 ± 12	1082 ± 125	N/A	N/A
16	50/50	29.4 ± 2.8	17 ± 4	526 ± 15	0.28	777
16	30/70	26.2 ± 1.9	17 ± 3	537 ± 41	0.38	672
16	10/90	22.3 ± 2.0	20 ± 4	489 ± 50	0.40	646
32	50/50	32.6 ± 1.1	18 ± 5	570 ± 32	0.25	812
32	30/70	19.8 ± 1.1	16 ± 3	449 ± 56	0.38	672
32	10/90	18.2 ± 1.8	29 ± 3	402 ± 31	0.40	646
64	50/50	24.5 ± 2.4	16 ± 2	530 ± 24	0.35	698
64	30/70	19.2 ± 1.7	16 ± 1	522 ± 48	0.38	672
64	10/90	15.9 ± 1.5	13 ± 1	398 ± 48	0.48	567
1	0/100	16.7 ± 0.7	15 ± 3	421 ± 15	0.28	777

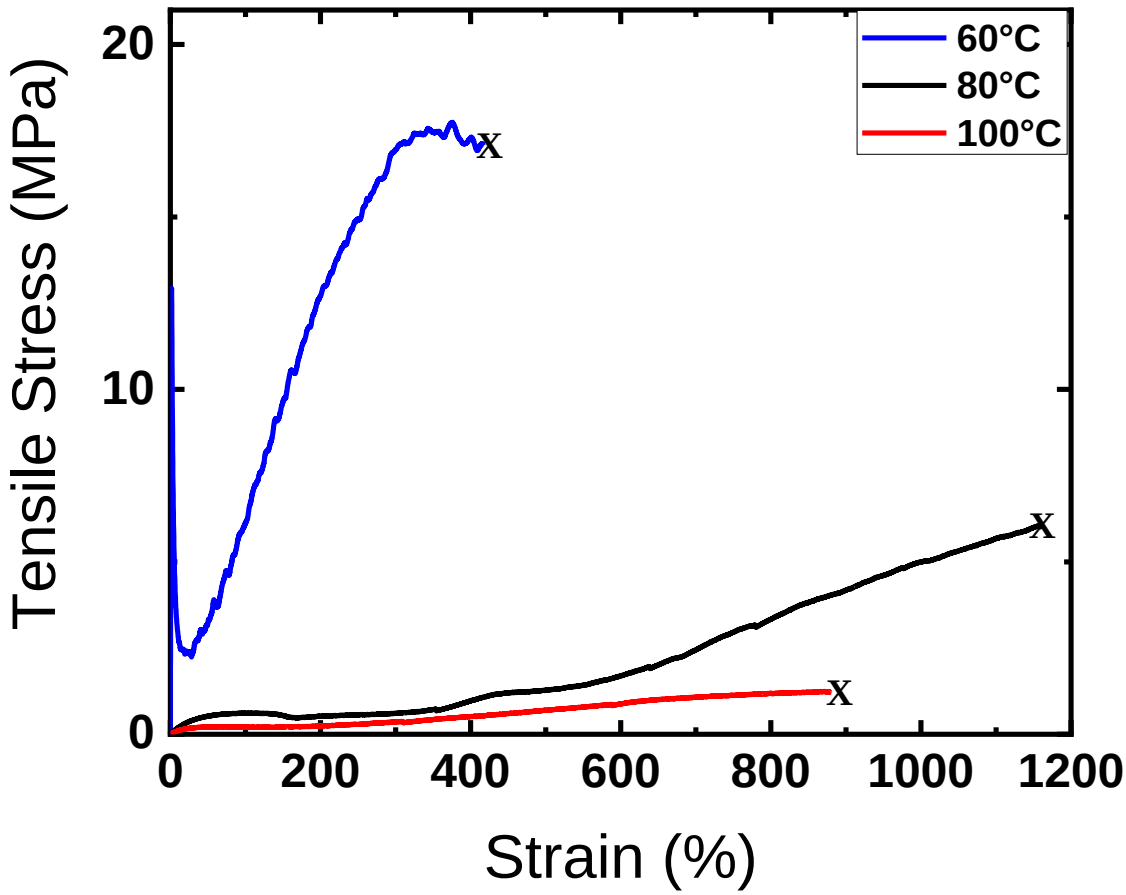

Figure 4.6 Mechanical properties of as-extruded PLA film control at different temperature.

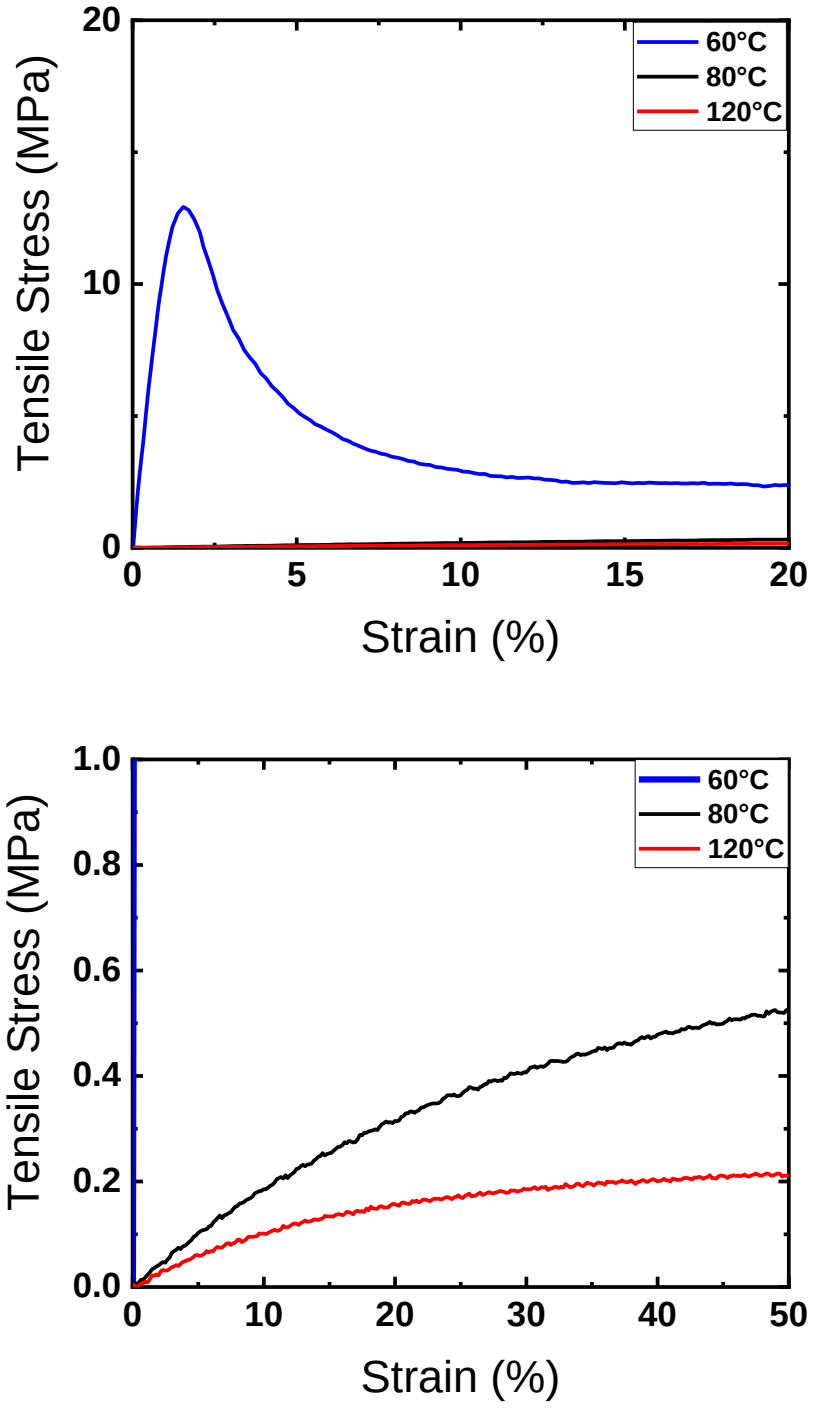

Figure 4.7 Mechanical properties at low strain and low stress of as-extruded PLA film control at different temperature.

Table 4.4 Mechanical properties of as-extruded PLA film control at different temperature.

Number of Layers	Temperature (°C)	Tensile Strength (MPa)	Elongation to Break (%)	Measured Young`s Modulus (MPa)
1 Layer	60	17.6 ± 3.5	458 ± 150	884 ± 82
1 Layer	80	6.9 ± 2.6	1241 ± 159	2.0 ± 0.1
1 Layer	100	1.4 ± 0.2	894 ± 143	1.4 ± 0.2

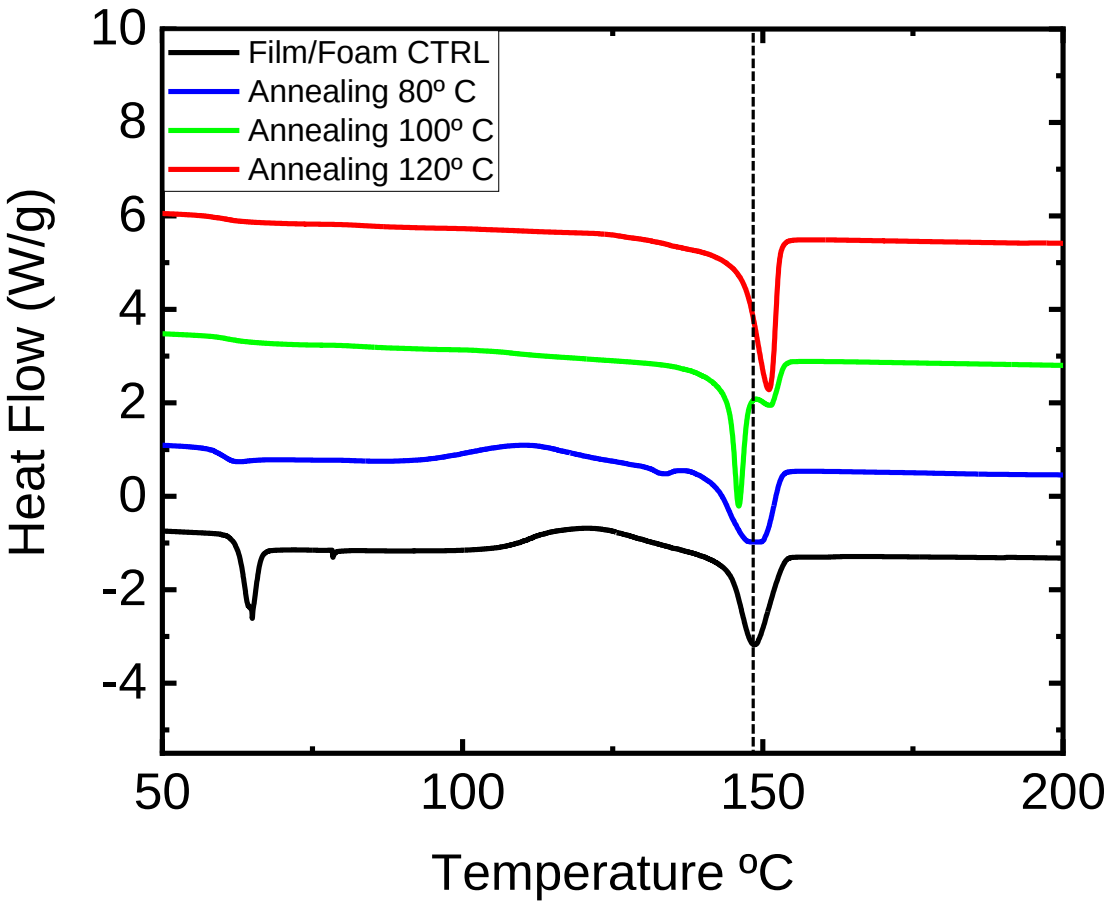

Figure 4.8 DSC heating thermograms of 32 layers PLA/PLA multilayer film/foam 50/50 composition before and after annealing process at different temperatures for 60 minutes.

Table 4.5 Cold Crystallization Temperature, Melting Temperature and Crystallinity of 32 layers PLA Multilayer Film/Foam 50/50 Composition Before and After Annealing Process at Different Temperatures for 60 Minutes Based on DSC.

Temp. Annealing (°C)	**PLA T_c (°C)**	**ΔH (J/g)**	**PLA T_m (°C)**	**ΔH (J/g)**	**Crystallinity (%)**
N/A	121	14.9	149	18.1	3.5 ± 0.9
80	108	8.4	149	21.5	14.0 ± 1.2
100	N/A	N/A	144/150	25.5	27.4 ± 2.3
120	N/A	N/A	150	31.9	34.3 ± 2.9

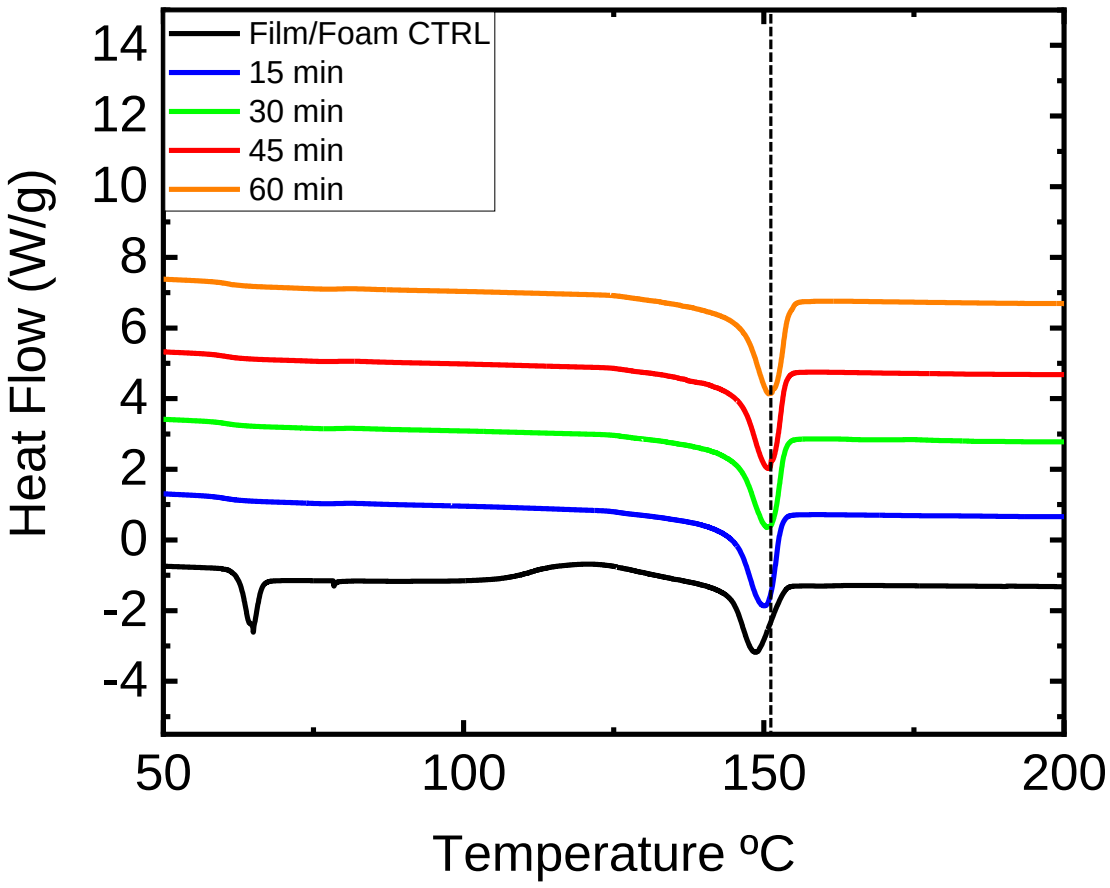

Figure 4.9 DSC heating thermograms of 32 layers PLA/PLA multilayer film/foam 50/50 composition before and after annealing process at 120°C at different times.

Table 4.6 Cold Crystallization Temperature, Melting Temperature and Crystallinity of 32 layers PLA Multilayer Film/Foam 50/50 Composition Before and After Annealing Process at 120 °C at Different Times Based on DSC.

Time Annealing (min)	**PLA T_c (°C)**	**ΔH (J/g)**	**PLA T_m (°C)**	**ΔH (J/g)**	**Crystallinity (%)**
N/A	125.7	11.41	149.8	13.8	2.6 ± 0.7
15	N/A	N/A	149.6	28.6	30.8 ± 2.5
30	N/A	N/A	150	31.8	34.3 ± 2.9
45	N/A	N/A	150.3	32.7	35.2 ± 2.7
60	N/A	N/A	150.6	31.8	34.2 ± 2.7

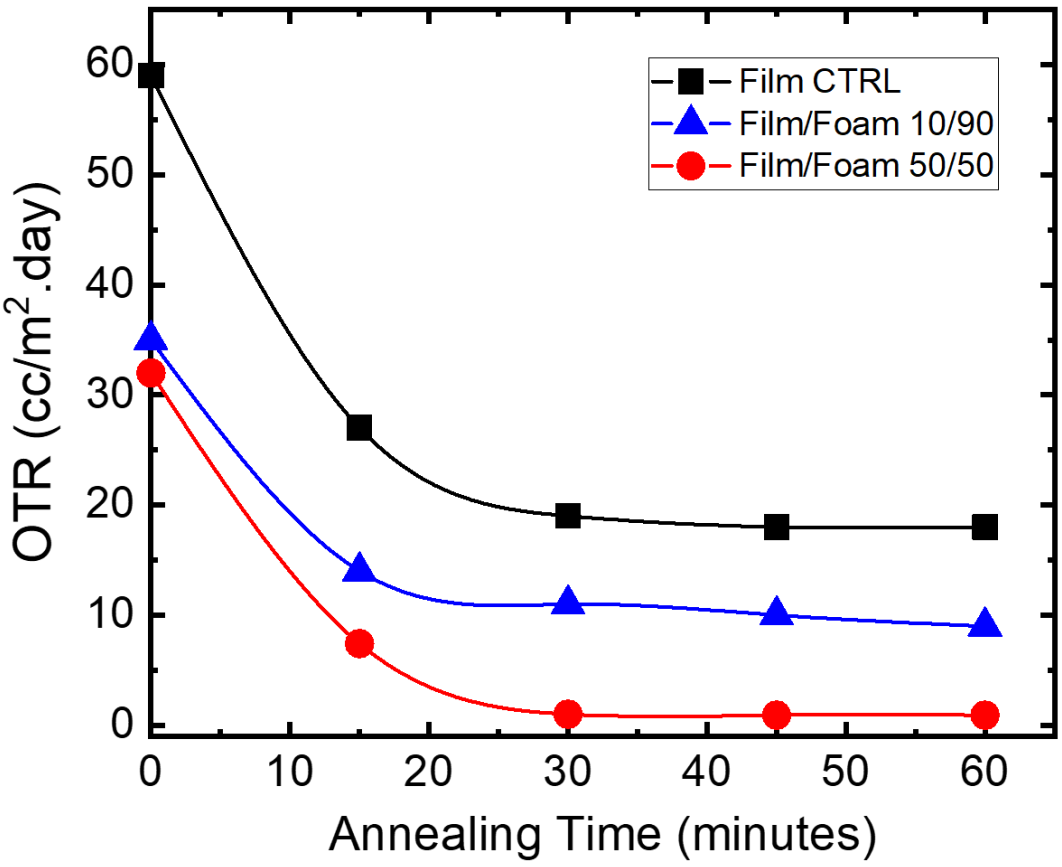

Figure 4.10 OTR of PLA film Control and PLA/PLA multilayer film/foam 32 layers as a function of annealing process time at 120°C.

Table 4.7 OTR of PLA film Control and PLA/PLA multilayer film/foam 32 layers as a function of annealing process time at 120°C.

Time Annealing (min)	**Film CTRL $cm^3/(m^2.day)$**	**PLA Film/Foam (10/90) $cm^3/(m^2.day)$**	**PLA Film/Foam (50/50) $cm^3/(m^2.day)$**
N/A	59 ± 5	35 ± 3	32 ± 2
15	27 ± 3	14 ± 2	8 ± 1
30	19 ± 2	11 ± 1	1.0 ± 0.1
45	18 ± 2	10 ± 2	0.9 ± 0.1
60	18 ± 2	9 ± 1	0.9 ± 0.1

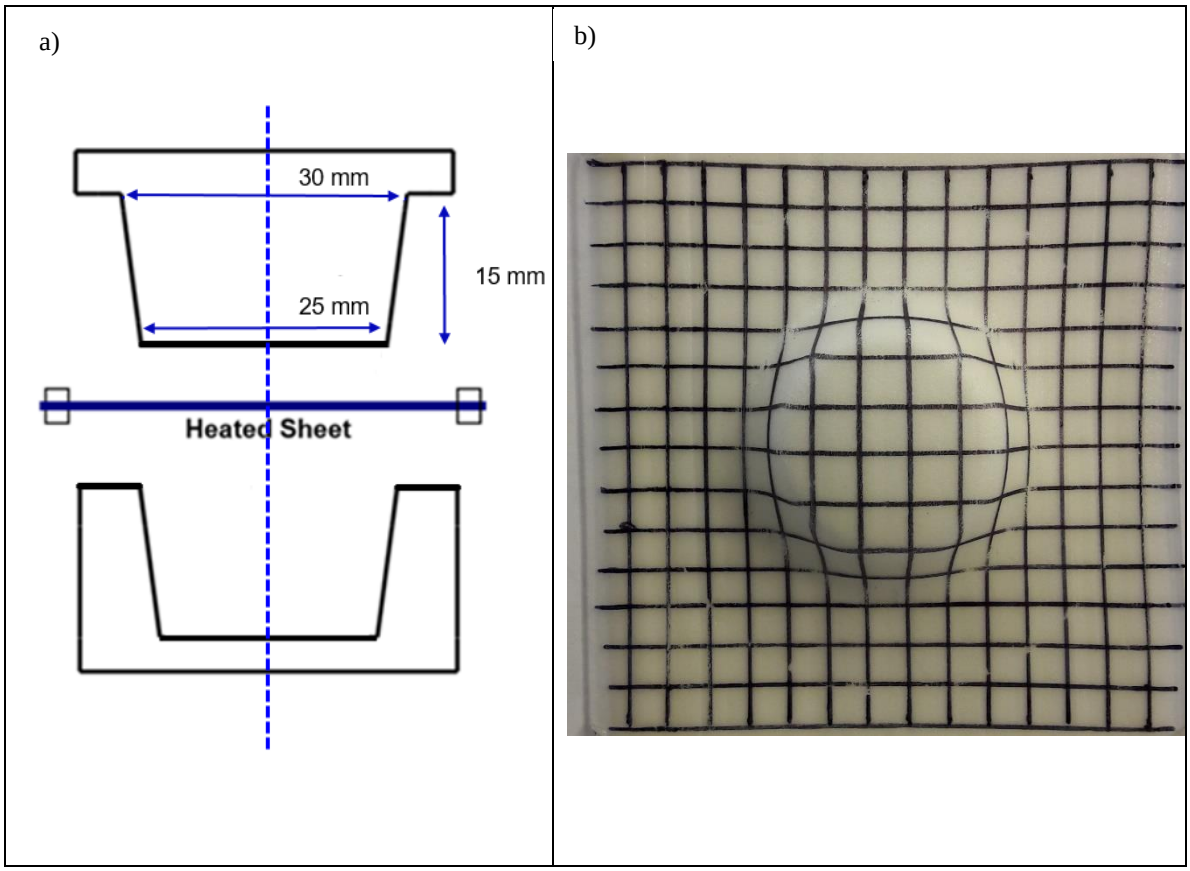

Figure 4.11 (a) Truncated cone mold dimensions. (b) Mechanically thermoformed PLA/PLA multilayer film/foam with composition of 10/90 in volume.

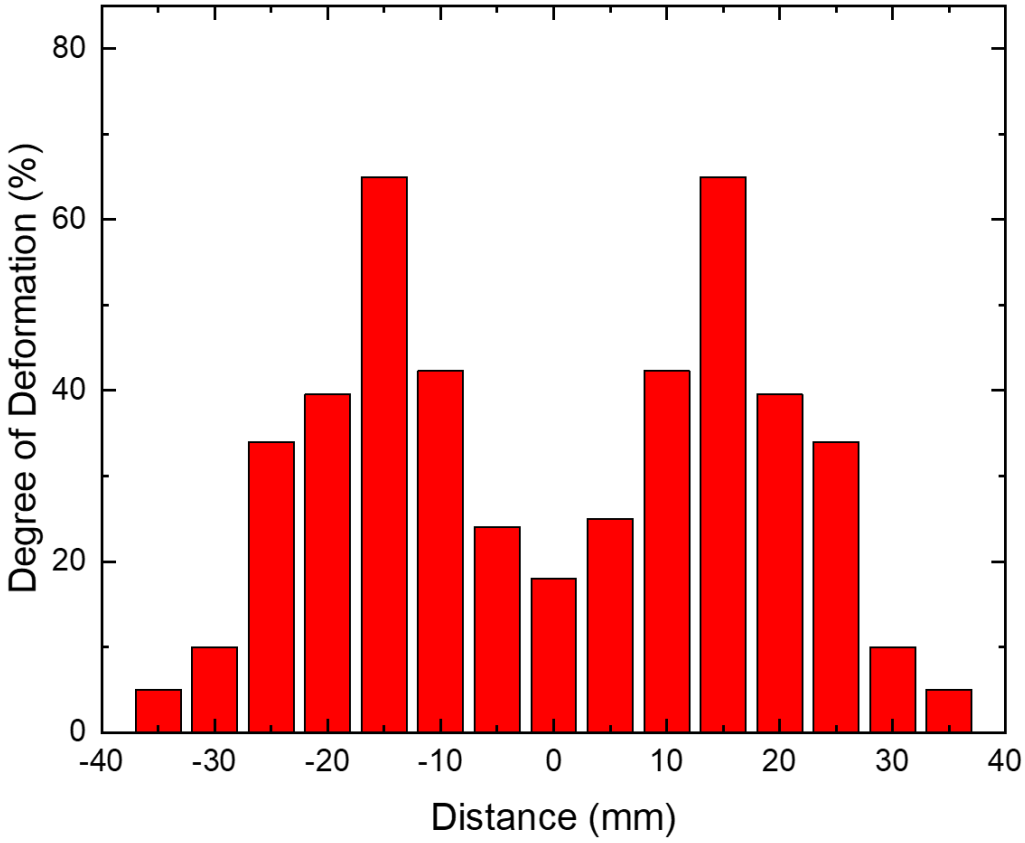

Figure 4.12 Local strain of PLA/PLA multilayer film/foam thermoformed at 80°C.

BIBLIOGRAPHY

A. P. Ranade, A. Hiltner, E. Baer, and D. G. Bland, “Structure-Property Relationships in Coextruded Foam/Film Microlayers,” J. Cell. Plast., vol. 40, no. 6, pp. 497–507, Nov. 2004, doi: 10.1177/0021955X04048425.

B. A. Blakistone, Ed., Principles and Applications of Modified Atmosphere Packaging of Foods. Boston, MA: Springer US, 1998.

B. Gupta, N. Revagade, and J. Hilborn, “Poly(lactic acid) fiber: An overview,” Prog. Polym. Sci., vol. 32, no. 4, pp. 455–482, Apr. 2007, doi: 10.1016/j.progpolymsci.2007.01.005.

B. Jeon, H. K. Kim, S. W. Cha, S. J. Lee, M.-S. Han, and K. S. Lee, “Microcellular foam processing of biodegradable polymers — review,” Int. J. Precis. Eng. Manuf., vol. 14, no. 4, pp. 679–690, Apr. 2013, doi: 10.1007/s12541-013-0092-0.

C. Souza, J. Feng, A. Olah, G. Wnek, and E. Baer, “Thermoformable high oxygen barrier multilayer EVOH/LDPE film/foam,” J. Appl. Polym. Sci., vol. 137, no. 30, p. 48903, Aug. 2020, doi: 10.1002/app.48903.

C.-Y. Lai, A. Hiltner, E. Baer, and L. T. J. Korley, “Deformation of Confined Poly(ethylene oxide) in Multilayer Films,” ACS Appl. Mater. Interfaces, vol. 4, no. 4, pp. 2218–2227, Apr. 2012, doi: 10.1021/am300240r.

D. Bhattacharyya, M. Bowis, and K. Jayaraman, “Thermoforming woodfibre–polypropylene composite sheets,” Compos. Sci. Technol., vol. 63, no. 3–4, pp. 353–365, Feb. 2003, doi: 10.1016/S0266-3538(02)00214-2.

D. Jarus, A. Hiltner, and E. Baer, “Barrier properties of polypropylene/polyamide blends produced by microlayer coextrusion,” Polymer (Guildf)., vol. 43, no. 8, pp. 2401–2408, Apr. 2002, doi: 10.1016/S0032-3861(01)00790-X.

Daniel Klempner, Handbook of Polymeric Foams and Foam Technology, 2nd Editio. Hanser Publications, 2004.

E. B. Obi, Polymeric foams structure-property-performance: a design guide. William Andrew, 2018.

E. Baer and A. Moet, High performance polymers- Structure, properties, composites, fibers(Book). Munich/New York: Hanser Publishers/Oxford University Press, 1991.

E. Baer, A. Hiltner, and D. Jarus, “Relationship of hierarchical structure to mechanical properties,” Macromol. Symp., vol. 147, no. 1, pp. 37–61, Dec. 1999, doi: 10.1002/masy.19991470106.

E. Baer, A. Hiltner, and H. Keith, “Hierarchical structure in polymeric materials,” Science (80-.)., vol. 235, no. 4792, pp. 1015–1022, Feb. 1987, doi: 10.1126/science.3823866.

E. Giménez, J. M. Lagarón, L. Cabedo, R. Gavara, and J. J. Saura, “Study of the thermoformability of ethylene-vinyl alcohol copolymer based barrier blends of interest in food packaging applications,” J. Appl. Polym. Sci., vol. 91, no. 6, pp. 3851–3855, Mar. 2004, doi: 10.1002/app.13584.

E. Giménez, J. M. Lagarón, M. L. Maspoch, L. Cabedo, and J. J. Saura, “Uniaxial tensile behavior and thermoforming characteristics of high barrier EVOH-based blends of interest in food packaging,” Polym. Eng. Sci., vol. 44, no. 3, pp. 598–608, Mar. 2004, doi: 10.1002/pen.20054.

F. Carosio et al., “Efficient Gas and Water Vapor Barrier Properties of Thin Poly(lactic acid) Packaging Films: Functionalization with Moisture Resistant Nafion and Clay Multilayers,” Chem. Mater., vol. 26, no. 19, pp. 5459–5466, Oct. 2014, doi: 10.1021/cm501359e.

F. M. Duarte and J. A. Covas, “Multilayer plug concept to enhance thickness distribution control of deep thermoformed parts,” Plast. Rubber Compos., vol. 37, no. 7, pp. 293–300, Sep. 2008, doi: 10.1179/174328908X314316.

F. Tihminlioglu, İ. D. Atik, and B. Özen, “Water vapor and oxygen-barrier performance of corn–zein coated polypropylene films,” J. Food Eng., vol. 96, no. 3, pp. 342–347, Feb. 2010, doi: 10.1016/j.jfoodeng.2009.08.018.

H. Li and M. A. Huneault, “Crystallization of PLA/Thermoplastic Starch Blends,” Int. Polym. Process., vol. 23, no. 5, pp. 412–418, Nov. 2008, doi: 10.3139/217.2185.

H. Wu, J. Zhang, C. Zhang, J. Feng, M. A. Rahman, and E. Baer, “Structure–Properties Relationship of a Novel Multilayer Film/Foam Material Produced through Co-extrusion and Orientation,” Ind. Eng. Chem. Res., vol. 55, no. 41, pp. 10947–10954, Oct. 2016, doi: 10.1021/acs.iecr.6b03418.

J. Feng et al., “Breakup behavior of nanolayers in polymeric multilayer systems — Creation of nanosheets and nanodroplets,” Polymer (Guildf)., vol. 143, pp. 19–27, May 2018, doi: 10.1016/j.polymer.2018.03.049.

J. Feng, Z. Li, A. Olah, and E. Baer, “High oxygen barrier multilayer EVOH/LDPE film/foam,” J. Appl. Polym. Sci., vol. 135, no. 26, p. 46425, Jul. 2018, doi: 10.1002/app.46425.

J. L. Throne, Understanding Thermoforming. München: Carl Hanser Verlag GmbH & Co. KG, 2008.

J. Lange and Y. Wyser, “Recent innovations in barrier technologies for plastic packaging?a review,” Packag. Technol. Sci., vol. 16, no. 4, pp. 149–158, Jul. 2003, doi: 10.1002/pts.621.

J. M. Carr, D. S. Langhe, M. T. Ponting, A. Hiltner, and E. Baer, “Confined crystallization in polymer nanolayered films: A review,” J. Mater. Res., vol. 27, no. 10, pp. 1326–1350, May 2012, doi: 10.1557/jmr.2012.17.

J. R. W. Jr., Multilayer Flexible Packaging, First Edit. Elsevier, 2010.

J. Wang, D. J. Gardner, N. M. Stark, D. W. Bousfield, M. Tajvidi, and Z. Cai, "Moisture and Oxygen Barrier Properties of Cellulose Nanomaterial-Based Films," ACS Sustain. Chem. Eng., vol. 6, no. 1, pp. 49–70, Jan. 2018, doi: 10.1021/acssuschemeng.7b03523.

L. J. Gibson and M. F. Ashby, Cellular Solids. Cambridge University Press, 1997.

L. M. Matuana, O. Faruk, and C. A. Diaz, "Cell morphology of extrusion foamed poly(lactic acid) using endothermic chemical foaming agent," Bioresour. Technol., vol. 100, no. 23, pp. 5947–5954, Dec. 2009, doi: 10.1016/j.biortech.2009.06.063.

L. MATHIEU, T. MUELLER, P. BOURBAN, D. PIOLETTI, R. MULLER, and J. MANSON, "Architecture and properties of anisotropic polymer composite scaffolds for bone tissue engineering," Biomaterials, vol. 27, no. 6, pp. 905–916, Feb. 2006, doi: 10.1016/j.biomaterials.2005.07.015.

L. S. Kochar and J. L. Throne, "Thermoforming Multilayer Sheet; I: General Criteria," J. Plast. Film Sheeting, vol. 5, no. 3, pp. 186–208, Jul. 1989, doi: 10.1177/875608798900500308.

L. Yu, H. Liu, F. Xie, L. Chen, and X. Li, "Effect of annealing and orientation on microstructures and mechanical properties of polylactic acid," Polym. Eng. Sci., vol. 48, no. 4, pp. 634–641, Apr. 2008, doi: 10.1002/pen.20970.

L.-T. Lim, R. Auras, and M. Rubino, "Processing technologies for poly(lactic acid)," Prog. Polym. Sci., vol. 33, no. 8, pp. 820–852, Aug. 2008, doi: 10.1016/j.progpolymsci.2008.05.004.

M. A. Rahman and E. Baer, "Layer Integrity in Polyethylene Based Multilayer Film/Foams and their Properties," in SPE ANTEC: Orlando, FL., 2015.

M. A. Rahman, J. Wang, C. Zhang, A. Olah, and E. Baer, "Novel micro-/nano- porous cellular membranes by forced assembly co-extrusion technology," Eur. Polym. J., vol. 83, pp. 99–113, Oct. 2016, doi: 10.1016/j.eurpolymj.2016.08.015.

M. A. Rahman, R. Andrade, J. Maia, and E. Baer, "Viscosity contrast effects on the structure – Property relationship of multilayer soft film/foams," Polymer (Guildf)., vol. 69, pp. 110–122, Jul. 2015, doi: 10.1016/j.polymer.2015.05.051.

M. Buntinx et al., "Evaluation of the Thickness and Oxygen Transmission Rate before and after Thermoforming Mono- and Multi-layer Sheets into Trays with Variable Depth," Polymers (Basel)., vol. 6, no. 12, pp. 3019–3043, Dec. 2014, doi: 10.3390/polym6123019.

M. Drieskens, R. Peeters, J. Mullens, D. Franco, P. J. Lemstra, and D. G. Hristova-Bogaerds, "Structure versus properties relationship of poly(lactic acid). I. Effect of crystallinity on barrier properties," J. Polym. Sci. Part B Polym. Phys., vol. 47, no. 22, pp. 2247–2258, Nov. 2009, doi: 10.1002/polb.21822.

M. K. Pettersen, A. Nilsson, A. Espedal, and A. Kohler, “Prediction of oxygen transmission rate for thermoformed trays,” Packag. Technol. Sci., vol. 17, no. 6, pp. 321–332, Nov. 2004, doi: 10.1002/pts.669.

M. Mackey et al., “Reduction of Dielectric Hysteresis in Multilayered Films via Nanoconfinement,” Macromolecules, vol. 45, no. 4, pp. 1954–1962, Feb. 2012, doi: 10.1021/ma202267r.

M. Murariu and P. Dubois, “PLA composites: From production to properties,” Adv. Drug Deliv. Rev., vol. 107, pp. 17–46, Dec. 2016, doi: 10.1016/j.addr.2016.04.003.

M. Nofar and C. B. Park, “Poly (lactic acid) foaming,” Prog. Polym. Sci., vol. 39, no. 10, pp. 1721–1741, Oct. 2014, doi: 10.1016/j.progpolymsci.2014.04.001.

M. R. Kamal, I. A. Jinnah, and L. A. Utracki, “Permeability of oxygen and water vapor through polyethylene/polyamide films,” Polym. Eng. Sci., vol. 24, no. 17, pp. 1337–1347, Dec. 1984, doi: 10.1002/pen.760241711.

M. Siccardi, X. X. Garcia-Fonte, A. Simon, V. Pettarin, M. J. Abad, and C. Bernal, “Effect of the Processing-Induced Morphology on the Mechanical Properties of Biodegradable Extruded Films Based on Poly(lactic acid) (PLA) Blends,” J. Polym. Environ., vol. 27, no. 11, pp. 2325–2333, Nov. 2019, doi: 10.1007/s10924-019-01512-0.

M. Yasuniwa, S. Tsubakihara, Y. Sugimoto, and C. Nakafuku, “Thermal analysis of the double-melting behavior of poly(L-lactic acid),” J. Polym. Sci. Part B Polym. Phys., vol. 42, no. 1, pp. 25–32, Jan. 2004, doi: 10.1002/polb.10674.

N. Alipour et al., “Structure and properties of polyethylene-based and EVOH-based multilayered films with layer thicknesses of 150nm and greater,” Eur. Polym. J., vol. 64, pp. 36–51, Mar. 2015, doi: 10.1016/j.eurpolymj.2014.12.011.

N. Rosenzweig, M. Narkis, and Z. Tadmor, “Wall thickness distribution in thermoforming,” Polym. Eng. Sci., vol. 19, no. 13, pp. 946–951, Oct. 1979, doi: 10.1002/pen.760191311.

S. E. M. Selke, Understanding Plastic Packaging Technology. New York: Hanser Publications, 1997.

S. Ebnesajjad, Plastic Films in Food Packaging Materials, Technology, and Applications. Elsevier, 2013.

S. Ji, K. Yin, M. Mackey, A. Brister, M. Ponting, and E. Baer, “Polymeric nanolayered gradient refractive index lenses: technology review and introduction of spherical gradient refractive index ball lenses,” Opt. Eng., vol. 52, no. 11, p. 112105, Jul. 2013, doi: 10.1117/1.OE.52.11.112105.

S. Pilla, S. G. Kim, G. K. Auer, S. Gong, and C. B. Park, “Microcellular extrusion-foaming of polylactide with chain-extender,” Polym. Eng. Sci., vol. 49, no. 8, pp. 1653–1660, Aug.

2009, doi: 10.1002/pen.21385.

S. Saeidlou, M. A. Huneault, H. Li, and C. B. Park, “Poly(lactic acid) crystallization,” Prog. Polym. Sci., vol. 37, no. 12, pp. 1657–1677, Dec. 2012, doi: 10.1016/j.progpolymsci.2012.07.005.

S. T. Lee and C. B. Park, Foam Extrusion: Principles and Practice, Second Edi. CRC Press, 2014.

S. T. Lee, C. B. Park, and N. S. Ramesh, Polymeric foams: Mechanisms and materials. 2006.

S. T. Lee, L. Kareko, and J. Jun, “Study of Thermoplastic PLA Foam Extrusion,” J. Cell. Plast., vol. 44, no. 4, pp. 293–305, Jul. 2008, doi: 10.1177/0021955X08088859.

S.-T. Lee and N. S. Ramesh, “Gas loss during foam sheet formation,” Adv. Polym. Technol., vol. 15, no. 4, pp. 297–305, 1996, doi: 10.1002/adv.1996.060150403.

S.-T. Lee and N. S. Ramesh, Polymeric Foams Mechanisms and Materials. CRC Press, 2004.

T. Schuman, S. Nazarenko, E. . Stepanov, S. . Magonov, A. Hiltner, and E. Baer, “Solid state structure and melting behavior of interdiffused polyethylenes in microlayers,” Polymer (Guildf)., vol. 40, no. 26, pp. 7373–7385, Dec. 1999, doi: 10.1016/S0032-3861(99)00013-0.

T. Standau, C. Zhao, S. Murillo Castellón, C. Bonten, and V. Altstädt, “Chemical Modification and Foam Processing of Polylactide (PLA),” Polymers (Basel)., vol. 11, no. 2, p. 306, Feb. 2019, doi: 10.3390/polym11020306.

T. Takayama, M. Todo, and H. Tsuji, “Effect of annealing on the mechanical properties of PLA/PCL and PLA/PCL/LTI polymer blends,” J. Mech. Behav. Biomed. Mater., vol. 4, no. 3, pp. 255–260, Apr. 2011, doi: 10.1016/j.jmbbm.2010.10.003.

V. Maquet et al., “Peripheral nerve regeneration using bioresorbable macroporous polylactide scaffolds,” J. Biomed. Mater. Res., vol. 52, no. 4, pp. 639–651, Dec. 2000, doi: 10.1002/1097-4636(20001215)52:4<639::AID-JBM8>3.0.CO;2-G.

W. Busby, N. R. Cameron, and C. A. Jahoda, “Tissue engineering matrixes by emulsion templating,” Polym. Int., vol. 51, no. 10, pp. 871–881, Oct. 2002, doi: 10.1002/pi.934.

Y. Srithep, P. Nealey, and L.-S. Turng, “Effects of annealing time and temperature on the crystallinity and heat resistance behavior of injection-molded poly(lactic acid),” Polym. Eng. Sci., vol. 53, no. 3, pp. 580–588, Mar. 2013, doi: 10.1002/pen.23304.

Z. Li, A. Olah, and E. Baer, “Micro- and nano-layered processing of new polymeric systems,” Prog. Polym. Sci., vol. 102, p. 101210, Mar. 2020, doi:

10.1016/j.progpolymsci.2020.101210.